US009557285B2

(12) **United States Patent**
Gole

(10) **Patent No.: US 9,557,285 B2**
(45) **Date of Patent: Jan. 31, 2017**

(54) **GAS SENSORS AND METHODS OF PREPARATION THEREOF**

(75) Inventor: **James L. Gole**, Atlanta, GA (US)

(73) Assignee: **GEORGIA TECH RESEARCH CORPORATION**, Atlanta, GA (US)

(*) Notice: Subject to any disclaimer, the term of this patent is extended or adjusted under 35 U.S.C. 154(b) by 277 days.

(21) Appl. No.: **14/240,691**

(22) PCT Filed: **Aug. 21, 2012**

(86) PCT No.: **PCT/US2012/051721**

§ 371 (c)(1),
(2), (4) Date: **Feb. 24, 2014**

(87) PCT Pub. No.: **WO2013/028691**

PCT Pub. Date: **Feb. 28, 2013**

(65) **Prior Publication Data**

US 2014/0223997 A1 Aug. 14, 2014

Related U.S. Application Data

(60) Provisional application No. 61/527,294, filed on Aug. 25, 2011.

(51) **Int. Cl.**
G01N 27/06 (2006.01)
B82Y 15/00 (2011.01)
G01N 27/12 (2006.01)

(52) **U.S. Cl.**
CPC *G01N 27/06* (2013.01); *B82Y 15/00* (2013.01); *G01N 27/127* (2013.01)

(58) **Field of Classification Search**
CPC G01N 27/403; G01N 27/02; G01N 27/128;
G01N 2033/0095; G01N 27/127; G01N
33/0027; G01N 27/414; B82Y 15/00
See application file for complete search history.

(56) **References Cited**

U.S. PATENT DOCUMENTS

4,542,640 A	9/1985	Clifford	
5,726,463 A *	3/1998	Brown	H01L 29/1608 257/288
7,452,126 B2	11/2008	Arndt	
7,459,732 B2 *	12/2008	Fleischer	G01N 27/002 257/213

(Continued)

OTHER PUBLICATIONS

International Search Report & Written Opinion—Nov. 16, 2012.

Primary Examiner — Francis Gray
(74) *Attorney, Agent, or Firm* — Thomas I Horstemeyer, LLP

(57) **ABSTRACT**

Embodiments of the present disclosure include sensors, arrays of conductometric sensors, devices including conductometric sensors, methods of making conductometric sensors, methods of using conductometric gas sensors, and the like. One exemplary embodiment of a device, among others, includes: a conductometric gas sensor including a n-type substrate having a porous layer, wherein a plurality of 'nanostructures are disposed on a portion of the porous layer, wherein the nanostructure provides a fractional coverage on the porous layer, wherein the conductometric gas sensor is operative to transduce the presence of a gas into an impedance change, wherein the impedance change correlates to the gas concentration.

63 Claims, 28 Drawing Sheets
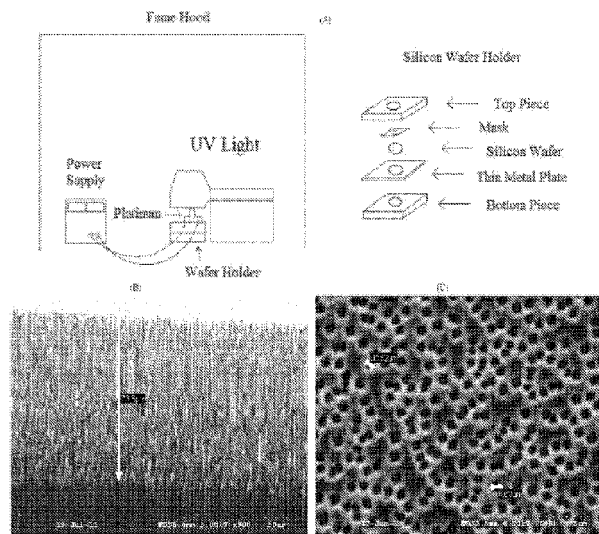
(56)   **References Cited**

U.S. PATENT DOCUMENTS

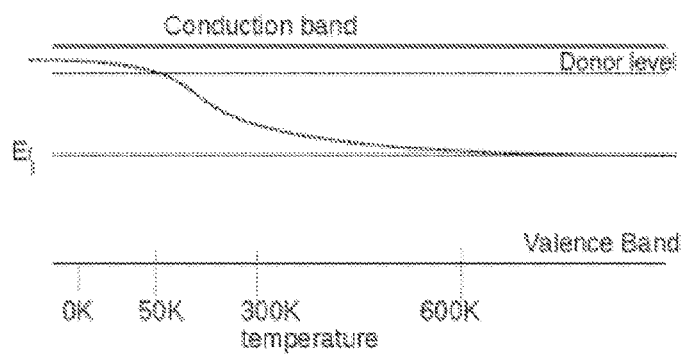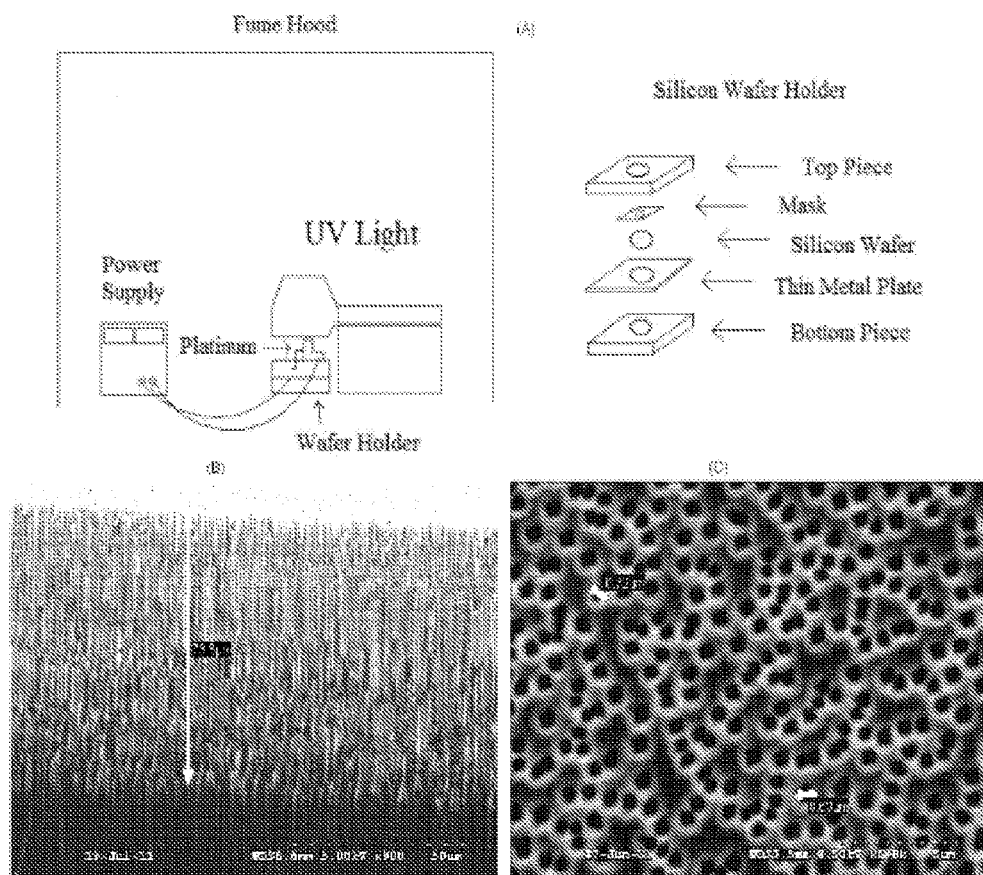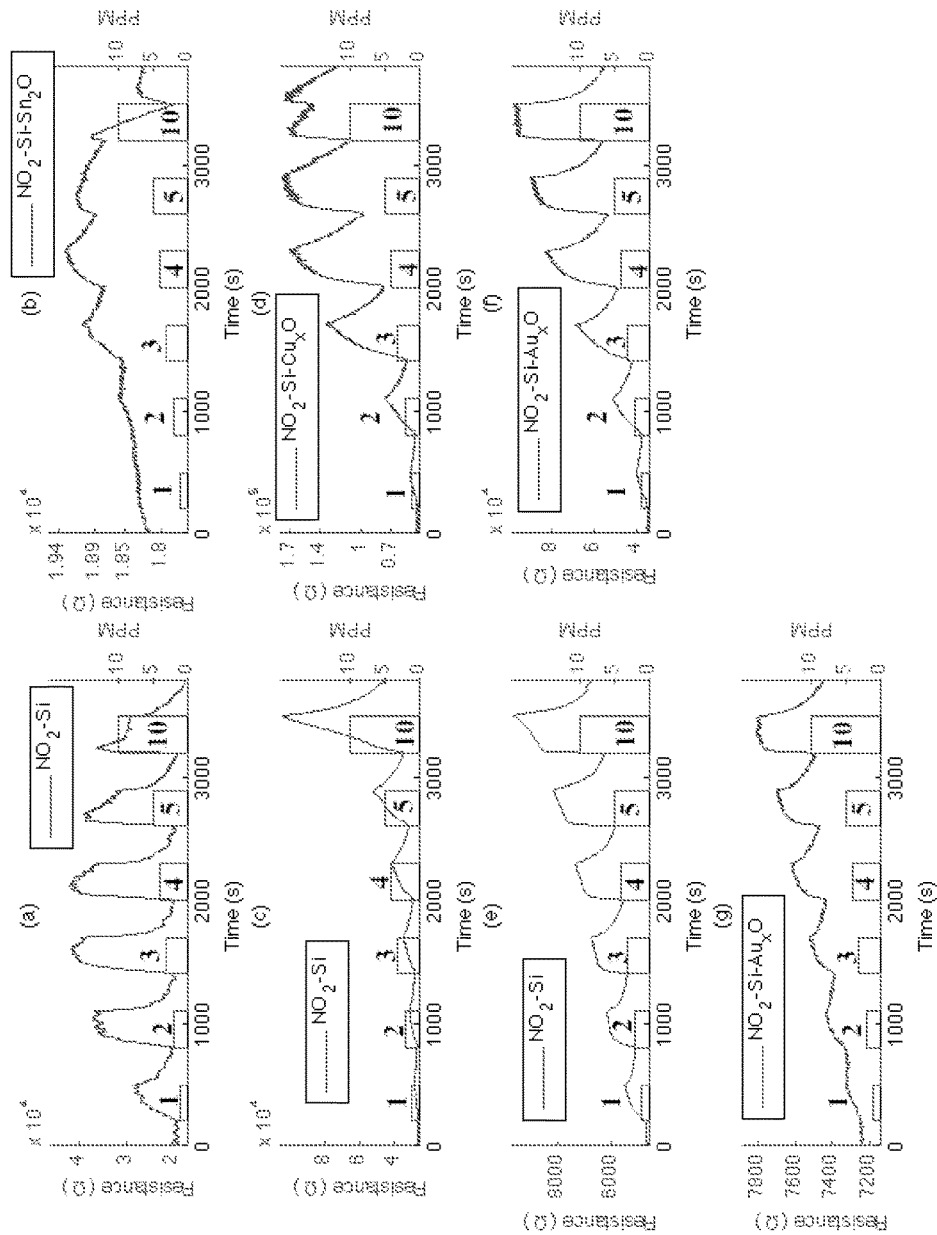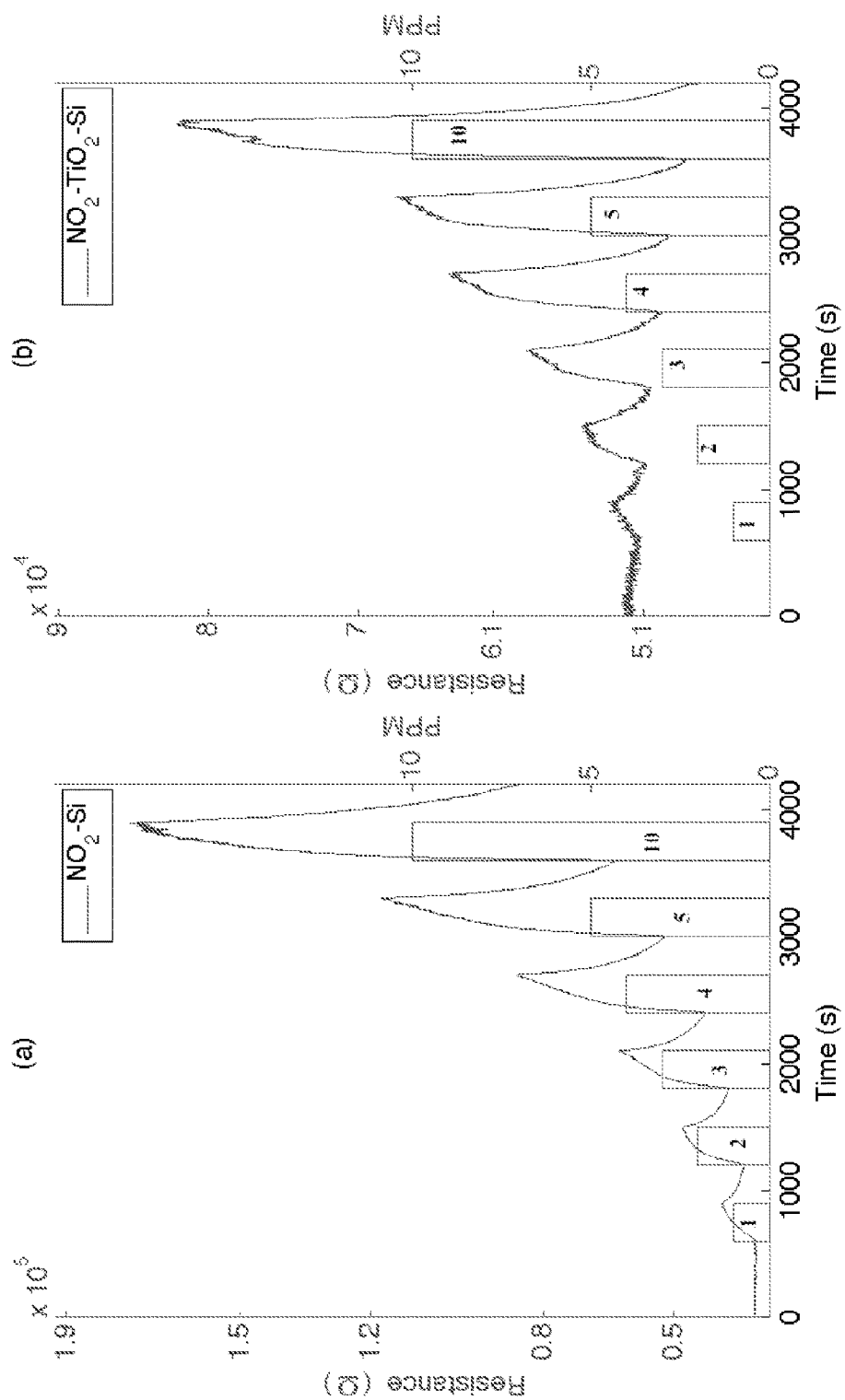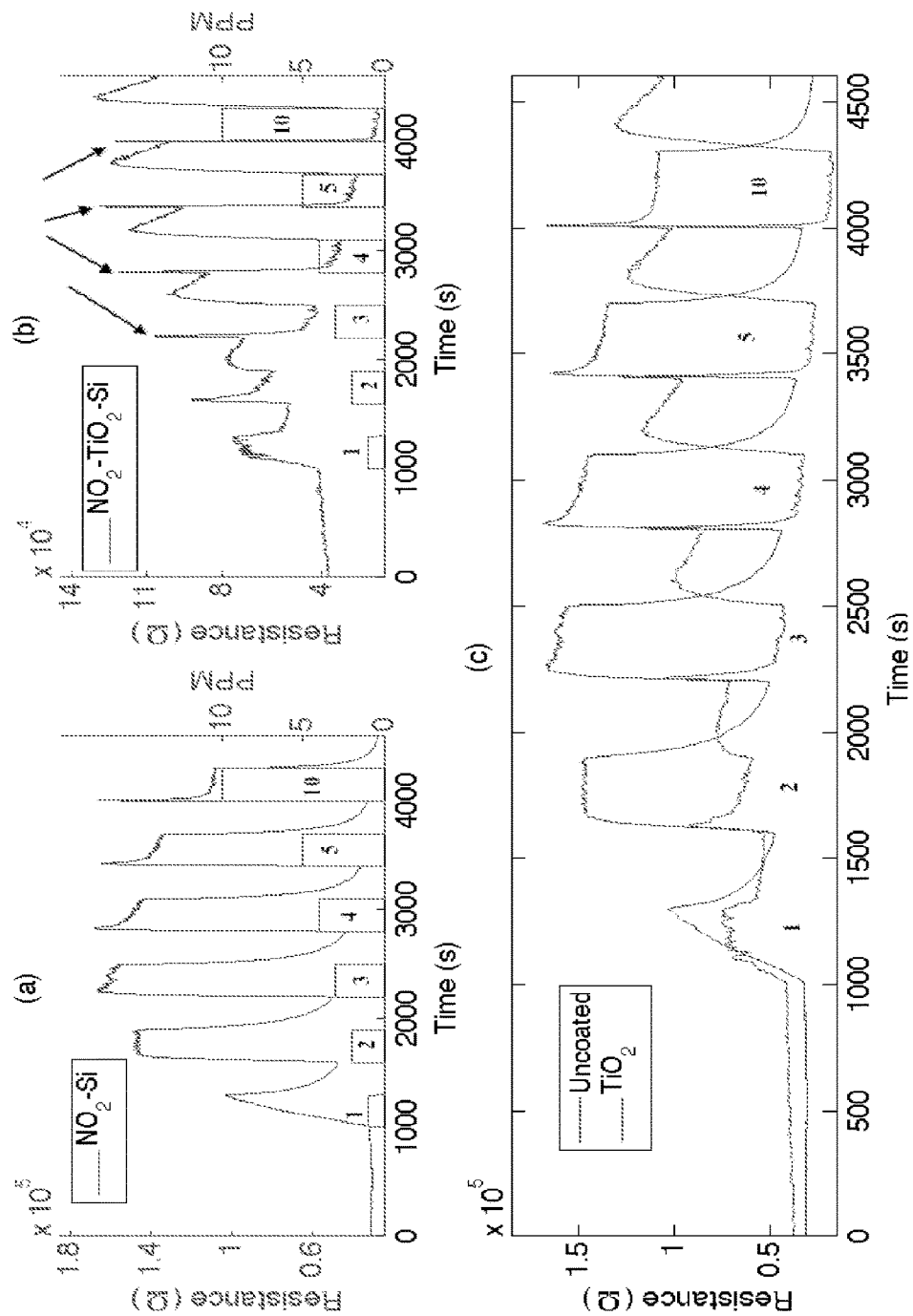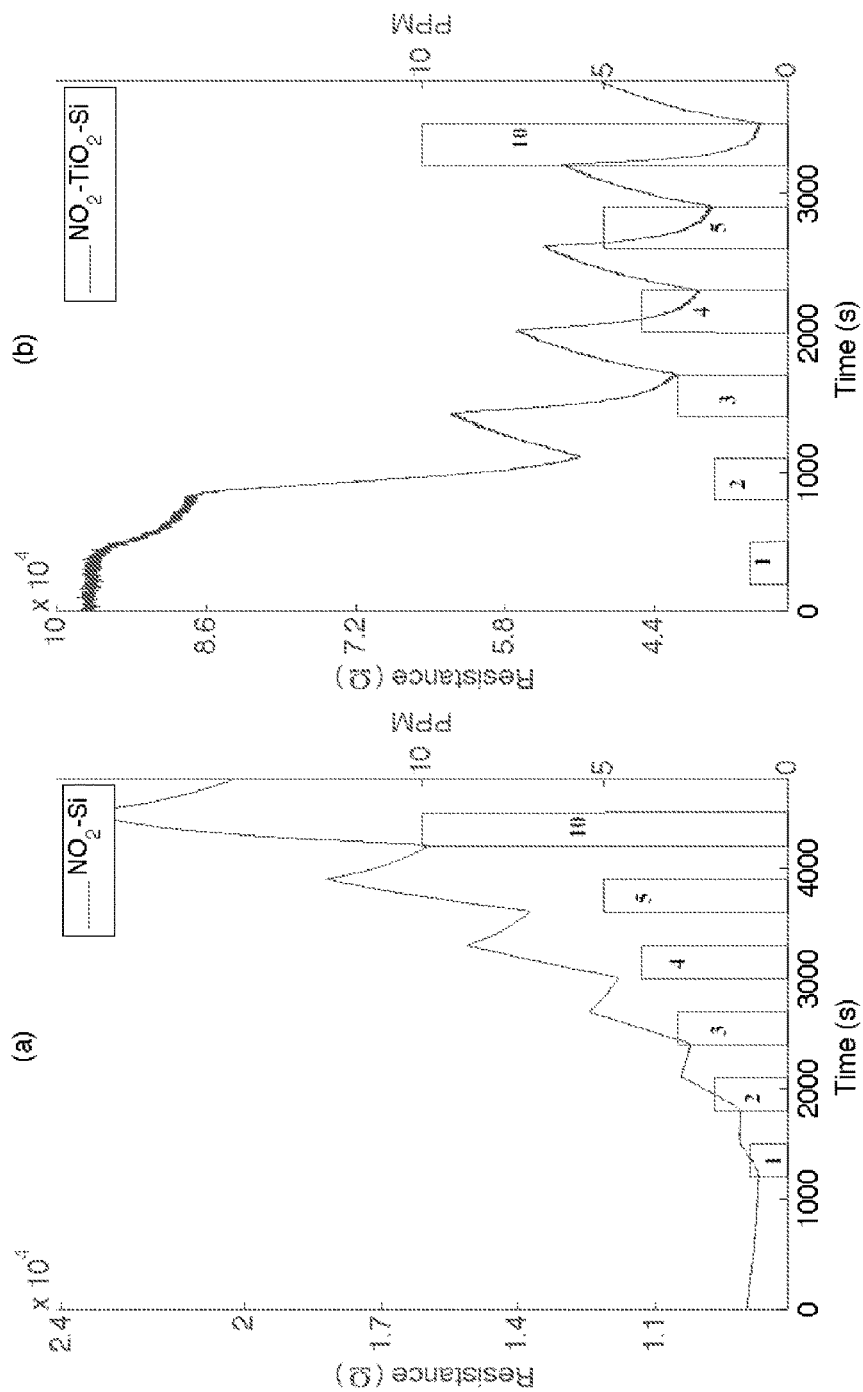|				
7,598,584	B2 *	10/2009	Ohta	H01L 31/103 257/184
7,933,535	B2	4/2011	Deguchi	
2005/0193800	A1 *	9/2005	DeBoer	G01N 27/128 73/1.06
2007/0140908	A1	6/2007	Mizuguchi	
2008/0110241	A1	5/2008	Rothschild	
2010/0147684	A1	6/2010	Park	
2010/0154517	A1	6/2010	Sammoura	
2012/0086021	A1 *	4/2012	Wang	G01N 21/658 257/84

* cited by examiner

FIG. 1.1

FIG. 1.2

FIG. 1.3

FIG. 1.4

FIG. 1.5

FIG. 1.6
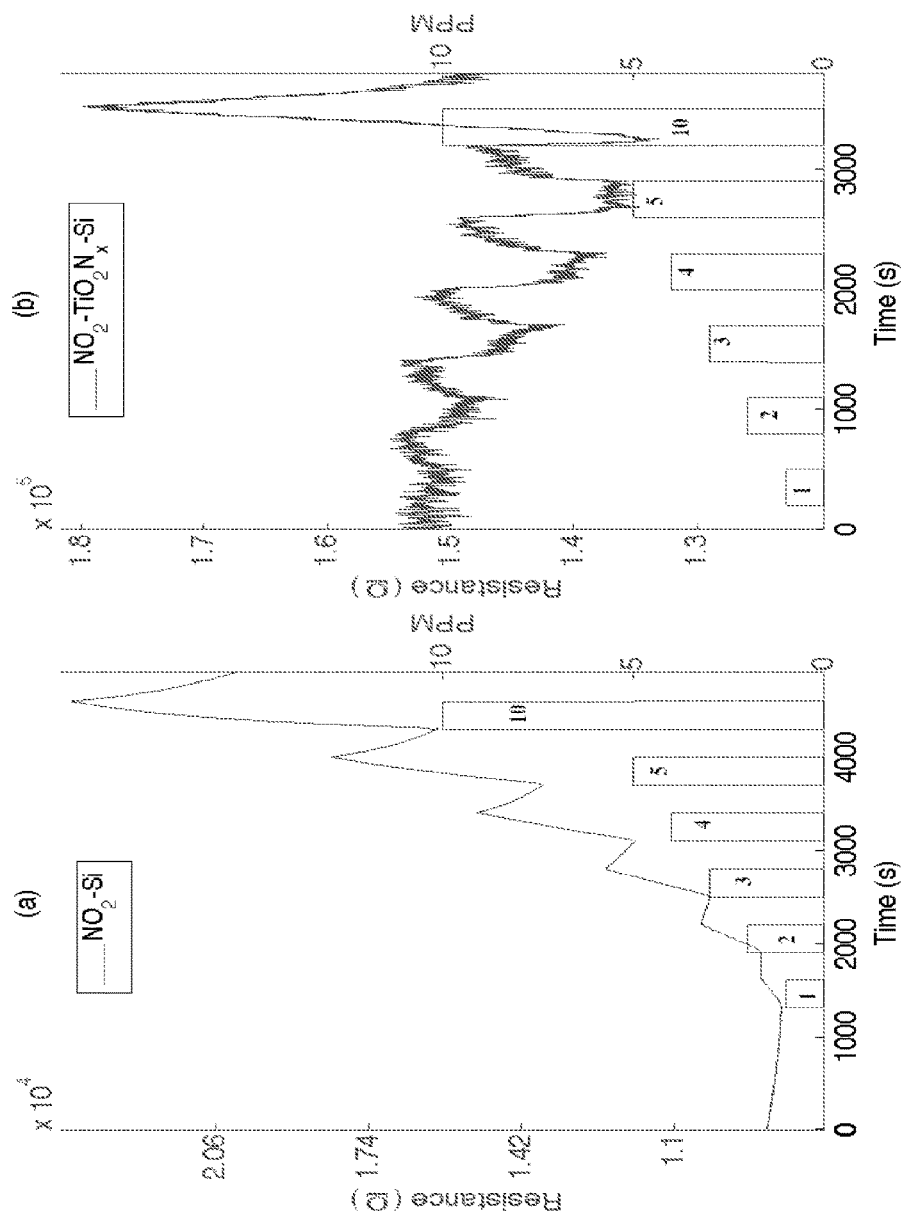
FIG. 1.7
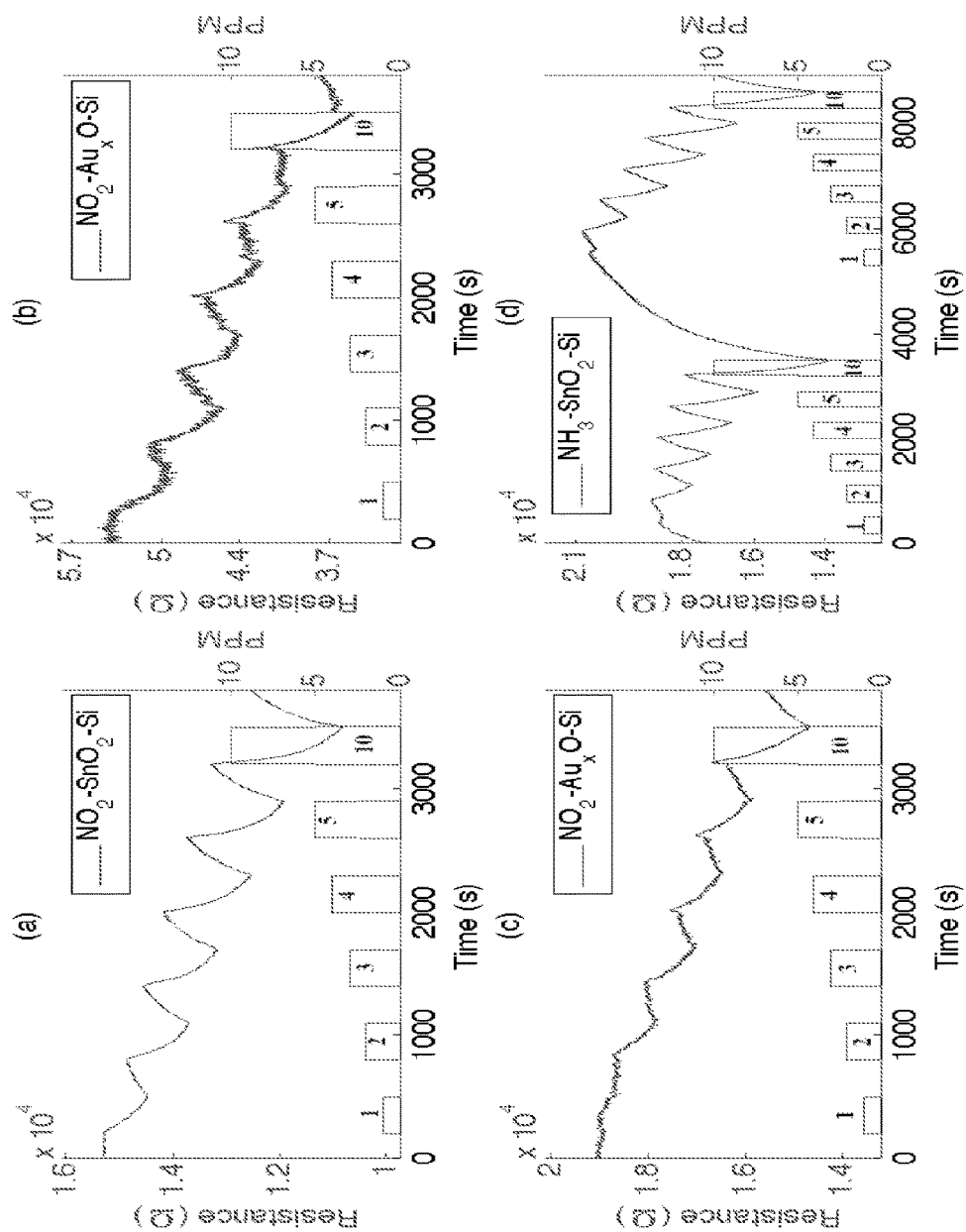
FIG. 1.8
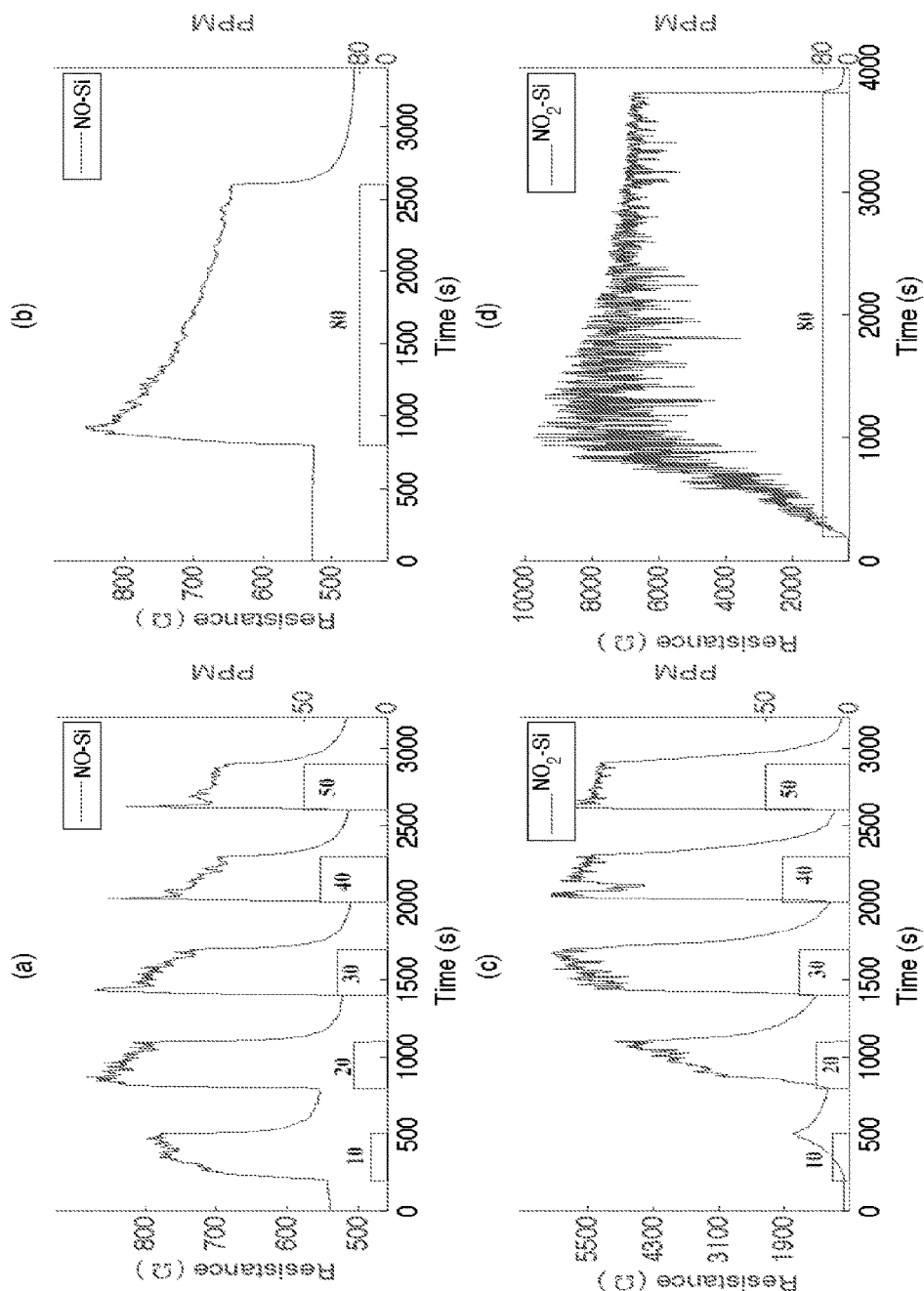
FIG. 1.9
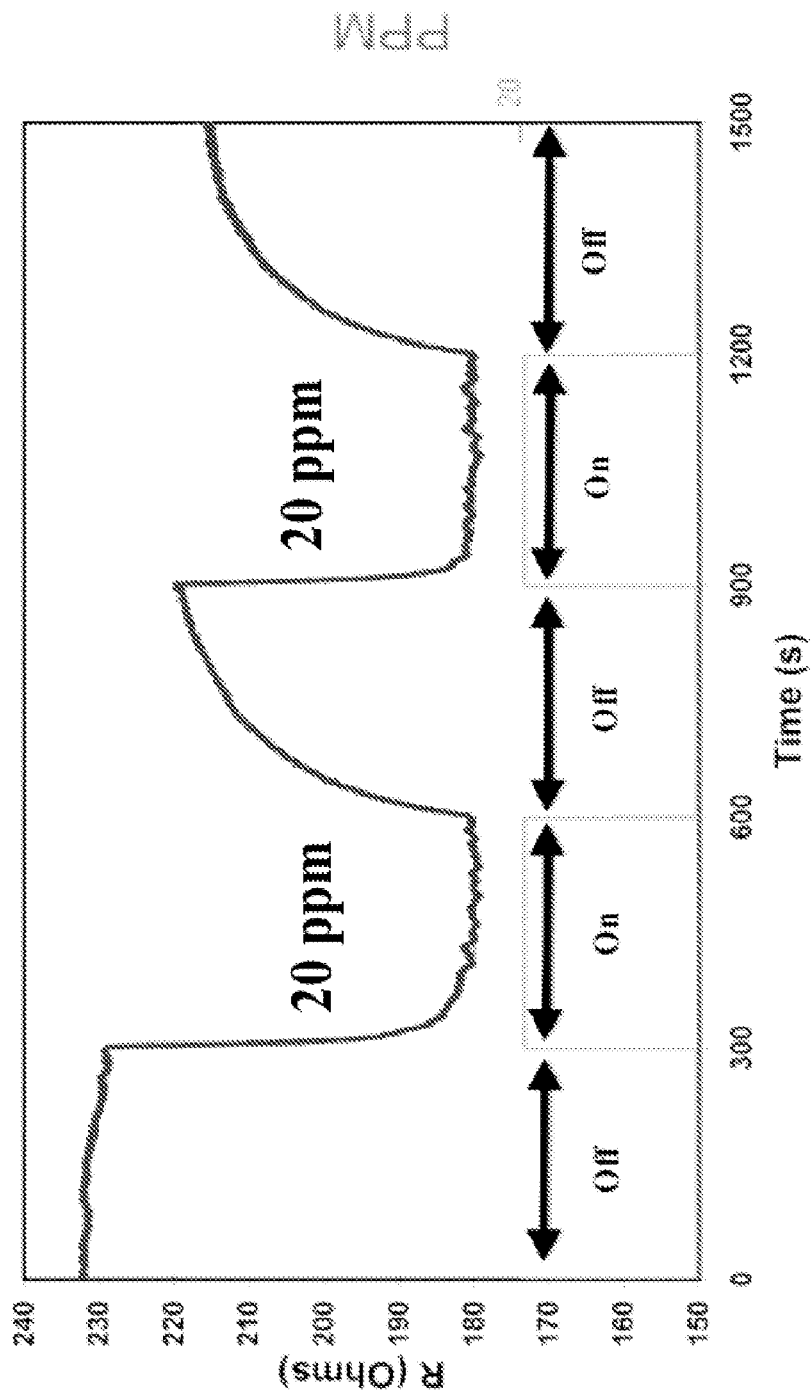
FIG. 1.10

FIG. 1.11

Table 1

Hard	Borderline	Soft
Acids H$^+$, Li$^+$, Na$^+$, K$^+$	Fe^{2+}, Co^{2+}, Ni^{2+}	Cu$^+$, Au$^+$, Ag$^+$, Tl$^+$, Hg$^+$
Be^{2+}, Mg^{2+}, Ca^{2+}	Cu^{2+}, Zn^{2+}, Pb^{2+}	Pd^{2+}, Cd^{2+},
Pt^{2+}, Hg^{2+}		
Cr^{2+}, Cr^{3+}, Al^{3+}	BBr$_3$, Sn^{+2}, NO$_2$	BH$_3$, NO
SO$_3$, BF$_3$, Sn^{+4}, Ti^{+4}		
Bases F$^-$, OH$^-$, H$_2$O, NH$_3$	NO$_2^-$, SO$_3^{2-}$, Br$^-$	H$^-$, R$^-$, CN$^-$, CO, I
CO$_3^{2-}$, NO$_3^-$, O^{2-}	N$_3^-$, N$_2$, H$_2$S, SO$_2$	SCN$^-$, R$_3$P, C$_6$H$_5$
SO$_4^{2-}$, PO$_4^{3-}$, ClO$_4^-$	C$_6$H$_5$N, SCN	R$_2$S, NO

Table 2

	TiO$_2$	SnO$_2$	NiO	Cu$_x$O	Au$_x$O
NO$_2$	0.75^1	0.5^2	(0.9-1)	>2	5

Table 3

	2 ppm	3 ppm	4 ppm	5 ppm	10 ppm
Elapsed time till peak maximum	32 s	15 s	11 s	9 s	4 s
Peak width s	57 s	14 s	8 s	5 s	1 s

FIG. 2.1

FIG. 2.2
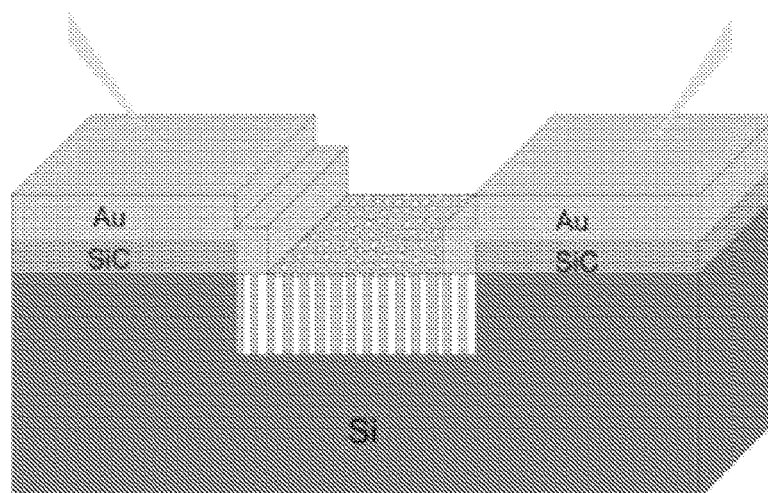
FIG. 2.3
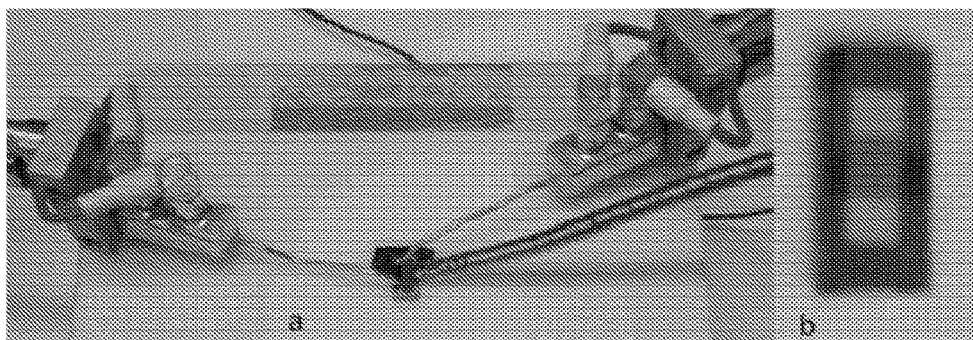
FIG. 2.4
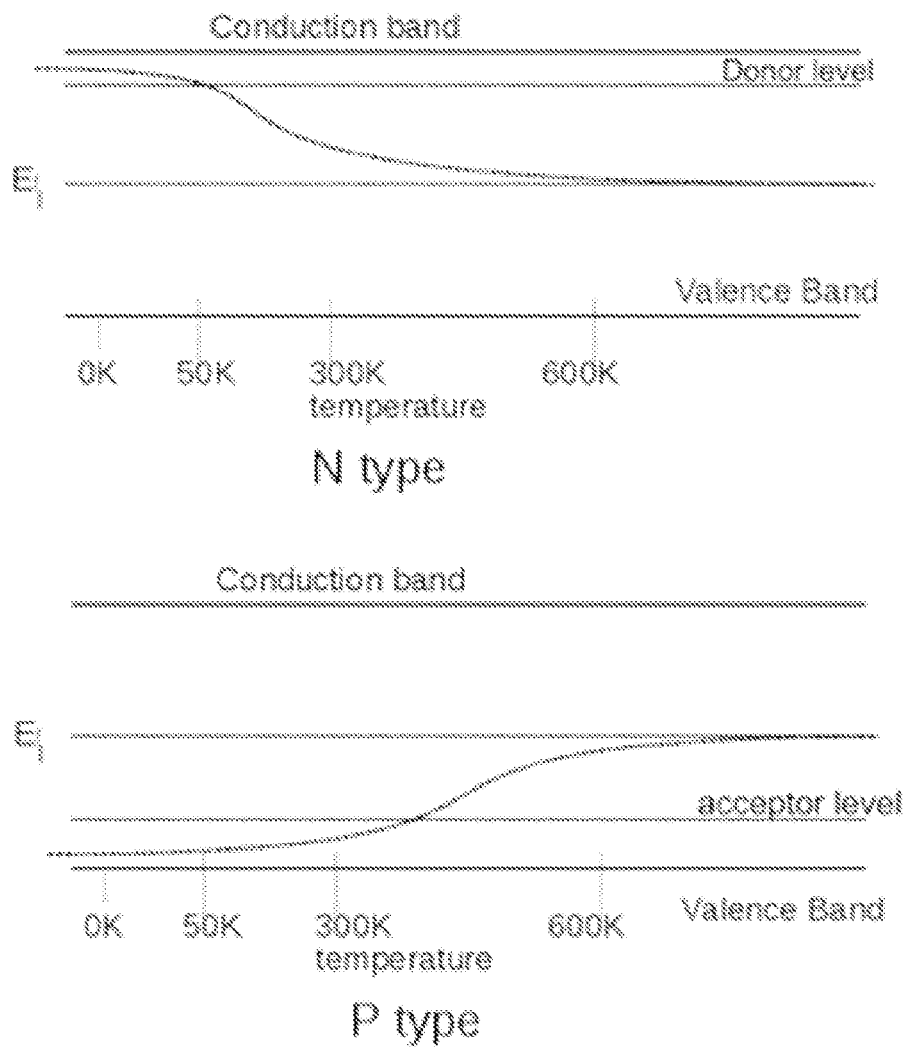
FIG. 2.5
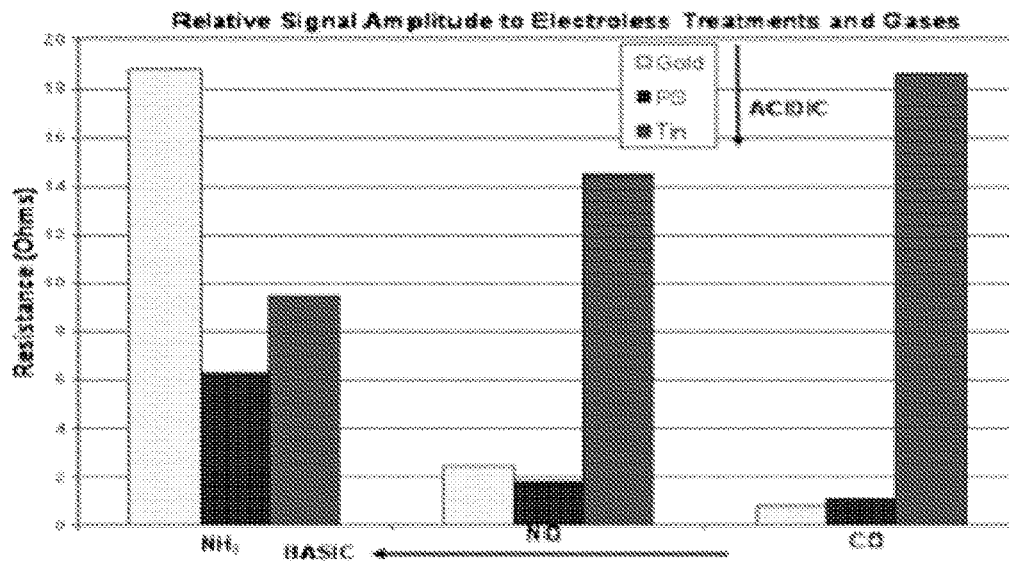
FIG. 2.6
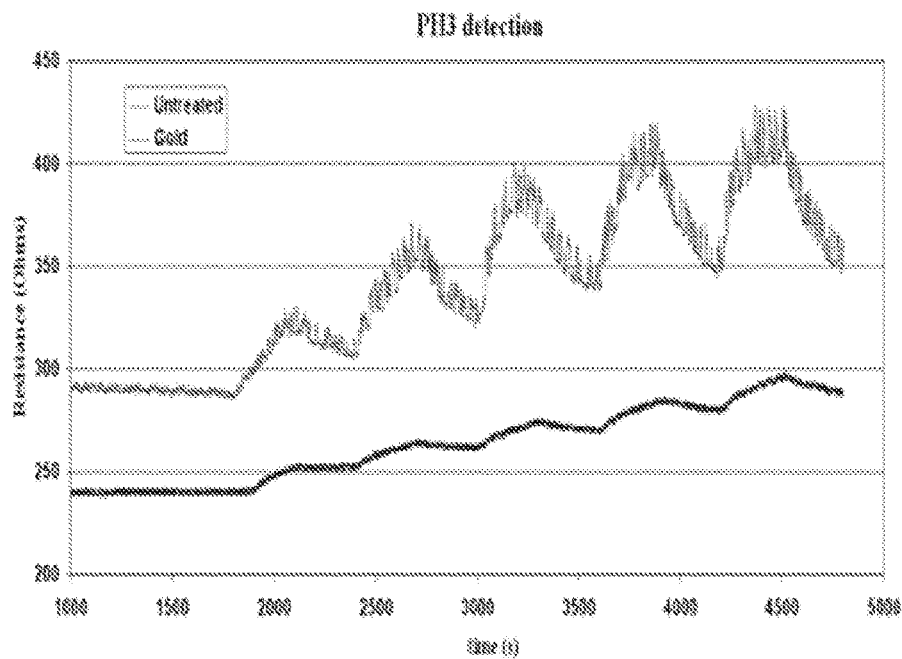
FIG. 2.7
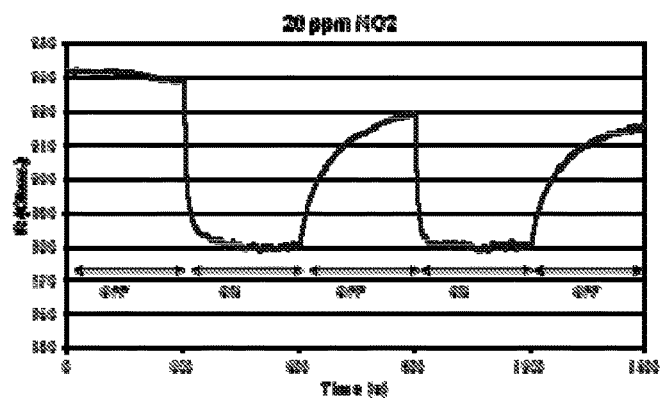
FIG. 2.8
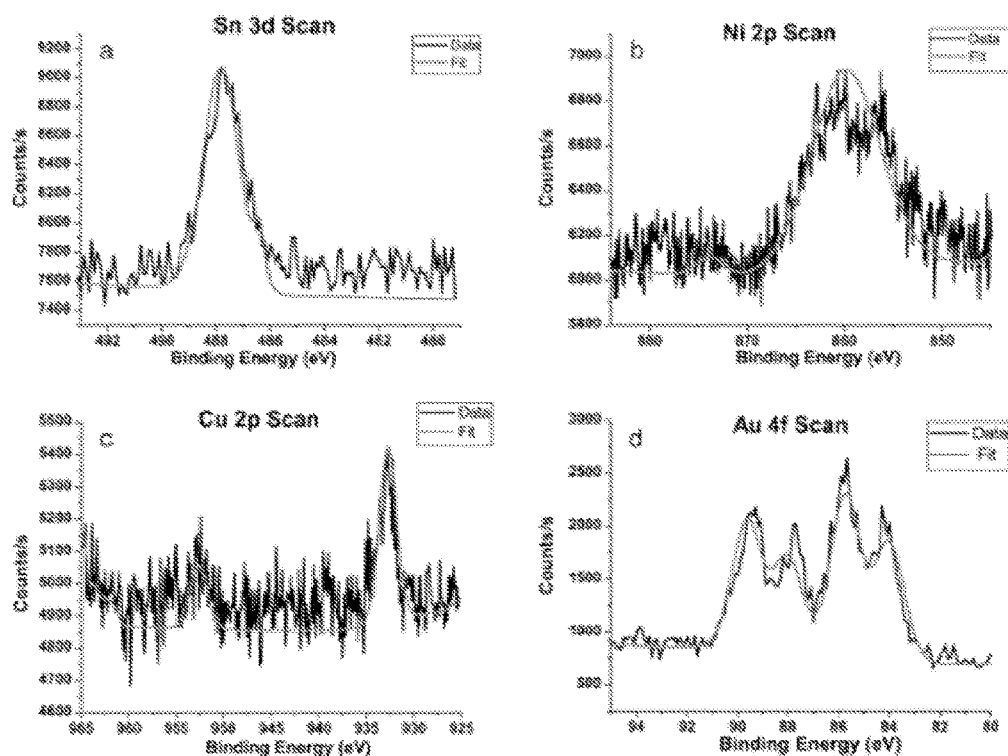
FIG. 2.9
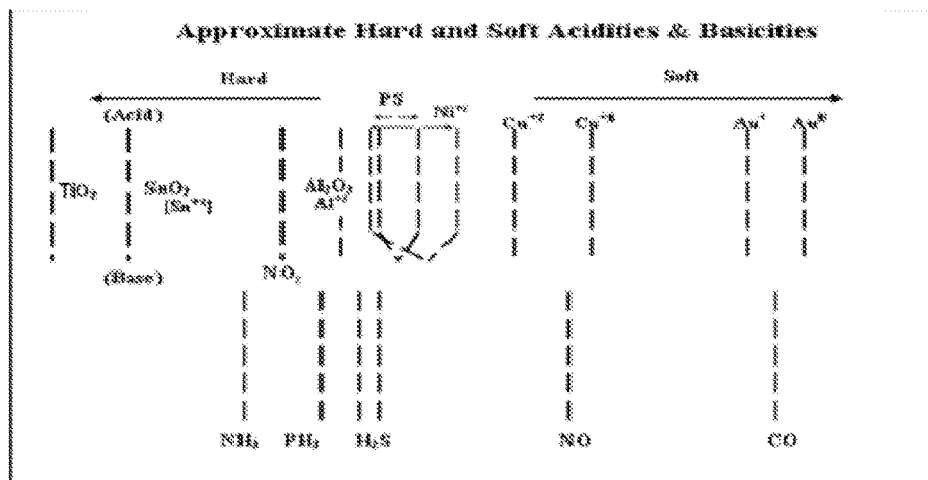
FIG. 2.10
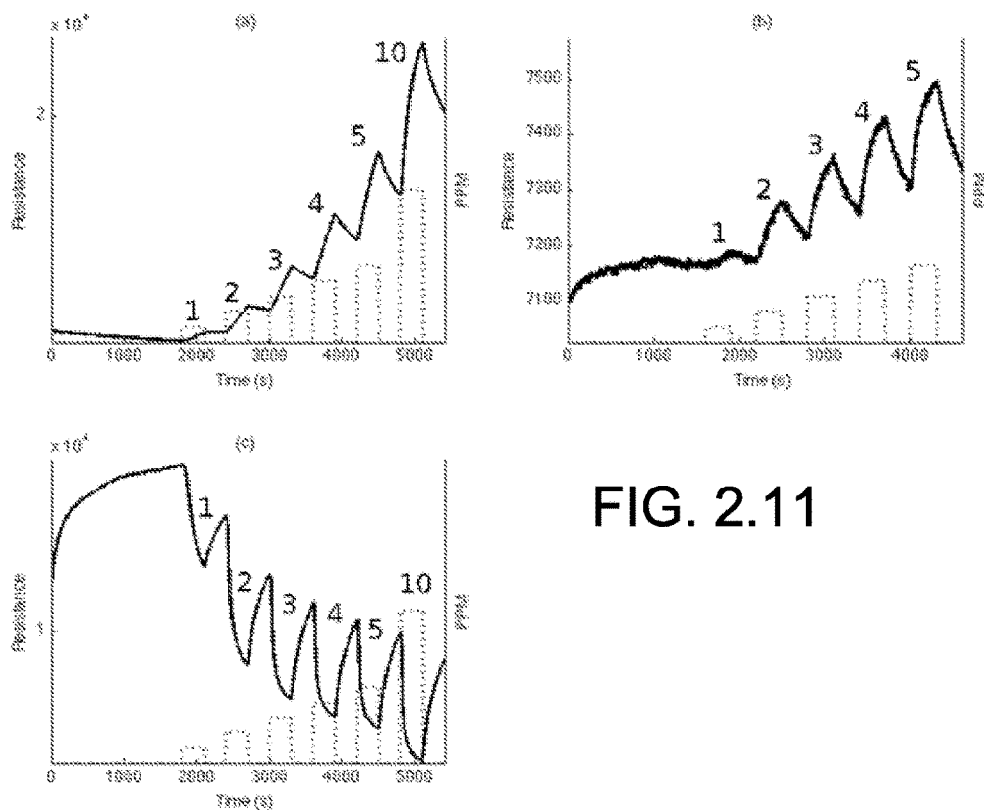
FIG. 2.11
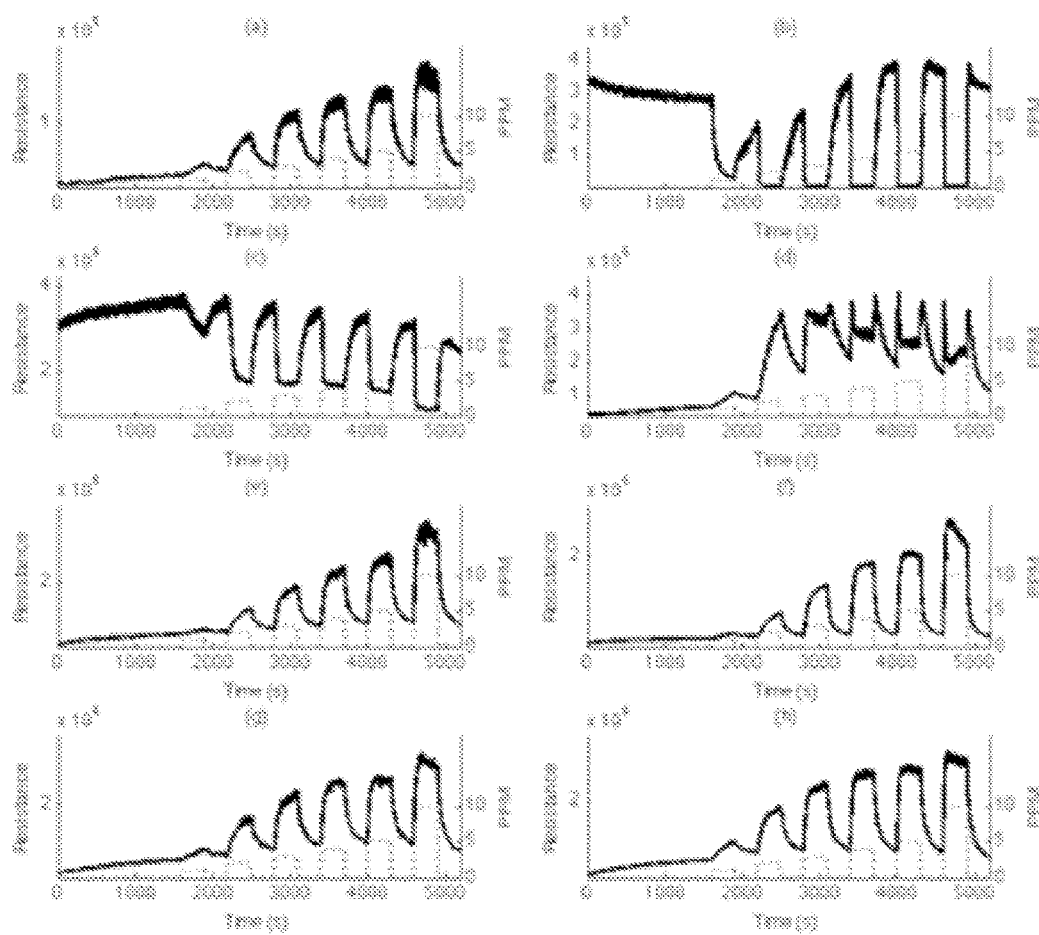
FIG. 2.12
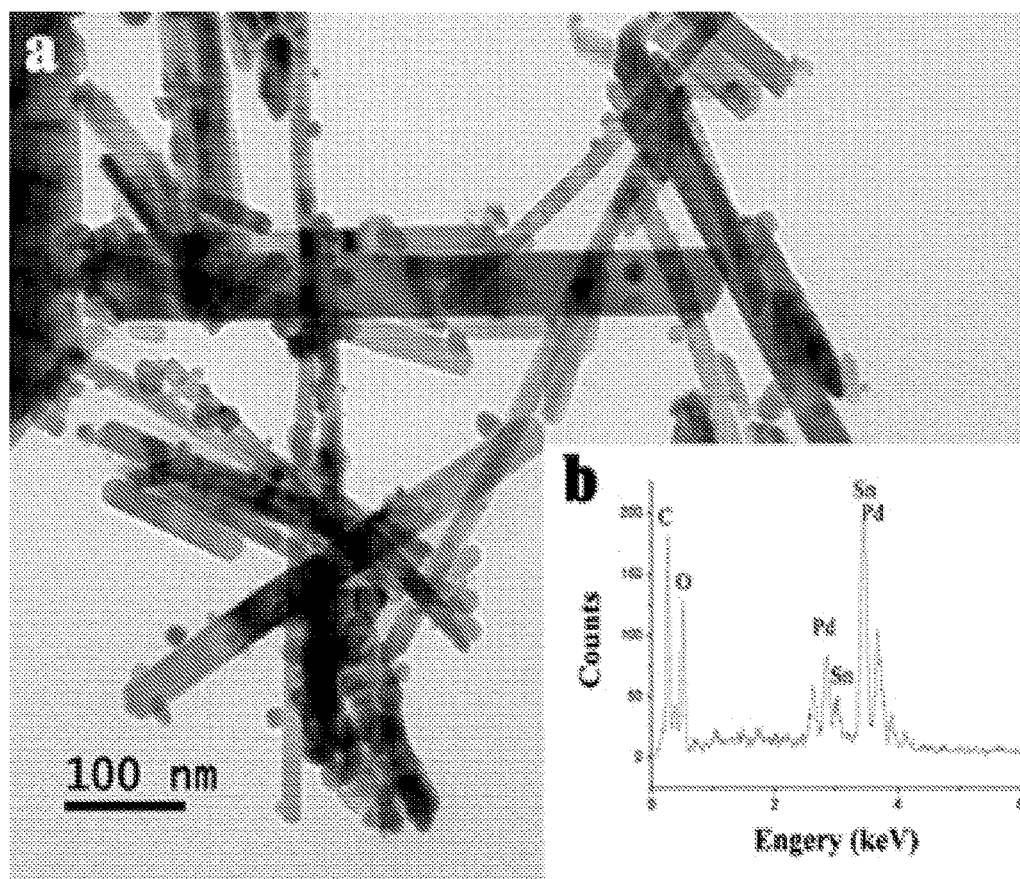
FIG. 2.13
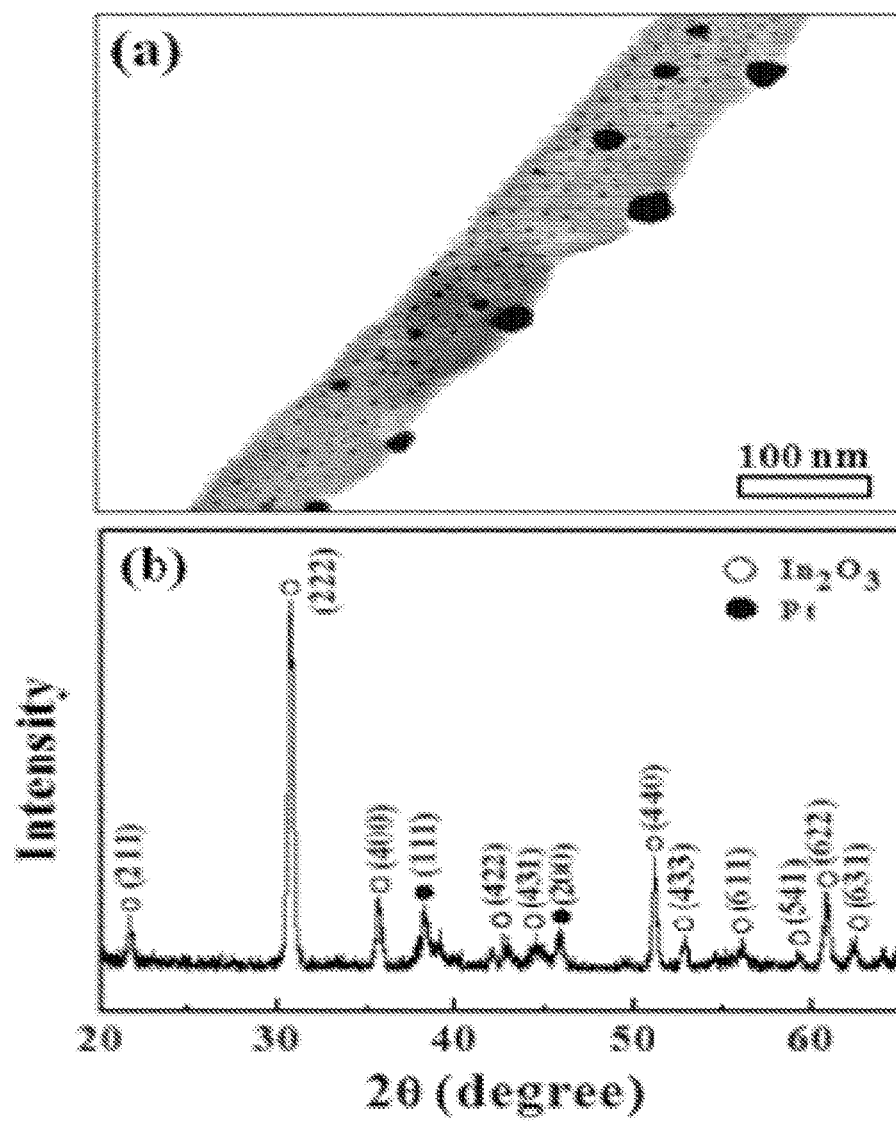
FIG. 2.14
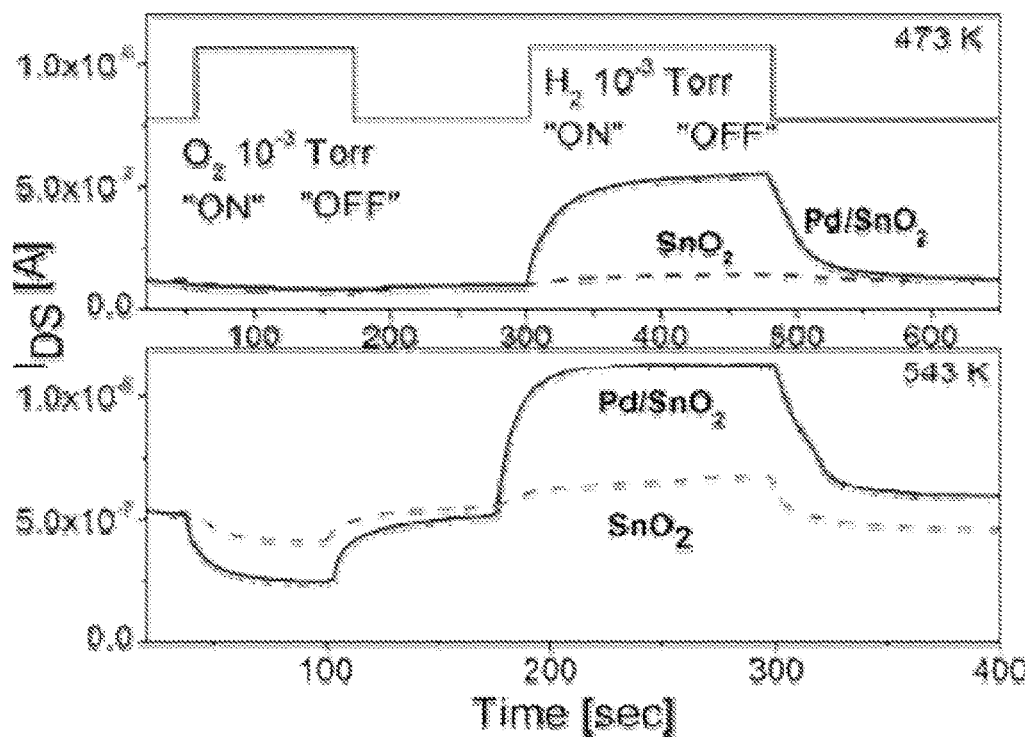
FIG. 2.15
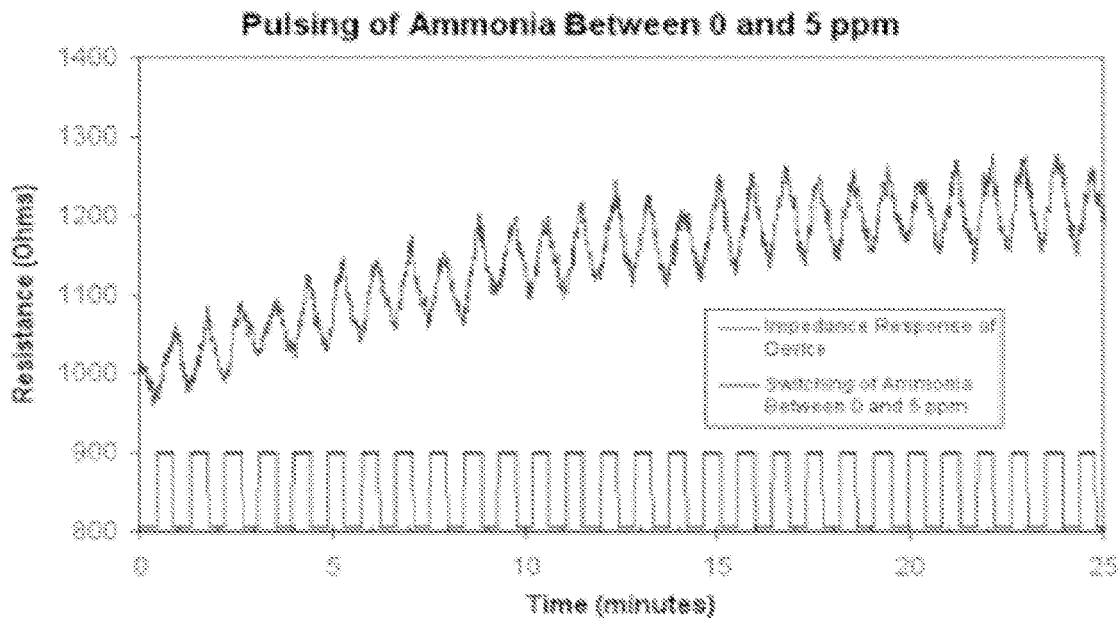
FIG. 2.16
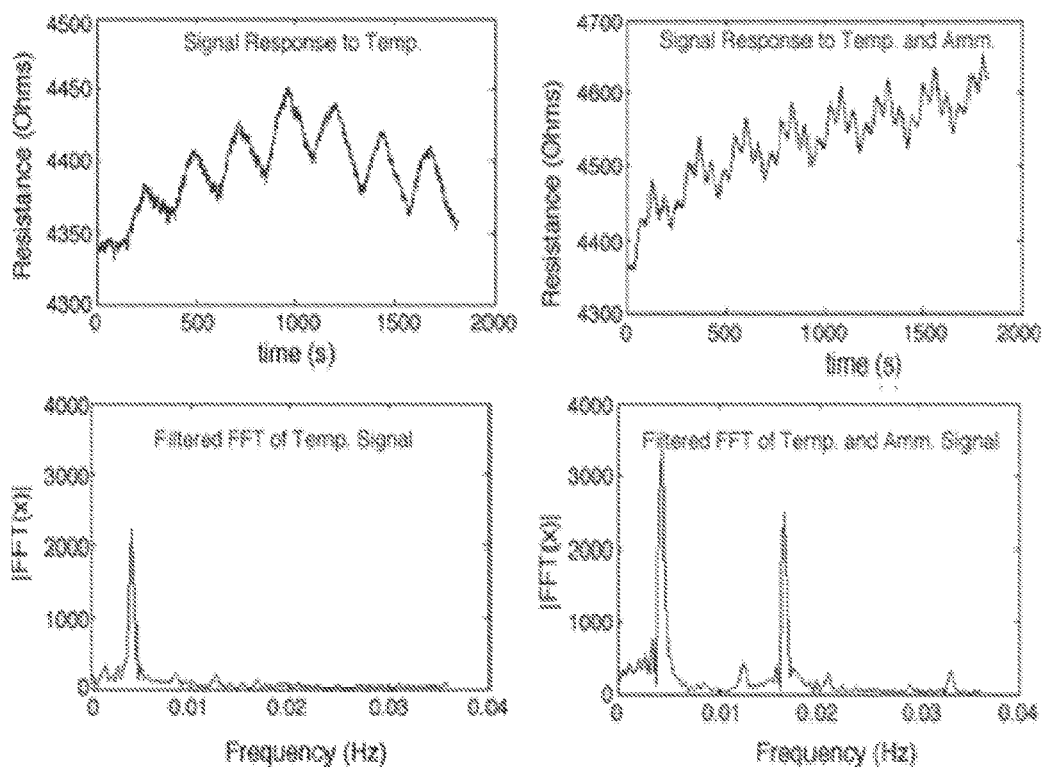
FIG. 2.17

FIG. 2.18

FIG. 2.19

FIG. 2.20

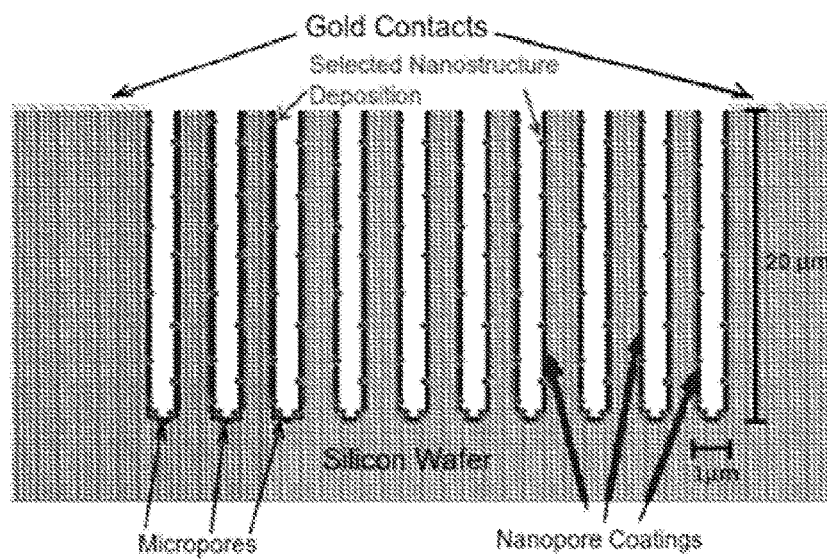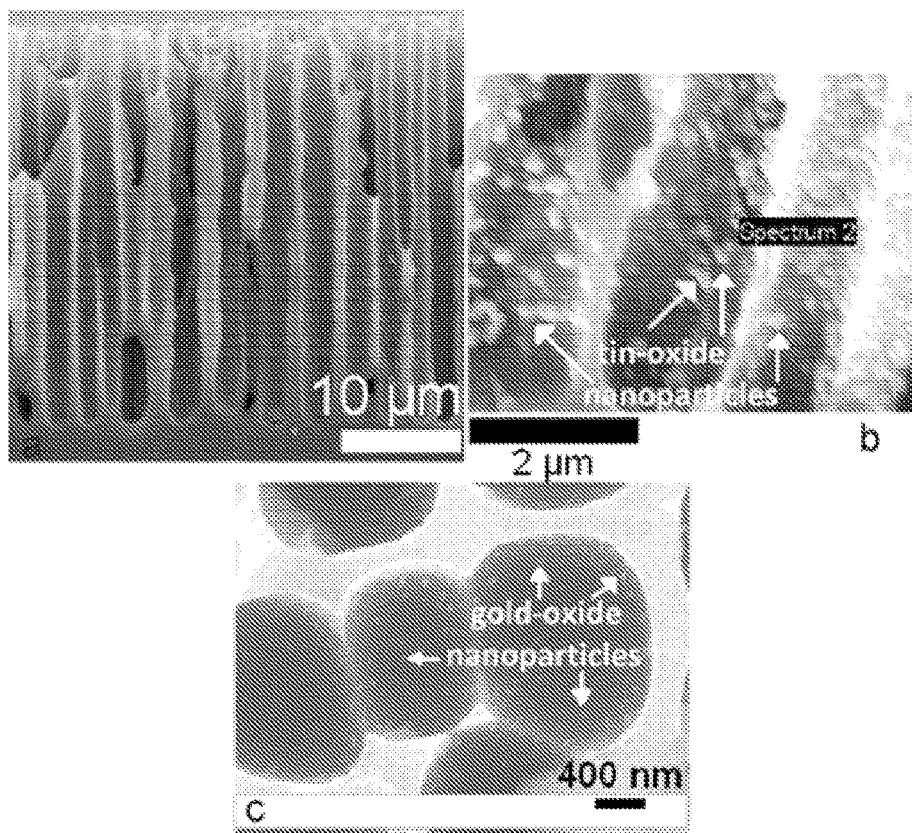Exposure to Ammonia in 20ppm NO background

FIG. 2.21

Metal Oxide Sensors

Porous Silicon Sensor
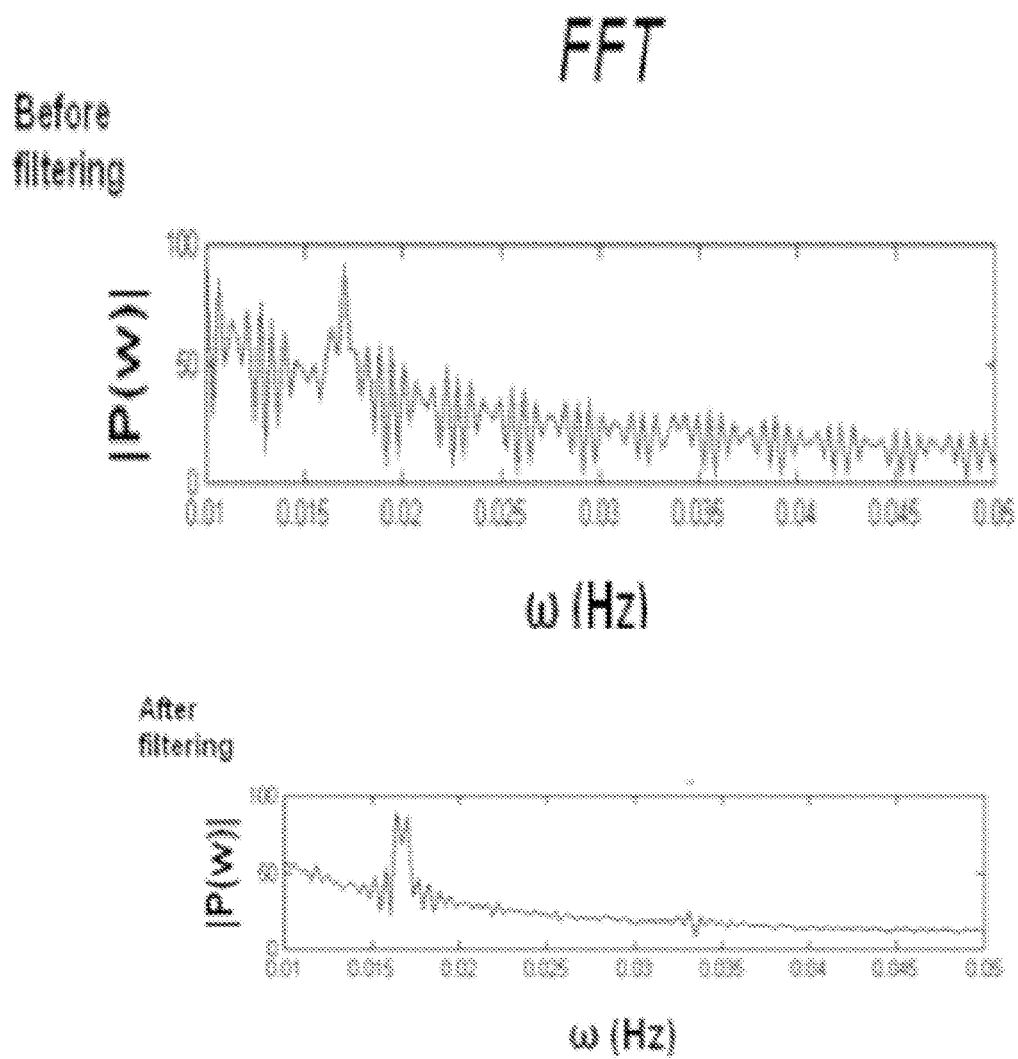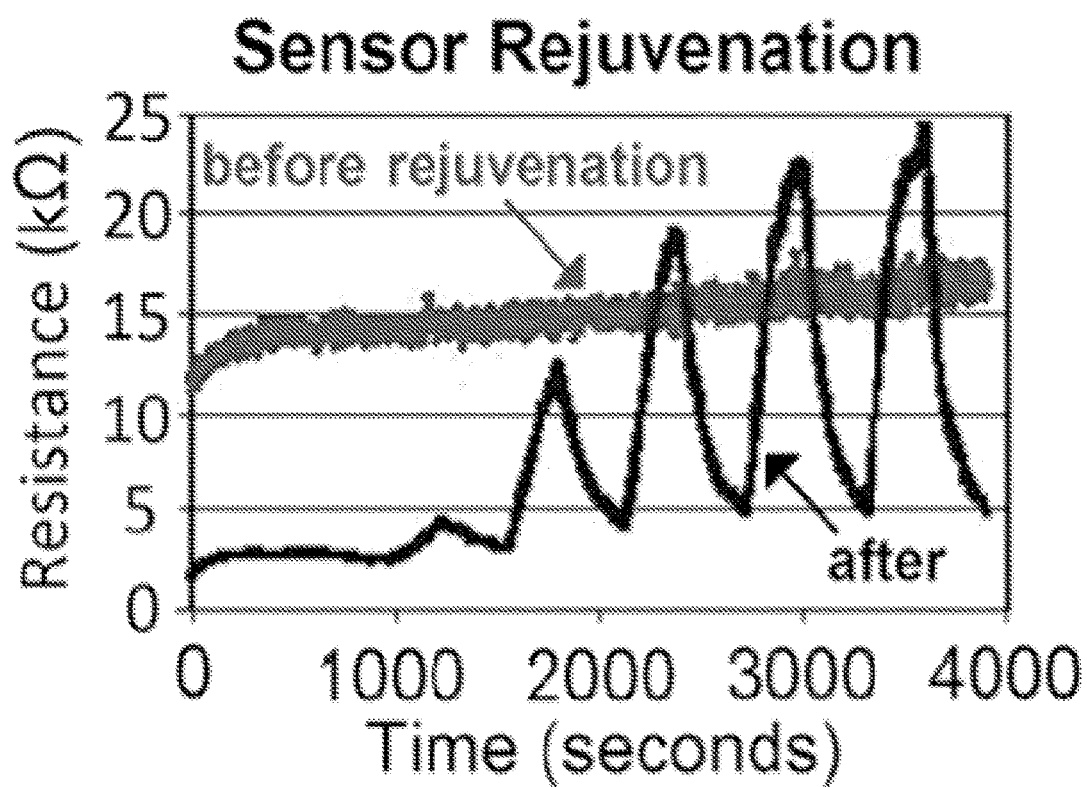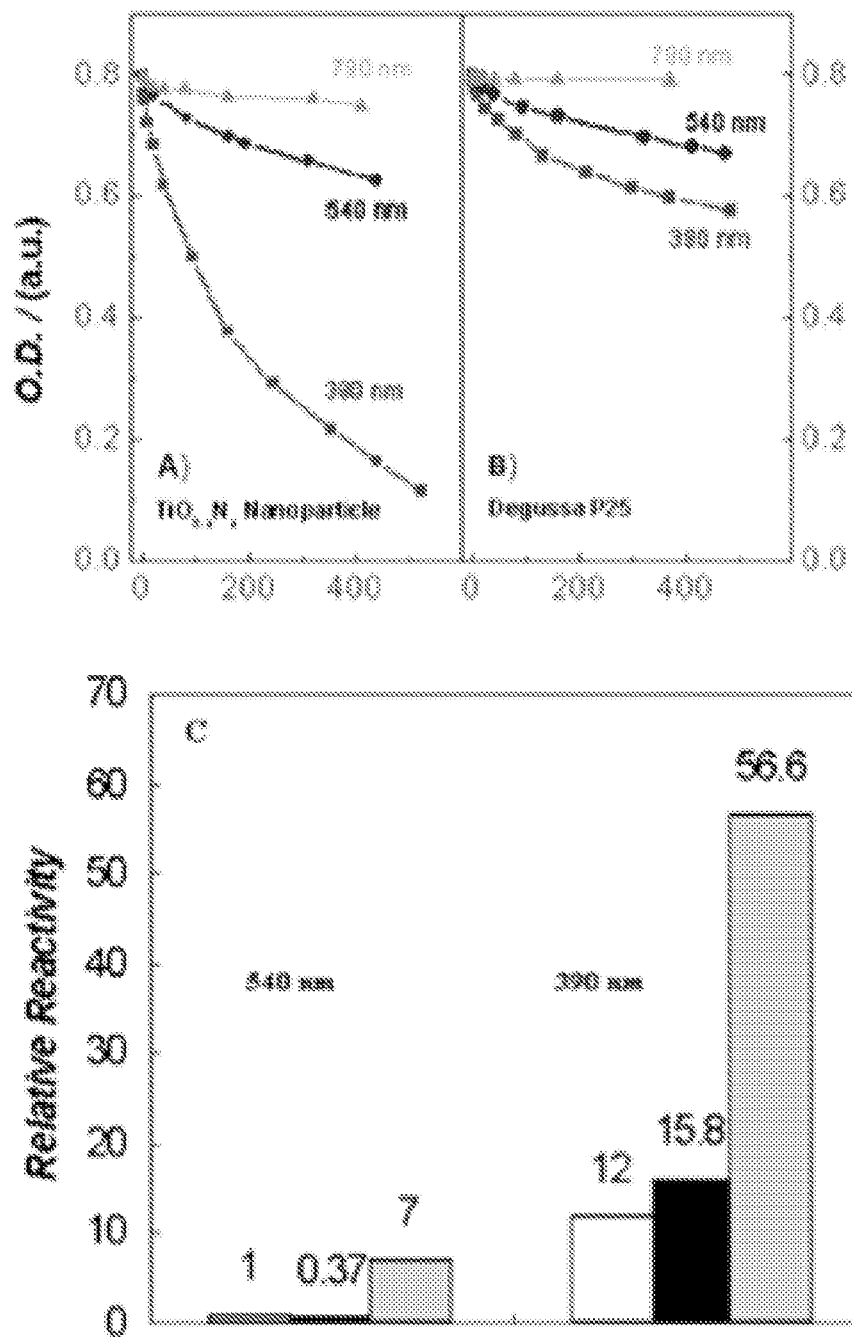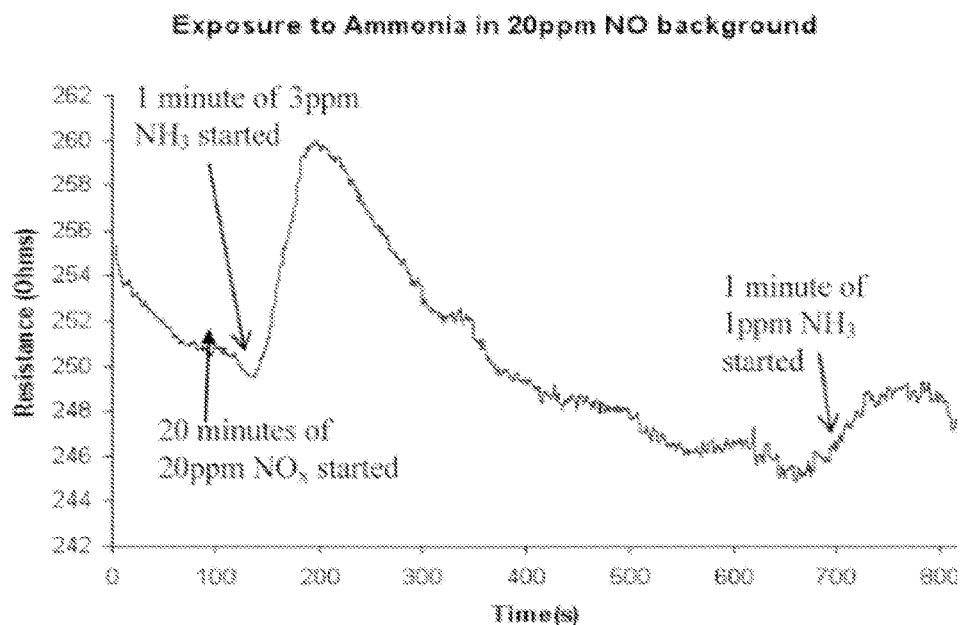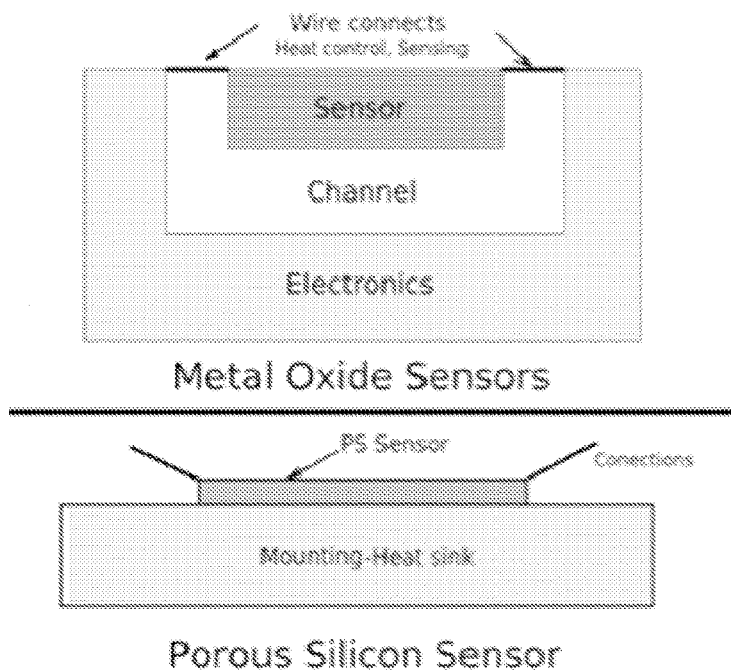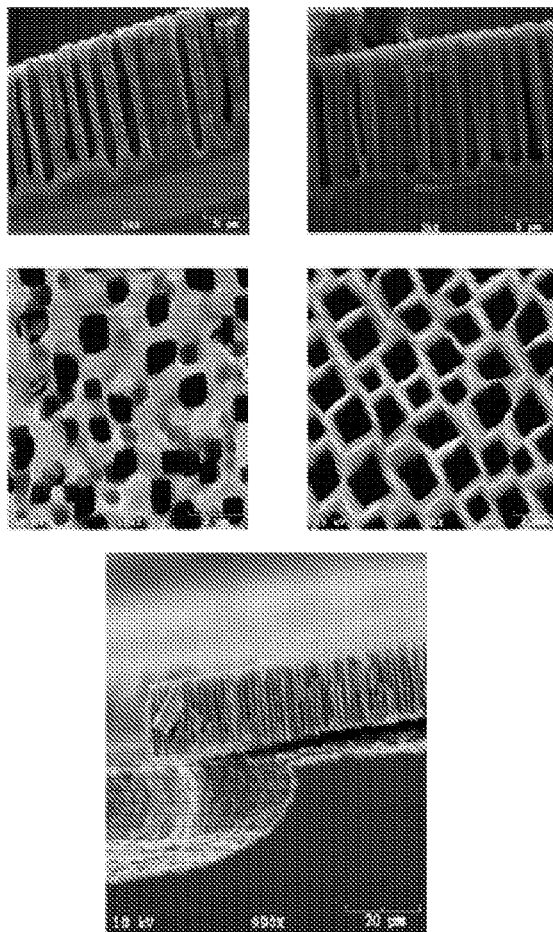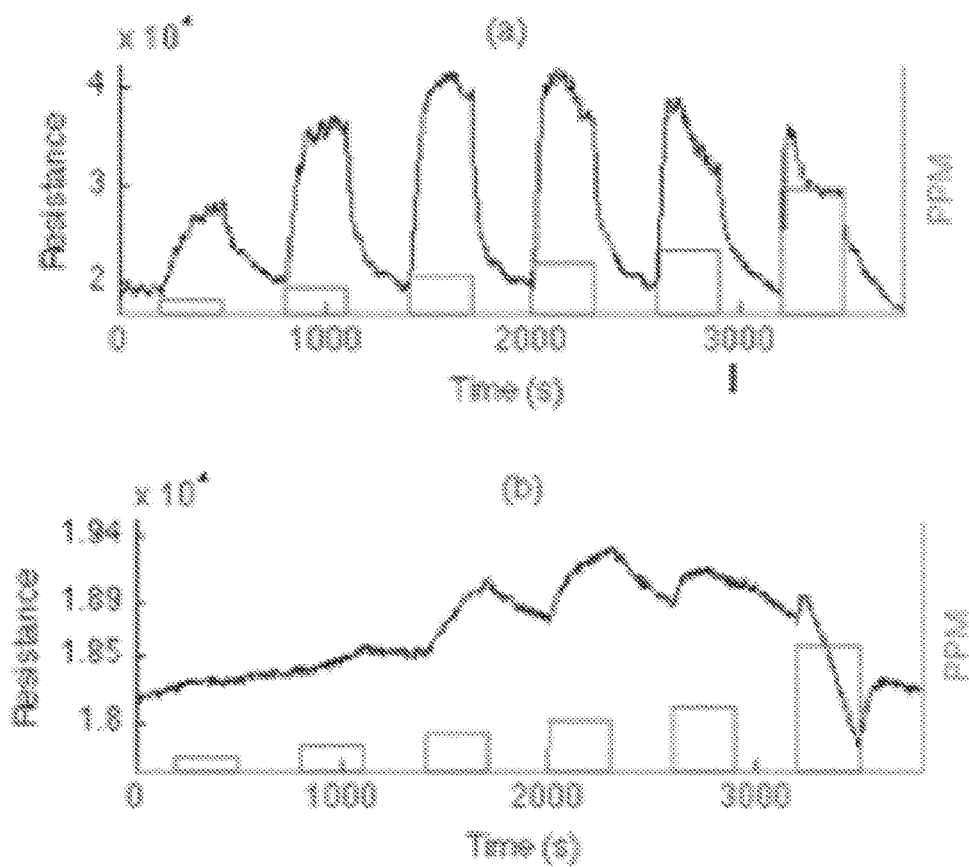
FIG. 2.22

FIG. 2.23

FIG. 2.24

Table 2/1

Hard	Borderline	Soft
Acids H^+, Li^+, Na^+, K^+ Ag^+, Tl^+, Hg^+	Fe^{2+}, Co^{2+}, Ni^{2+}	Cu^+, Au^+
Be^{2+}, Mg^{2+}, Ca^{2+} Pt^{2+}, Hg^{2+}	Cu^{2+}, Zn^{2+}, Pb^{2+} Cd^{2+}	Pd^{2+}
Cr^{2+}, Cr^{3+}, Al^{3+} SO_3, BF_3, Sn^{+4}, Ti^{+4}	BBr_3, Sn^{+2}, NO_2	BH_3, NO
Bases F^-, OH^-, H_2O, NH_3 CO, I	NO_2, SO_3^{2-}, Br^-	H^-, R^-, CN^-
CO_3^{2-}, NO_3^-, O^{2-} C_6H_5	N_3^-, N_2, H_2S, SO_2 R_3P	SCN^-
SO_4^{2-}, PO_4^{3-}, ClO_4^-	C_6H_5N, SCN	R_2S, NO

Table 2/2

	SnO_2	NiO	Cu_xO	Au_xO
PH_3	2	2.5	4	5
NO	7-10	3.5	1	1.5-2
NH_3	1.5	1.5-2	2-2.5	~3
SO_2	4	(2)	1+	2

Table 2/3

	TiO_2	SnO_2	NiO	Cu_xO	Au_xO
NO	-12*	-2*	4	1.2	1.5-2
NO_2	0.75	0.5**	(0.9-1)	1	1.5-2**
NH_3*	(3.5-4)	2.5	1.5	2	3

FIG. 2.25

GAS SENSORS AND METHODS OF PREPARATION THEREOF

CROSS-REFERENCE TO RELATED APPLICATION

This application is the 35 U.S.C. §371 national stage of PCT Application No. PCT/US2012/051721, entitled "Gas Sensors and Methods of Preparation Thereof" and filed Aug. 21, 2012, which is herein incorporated by reference in its entirety and which also claims priority to, and the benefit of, U.S. patent application No. 61/527,294, filed Aug. 25, 2011, which is herein incorporated by reference in its entirety.

BACKGROUND

Porous silicon (PS) has drawn considerable attention for sensor applications. Its luminescence properties, large surface area, and compatibility with silicon based technologies have been the driving force for this technology development. However, there exists a need in the industry to advance sensor technologies.

SUMMARY

Embodiments of the present disclosure include sensors, arrays of conductometric sensors, devices including conductometric sensors, methods of making conductometric sensors, methods of using conductometric gas sensors, and the like.

One exemplary embodiment of a device, among others, includes: a conductometric gas sensor including a n-type substrate having a porous layer, wherein a plurality of nanostructures are disposed on a portion of the porous layer, wherein the nanostructure provides a fractional coverage on the porous layer, wherein the conductometric gas sensor is operative to transduce the presence of a gas into an impedance change, wherein the impedance change correlates to the gas concentration.

One exemplary embodiment of a device, among others, includes: a conductometric porous silicon gas sensor including a n-type silicon substrate having a porous silicon layer, wherein a plurality of nanostructures are disposed on a portion of the porous silicon layer, wherein the conductometric porous silicon gas sensor is operative to transduce the presence of a gas into an impedance change, wherein the impedance change correlates to the gas concentration.

One exemplary embodiment of a method of detecting a concentration of a gas, among others, includes: providing a conductometric porous silicon gas sensor including a n-type silicon substrate having a porous silicon layer, wherein a plurality of nanostructures are disposed on a portion of the porous silicon layer, wherein the conductometric porous silicon gas sensor is operative to transduce the presence of a gas into an impedance change, wherein the impedance change correlates to the gas concentration; introducing the gas to the sensor; and measuring an impedance change in the sensor at room temperature.

Other devices, systems, methods, features, and advantages of the present disclosure will be or become apparent to one with skill in the art upon examination of the following detailed description. It is intended that all such additional devices, systems, methods, features, and advantages be included within this description, be within the scope of the present disclosure, and be protected by the accompanying claims.

BRIEF DESCRIPTION OF THE DRAWINGS

Many aspects of the disclosure can be better understood with reference to the following drawings. The components in the drawings are not necessarily to scale, emphasis instead being placed upon clearly illustrating the principles of the present disclosure. Moreover, in the drawings, like reference numerals designate corresponding parts throughout the several views.

FIG. **1.1** illustrates variations of the position of the Fermi Level with temperature for n-type semiconductors.

FIG. **1.2**(a) illustrates a schematic view of apparatus used to generate the micro/nanoporous structure in n-type silicon. FIG. **1.2**B illustrates the top and FIG. **1.2**C illustrates a side view of the pores.

FIGS. **1.3**(a-g) illustrates graphs of a comparison of responses to 1, 2, 3, 4, 5, and 10 ppm NO_2 for (a), (c), and (e) PS interfaces having an untreated n-type surface with those treated with (b) SnO_x (d) Cu_xO, and (f,g) Au_xO fractional nanostructured island depositions. The green saw-teeth boxes indicate the anaylte concentration and the range over which this concentration is exposed to the sensor interface. The numbers inside the graphs denote the ppm concentration of these exposures. See text for discussion.

FIGS. **1.4**(a) and (b) illustrates a comparison of NO_2 response to (a) an untreated and (b) a TiO_2 nanostructure deposited PS interfaces for low TiO_2 deposition. The green saw-teeth boxes indicate the anaylte concentration and the range over which this concentration is exposed to the sensor interface. The numbers inside the graphs denote the ppm concentration of these exposures. See text for discussion.

FIG. **1.5**(a) to (c) illustrates a comparison of responses to 1, 2, 3, 4, 5, and 10 ppm NO_2 for (a) a PS interface having an untreated n-type surface with (b) that treated with TiO_2 fractional nanostructured island depositions. The figure (c) corresponds to the overlap of the response observed for the untreated PS interface (blue) to that modified with TiO_2 (green). The arrows point to the measured peaks for the TiO_2 island system. The green saw-teeth boxes indicate the anaylte concentration and the range over which this concentration is exposed to the sensor interface. The numbers inside the graphs denote the ppm concentration of these exposures. See text for discussion.

FIGS. **1.6**(a) and (b) illustrates a comparison of NO_2 response to (a) an untreated and (b) a TiO_2 nanostructure deposited PS interface for TiO_2 depositions notably higher than those associated with FIGS. **1.4** and **1.5**. The response curve for the untreated n-type interface corresponds to an increase in resistance with NO_2 concentration, the TiO_2 decorated surface displays a decrease in resistance (increase in conductance) as TiO_2 facilitates electron extraction from NO_2. Here, the signal begins to saturate between 3 and 4 ppm*. The green saw-teeth boxes indicate the anaylte concentration and the range over which this concentration is exposed to the sensor interface. The numbers inside the graphs denote the ppm concentration of these exposures. See text for discussion.

FIGS. **1.7**(a) and (b) illustrates a comparison of NO_2 response to (a) an untreated and (b) a $TiO_{2-x}N_x$ treated PS interface. The green saw-teeth boxes indicate the anaylte concentration and the range over which this concentration is exposed to the sensor interface. The numbers inside the graphs denote the ppm concentration of these exposures. See text for discussion.

FIG. **1.8**(a) to (c) illustrates a comparison of responses to 1, 2, 3, 4, 5, and 10 ppm of analyte gas. FIG. **1.8**(a) NO_2 interacting with a SnO_x treated n-type PS surface 24 hours

after an initial exposure produced the response in FIG. 1.3(b). FIGS. 1.8 (b and c) corresponds to the response of Au$_x$O treated (10 and 30 s exposures) PS surfaces for the surfaces generating the responses in FIGS. 1.3 (f and g) 24 hours earlier. FIG. 1.8(d) corresponds to the response (two cycles) to NH$_3$ of an SnO$_x$ treated n-type PS surface also used in FIG. 1.8(a). Note that the time scale for this figure is compressed relative to FIGS. 1.8 (a, b, c). The green saw-teeth boxes indicate the anaylte concentration and the range over which this concentration is exposed to the sensor interface. The numbers inside the graphs denote the ppm concentration of these exposures.

FIG. 1.9 illustrates a comparison of responses for NO$_2$ and NO in the concentration range 10-80 ppm. FIGS. 1.9(a) and (b) for NO and FIGS. 1.9(c) and (d) for NO$_2$ depict the response to 10, 20, 30, 40, 50, and 80 ppm of these gases. FIGS. 1.9(b) and (d) represent higher resolution time scales. The change in resistance for NO$_2$ is a substantial 10,000 Ohms whereas that for NO approaches 800 Ohms. The green saw-teeth boxes indicate the anaylte concentration and the range over which this concentration is exposed to the sensor interface. The numbers inside the graphs denote the ppm concentration of these exposures.

FIG. 1.10 illustrates a response of NO$_2$ to a p-type PS sensor. Note that upon the introduction of NO$_2$ the resistance of the system "bottoms-out" as conductance is maximized[27]. The green saw-teeth boxes indicate the anaylte concentration and the range over which this concentration is exposed to the sensor interface. The numbers inside the graphs denote the ppm concentration of these exposures.

FIG. 1.11 illustrates Tables 1/I to 1/III, where: Table 1/1, Hard and soft acids and bases; Table 1/II, Relative increase or decrease in resistance (decrease or increase in conductance) of TiO$_2$, SnO$_x$, NiO, Cu$_x$O, and gold clustered oxide, Au$_x$O (x>>1) treated "n-type" PS interfaces. The table constitutes a response matrix for NO$_2$. (1) The competition between TiO$_2$ and NO$_2$ is a factor. (2) Chemisorption is a factor See text for discussion; and Table 1/III, Observed dynamic interplay resulting from the depletion of donor levels and subsequent reversing electron exchange associated with the interaction of NO$_2$ and a TiO$_2$ treated PS interface (FIG. 1.5). The elapsed time follows a linear inverse with concentration. See text for discussion.

FIG. 2.1 illustrates a schematic representation of PS sensor interface structure.

FIG. 2.2(a) illustrates a close up side view of hybrid porous silicon film. FIG. 2.2(b) illustrates nanoparticle tin-oxide coating on porous silicon micropores. FIG. 2.2(c) illustrates 10 to 30 nm Au$_x$O nanostructures on porous silicon.

FIG. 2.3 illustrates a porous Si gas sensor schematic. The resistance change is measured via precision microprobes when the porous silicon interface is exposed to a test gas. A SiC layer also serves as an insulation layer as the resistance response of the porous layer is measured through gold contacts.

FIG. 2.4(a) illustrates a configuration for gas sensor testing and FIG. 2.4(b) illustrates a top view of sensor showing the PS surface between gold pads for electrical connection.

FIG. 2.5 illustrates a variation of the position of the Fermi level with temperature.

FIG. 2.6 illustrates a comparison of responses for sensors consisting of an untreated PS interface with those treated with gold or tin to form the SnO$_x$ (x=1, 2) and gold clustered oxide AuxO nanostructured island deposits (FIG. 2.2). Note that the three bases, NH$_3$, NO, and CO introduced to the

treated "p-type" silicon result in a positive resistance change and that the relative responses to the strong (hard) base NH$_3$ and the weak (soft) bases NO and CO are distinct. The significant differences in relative response are maintained with improved interfaces whose S/N is up to two orders of magnitude greater (Seals et al. 2002; Lewis et al. 2005; Ozdemir and Gole 2008b). This represents earlier data whose resistance response (sensitivity) has been greatly improved whereas the ratios of resistance have remained the same.

FIG. 2.7 illustrates a PH$_3$ response to an electroless Au$_x$O coating. Here, 1, 2, 3, 4, 5 ppm of PH$_3$ is pulsed onto the sensor surface every 300 s. For the first 1800 s an N$_2$ purge is applied for resistance stabilization.

FIG. 2.8 illustrates a response of NO$_2$ to a p-type PS sensor. Note that upon the introduction of NO$_2$ the resistance of the system "bottoms-out" as conductance is maximized.

FIG. 2.9 illustrates XPS spectra of metal-based nanostructure deposited PS sensors and fitting curves (in red) to the spectra. FIG. 2.9 (a) illustrates a XPS stectrum of a dominantly SnO$_x$ deposited sensor. SnO (Sn^{2+}) has peaks in the range of 485.6-87.0 eV, SnO2 (Sn^{4+}) has peaks in the range of 486.1-487.1 eV. FIG. 2.9 (b) illustrates a XPS spectrum of a dominantly NiO$_x$ deposited sensor. Nickel has an oxidation peak (2p1/2) located ~871.8 eV for NiO (Ni^{2+}) and has peaks (2p3/2) in the range of 853.6-857.2 eV. Ni2O3 (Ni^{3+}) shows peaks from 855.8 eV to 856.5 eV. FIG. 2.9 (c) illustrates a XPS spectrum for a dominantly Cu$_x$O deposited PS surface. CuO (Cu^{2+}) has peaks (2p1/2) in the range of 952.5-952.7 eV and has peaks (2p3/2) in the range of 933.3-934.3 eV. Cu$_2$O (Cu^{1+}) has peaks in the range of 932.0-932.8 eV. FIG. 2.9 (d) illustrates a XPS spectrum of Au 4f5/2 and Au 4f7/2 doublets (NIST 2003) which demonstrate minimal oxidation.

FIG. 2.10 illustrates estimated hard and soft acidities and basicities based on resistance changes relative to a p-type porous silicon interface.

FIGS. 2.11(a-c) illustrates the response of n-type PS micro/nanostructured interface to 1, 2, 3, 4, 5 and 10 ppm NO$_2$ (a) and NH$_3$ (c) and 1-5 ppm NO (b). These gases were pulsed onto the PS interface with a 300 s half-cycle followed by a 300 s half-cycle UHP cleaning. The system was purged with UHP nitrogen 1800 s before operation. See text for discussion.

FIG. 2.12(a-g) illustrates the comparison of responses for 1, 2, 3, 4, 5, and 10 ppm NO for (a), (e), (g) sensors having of an untreated n-type PS interface with those treated with (b) TiO$_2$, (c) SnO$_x$, (d) NiO, (f) Cu$_x$O, and (h) AuxO fractional nanostructured island depositions. The untreated PS interface in (a) is that treated with TiO$_2$ in (b). The response for the untreated PS interface in (a) is duplicated precisely for the untreated PS interfaces to which we compare in (c) for SnO$_x$ and (d) for NiO. The untreated PS responses in (e) and (g) correlate with the CuxO (f) and AuxO responses in (h) respectively. NO was pulsed onto these interfaces with a 300 s half-cycle followed by a 300 s half-cycle UHP cleaning. The system was purged with UHP nitrogen for 1800 s before operation.

FIG. 2.13(a) illustrates a TEM image and FIG. 2.13(b) illustrates a EDS (inset) of Pd nanoparticles on SnO$_2$ nanowires.

FIG. 2.14(a) illustrates a low magnification TEM image of an 800° C.-annealed, core-shell nanowire. FIG. 2.14(b) illustrates a corresponding XRD Spectrum.

FIG. 2.15(a) illustrates a schematic view of the formation of electron depleted regions beneath and in the immediate vicinity of two Pd nanoparticles. FIG. 2.15 illustrates a

response of a pristine (dashed line) and Pd-functionalized (solid line) nanostructure to sequential oxygen and hydrogen pulses at 473° K (top pane) and 543° K (bottom).

FIG. **2.16** illustrates a gas sensor response to pulsing of ammonia between 0 and 5 ppm in research grade N_2.

FIG. **2.17** illustrates a FFT analysis of a gas pulsing experiment performed on a sensor (right) is compared to the signal of a device responding to the same external noise in the absence of no gas pulsing (left). The raw signal of each sensor is shown (top) as well as the filtered FFT of the sensor (bottom). Separate peaks are generated at a pulsing frequency (0.0167 Hz) and the heating frequency (0.0042) (Lewis et al. 2007).

FIG. **2.18** illustrates a FFT of PS gas response (top) before filtering and (bottom) after filtering.

FIG. **2.19** illustrates a response to NH_3 after a sensor is subjected to a rejuvenation process. The contaminated sensor response is in blue, the rejuvenated sensor response is in black.

FIG. **2.20** illustrates a comparison of photocatalytic degredation of methylene blue for $TiO_{2-x}N_x$ nanoparticles and nitrided Degussa P25. White column indicates Degussa P25; black center column indicates nitrided Degussa; grey column indicates $TiO_{2-x}N_x$ nanocolloid (Chen et al. 2005; Gole et al. 2004).

FIG. **2.21** illustrates the selectivity of a PS device to NH_3 in 20 ppm NO_x. The response time (<10 seconds) of the gas sensor is also demonstrated.

FIG. **2.22** illustrates a comparison of a metal oxide (usually SnO_2 or WO_3) elevated temperature (150-500° C.) heat controlled sensors separated from their electronics by a channel with a heat sunk PS sensor operating at room temperature and capable of operation to temperatures of at least 80° C.

FIG. **2.23** illustrates SEM micrographs of a porous silicon filter. In the top images, the tips of the pores can be seen before (left) and after (right) they begin to spread out in their face directions. The second row of images show the front (left) and back (right) of a filter. Note that pore spreading is significant in the filter back. The final image represents the direct Lift-off of PS-based film-filter (~20 microns) from the surface of an etched PS film. Pore diameter is approximately one micron.

FIGS. **2.24**(a) and (b) illustrate a comparison of responses to 1, 2, 3, 4, 5, and 10 ppm NO_2 for (a) a particular untreated n-type PS interface and (b) an interface treated with a fractional deposition of nanostructured SnO_x, NO_2 was pulsed onto the interfaces with a 300 s half cycle followed by a 300 s half cycle UHP nitrogen cleaning. FIG. **2.24**(b) is suggested to result, at least in part, from the chemisorptive SnO_x—NO_2— interaction.

FIG. **2.25** illustrates Tables 2/1, 2/2, and 2/3. Table 2/1 describes hard and soft acids and bases. Table 2/2 describes the relative increase in response (increase in resistance) of SnO_2, NiO, Cu_xO, and gold clustered oxide, Au_xO treated "p-type" PS interfaces relative to the untreated interface. Table 2/2 constitutes a response matrix to the gases PH_3, NO, NH_3, and SO_2. Table 2/3 describes the relative increase or decrease in resistance (decrease or increase in conductance) of TiO_2, SnO_x, NiO, Cu_xO, and gold clustered oxide, Au_xO treated "n-type" PS interfaces. The table constitutes a response matrix for the gases NO, NO_2, and NH_3. * indicates decrease in resistance with analyte exposure ** indicates initial response.

DETAILED DESCRIPTION

Before the present disclosure is described in greater detail, it is to be understood that this disclosure is not limited to

particular embodiments described, and as such may, of course, vary. It is also to be understood that the terminology used herein is for the purpose of describing particular embodiments only, and is not intended to be limiting, since the scope of the present disclosure will be limited only by the appended claims.

Where a range of values is provided, it is understood that each intervening value, to the tenth of the unit of the lower limit unless the context clearly dictates otherwise, between the upper and lower limit of that range and any other stated or intervening value in that stated range, is encompassed within the disclosure. The upper and lower limits of these smaller ranges may independently be included in the smaller ranges and are also encompassed within the disclosure, subject to any specifically excluded limit in the stated range. Where the stated range includes one or both of the limits, ranges excluding either or both of those included limits are also included in the disclosure.

Unless defined otherwise, all technical and scientific terms used herein have the same meaning as commonly understood by one of ordinary skill in the art to which this disclosure belongs. Although any methods and materials similar or equivalent to those described herein can also be used in the practice or testing of the present disclosure, the preferred methods and materials are now described.

All publications and patents cited in this specification are herein incorporated by reference as if each individual publication or patent were specifically and individually indicated to be incorporated by reference and are incorporated herein by reference to disclose and describe the methods and/or materials in connection with which the publications are cited. The citation of any publication is for its disclosure prior to the filing date and should not be construed as an admission that the present disclosure is not entitled to antedate such publication by virtue of prior disclosure. Further, the dates of publication provided could be different from the actual publication dates that may need to be independently confirmed.

As will be apparent to those of skill in the art upon reading this disclosure, each of the individual embodiments described and illustrated herein has discrete components and features which may be readily separated from or combined with the features of any of the other several embodiments without departing from the scope or spirit of the present disclosure. Any recited method can be carried out in the order of events recited or in any other order that is logically possible.

Embodiments of the present disclosure will employ, unless otherwise indicated, techniques of chemistry, material sceince, and the like, which are within the skill of the art. Such techniques are explained fully in the literature.

The following examples are put forth so as to provide those of ordinary skill in the art with a complete disclosure and description of how to perform the methods and use the probes disclosed and claimed herein. Efforts have been made to ensure accuracy with respect to numbers (e.g., amounts, temperature, etc.), but some errors and deviations should be accounted for. Unless indicated otherwise, parts are parts by weight, temperature is in ° C., and pressure is at or near atmospheric. Standard temperature and pressure are defined as 20° C. and 1 atmosphere.

Before the embodiments of the present disclosure are described in detail, it is to be understood that, unless otherwise indicated, the present disclosure is not limited to particular materials, reagents, reaction materials, manufacturing processes, or the like, as such can vary. It is also to be understood that the terminology used herein is for purposes

of describing particular embodiments only, and is not intended to be limiting. It is also possible in the present disclosure that steps can be executed in different sequence where this is logically possible.

It must be noted that, as used in the specification and the appended claims, the singular forms "a," "an," and "the" include plural referents unless the context clearly dictates otherwise. Thus, for example, reference to "a compound" includes a plurality of compounds. In this specification and in the claims that follow, reference will be made to a number of terms that shall be defined to have the following meanings unless a contrary intention is apparent.

DEFINITIONS

The term "detectable" refers to the ability to detect a signal over the background signal.

The term "detectable signal" is a signal derived from an impedance change upon the interaction of a gas with a porous silicon layer or a porous silicon layer having a nanostructured deposit on the porous silicon layer. The detectable signal is detectable and distinguishable from other background acoustic signals that are generated from the host. In other words, there is a measurable and statistically significant difference (e.g., a statistically significant difference is enough of a difference to distinguish among the detectable signal and the background, such as about 0.1%, 1%, 3%, 5%, 10%, 15%, 20%, 25%, 30%, 40% or more difference between the detectable signal and the background) between detectable signal and the background. Standards and/or calibration curves and/or arrays of porous silicon sensors can be used to determine the relative intensity of the detectable signal and/or the background.

Discussion

Embodiments of the present disclosure include sensors, arrays of conductometric sensors, devices including conductometric sensors, methods of making conductometric sensors, methods of using conductometric gas sensors, and the like. In an embodiment, the present disclosure includes porous silicon (PS) sensors, arrays of conductometric PS sensors, devices including conductometric PS sensors, methods of making conductometric PS sensors, methods of using conductometric PS gas sensors, and the like.

Embodiments of the present disclosure can be understood based on the Inverse Hard/Soft Acid/Base (IHSAB) principle/approach. The Inverse Hard/Soft Acid/Base (IHSAB) principle/approach, as it correlates with a basis in physisorption (electron transduction), complements the HSAB principle for hard/soft acid/base interactions and can be correlated with a basis in density functional theory (DFT). The basis for correlation follows the principle that soft-soft acid/base interactions produce significant covalent bonding and hard-hard combinations produce significant ionic bonding. The HSAB principle states that hard acids prefer to coordinate to hard bases and soft acids prefer to coordinate to soft bases. In contrast, the driving principle to promote physisorption (electron transduction) represents the inverse of that necessary to form strong chemical bonds. This principle is manifest through the interactions of metal oxide nanostructures as they influence the nature of the majority carriers in a p- or n-type semiconductor. In an embodiment, nanoporous silicon layers positioned on porous silicon (PS) micropores facilitate the deposition of nanostructured metal/metal oxides which provide distinctly higher variable sensitivities and selectivity for a given extrinsic semiconductor interface. In an embodiment, the PS surface is treated with fractional depositions (e.g., islands of nanostructures), much

less than a monolayer to insure that the nanostructures do not begin to cross talk and, in so doing diminish signal to noise. This deposition can be made to produce a dominant physisorptive (sensors) or chemisorptive (micro-reactors) character at the semiconductor interface as the deposited nanostructures act to focus the nature of the surface interaction. However, the nature of the extrinsic semiconductor, the manner in which its donor and/or acceptor levels can be manipulated, and its transformation to intrinsic character also represent important variables.

An embodiment of the present disclosure describes a conductometric gas sensor that is operative to measure an impedance change that corresponds to a gas concentration (e.g., a gas concentration can be determined based on the impedance change or the magnitude of the impedance change and this concentration can be independently evaluated for calibration). More particularly, the conductometric sensor transduces the presence of a gas into an impedance signal, which is measured by another device in communication with the conductometric sensor. Therefore, the term "measure" used in reference to the conductometric sensor can include the conductometric sensor in combination with another circuit or device (e.g., impedance analyzer, sensor and shunt circuit, and the like) to measure the impedance (e.g., the detectable signal). The conductometric can be used to detect gases or liquids. In particular, conductometric sensors, in accordance with the present disclosure, have a rapid and reversible response to analyte gases at room temperature.

In an embodiment, the n-type semiconductor is PS, so the sensor can be referred to as a conductometric PS gas sensor (also referred to as a "PS gas sensor" or "conductometric PS sensor"). Although some embodiments of the present disclosure are described as PS, other n-type semiconductor materials can be used and include a porous layer. There is not intention to limit embodiments of the present disclosure to PS.

In an embodiment, the conductometric PS gas sensor can be made from an n-type PS substrate. In an embodiment, a conductometric PS gas sensor made from an n-type PS can operate at a lower concentration than p-type PS based conductometric PS gas sensors to extend down to the lowest parts per billion (ppb) (e.g., less than 100 ppb, less than about 75 ppb, less than about 50 ppb, less than about 25 ppb, about 1 to 100 ppb, about 1 to 75 ppb, about 1 to 50 ppb, about 1 to 25 ppb), while p-type PS based conductometric PS gas sensors operate in a linear fashion at pressures higher (greater than 5 ppm) than n-type PS based conductometric PS gas sensors. Thus, an embodiment of the present disclosure can include both p-type and n-type PS based conductometric PS gas sensors that can be used in a wide dynamic range of pressures. In general, these detection levels could be obtained where a different n-type semiconductor is being used. Detection abilities for some specific gases are given in the Examples.

Embodiments of the present disclosure provide for a concept that is predictive of significant and predictable changes in conductometric sensor (e.g., conductometric PS sensor) sensitivity for a variety of gases. Rapidly responding, reversible, sensitive, and selective conductometric PS sensors can be formed (1) with a highly efficient electrical contact to a porous silicon layer (e.g., a nanopore covered microporous layer) and (2) including deposited nanostructures (e.g., nanostructures as nanostructured fractional deposits), interacting with, and/or modifying of the porous silicon layer, using embodiments of the present disclosure. The nanostructures can be deposited as distinctly variable

nanostructures that can be chosen to be deposited on a portion (e.g, distinct islands) of the porous silicon layer, where the resulting conductometric PS sensors provide a range of sensitivities for a given analyte using a concept complementary to that of hard and soft acid-base interactions (HSAB) and commensurate with a basis in dominant physisorption. Physisorption interaction involves intermolecular forces (e.g., a van der Waals or comparable attraction) between the gas and nanostructured deposit. Physisorption interaction does not involve a significant change in the electronic orbital patterns of the nanostructured deposit and the gas. A physisorption interaction is a reversible interaction of the nanostructured deposit with the gas. A physisorption interaction is not a chemisorption reaction that involves a chemical reaction that may not be reversible. The concept, based on the reversible interaction of hard acids and bases with soft bases and acids corresponds (1) to the inverse of the HSAB concept and (2) to the selection of a conductometric PS sensor and a porous silicon surface (e.g., nanostructures islands) and analyte materials, which do not undergo strong covalent or ionic bonding but rather represent a much weaker mixed orbital interaction where a significant HOMO-LUMO and additional orbital mismatches dominate the interaction as a reversible physisorption interaction (electon transduction). Embodiments of the present disclosure provide for notably higher sensitivities and selectivity based on impedance changes.

An embodiment of the present disclosure can be advantageous for one or more of the following reasons: (1) its sensitivity and short recovery time (e.g., lower concentrations of a particular gas relative to p-type PS based sensors), (2) its operation at room temperature as well as at a single, readily accessible, temperature with an insensitivity to temperature drift, (3) its potential operation in a heat-sunk configuration allowing operation to a surface temperature of 80° C. even in highly elevated temperature environments (in sharp contrast to metal oxide sensors), (4) its ease of coating with diversity of gas-selective materials to form sensor arrays, (5) its low cost of fabrication, (6) its low cost and ease of rejuvenation after contamination, (7) its low cost of operation, and (8) its ability to rapidly assess false positives by operating the sensor in a pulsed gas mode.

It should be noted that the time frame for measuring the gas concentration depends, in part, on the particular application and gas being measured, where the presence of the gas can be measured in a time frame as short as 2 seconds in some embodiments, while in other embodiments, the time frame for a precise concentration measurement may be longer. It should be noted that impedance includes contributions from one or more of resistance, capacitance, and inductance, and measurement of impedance includes the measurement of one or more of resistance, capacitance, and inductance. In an embodiment, the impedance analyzer measures the resistance and capacitance only.

Embodiments of the present disclosure can be used to measure the concentration of a gas or a mixture of gases when the gas or the gas mixture is known or substantially known. For example, if the environment that the conductometric PS sensor is to be used in is known to include ammonia, the conductometric PS sensor can be used to measure the concentration of ammonia. In another example, if the environment that the conductometric PS sensor is to be used is known to include ammonia and H_2S, then an array matrix of conductometric PS sensors (e.g., 2, 3, 4, 6, 8, or more) can be used to measure the concentration of each gas or the relative concentration of each gas. In an embodiment, the array of conductometric PS sensors can be designed so that each of the conductometric PS sensors has a greater sensitivity for detection of a specific gas. In addition, the array of conductometric PS sensors allows the concentration of the gases to be compared to one another on relative terms.

In an embodiment, the conductometric PS sensor includes a silicon substrate (n-type), a protective layer on a portion of the silicon substrate, an n-type porous silicon (PS) layer (or region) on a portion of the silicon substrate that is not covered by the protective layer, and two or more distinct gold contacts disposed onto a portion of the PS region and the protective layer. A plurality of nanostructures (sometimes referred to as a "nanostructured deposit") can be disposed in a fractional manner (e.g., non-contiguous islands) on and/or within the n-type PS layer that are not covered by the contacts, which enables the conductometric PS sensor to respond more strongly to certain gases relative to others depending on the nanostructures used.

In an embodiment, the protective layer can include, but is not limited to, a silicon carbide layer, a silicon nitride layer, a silicon oxynitride (SiO_xN_y) layer, an insulating dielectric film, a ceramic layer, and combinations thereof. In an effort to be clear, the protective layer may be referred to as the silicon carbide layer hereinafter, but the protective layer could be any one of the layers described above in other embodiments.

In an embodiment, the n-type PS layer can include a macroporous/nanoporous hybrid framework. The nanopores are superimposed on the walls of the macropores. In an embodiment, the macropores can be about 0.5 to 20 μm deep and about 1 to 3 μm in diameter. In an embodiment, the nanopores can be about 1 to 20 nanometers in diameter.

In an embodiment, the contact can be disposed on and within the macroporous and nanoporous hybrid framework as well as extend above the n-type PS layer and onto the protective layer (e.g., silicon carbide layer). In other words, the material fills in a portion of the n-type PS layer and then forms a layer on top of the n-type PS layer. The contacts are distinct and separated from one another by a space or area (e.g., a portion of the PS layer and a portion of the protective layer). In an embodiment, the contact can include one or more contact portions. In other words, one portion can be disposed on the n-type PS layer and one portion disposed on the protective layer, but the two portions are contiguous in that a single metal layer extends from the n-type PS layer onto the top of the n-type PS layer and onto the protective layer. The contacts can be made of a metal or a combination of metals such as, for example, gold. In an embodiment, the contact includes a pre-coating layer usually titanium, and a metal layer usually gold, disposed onto the pre-coating layer. The pre-coating layer can be used to improve the electrical connection of the contact to the n-type PS layer.

As mentioned above, the exposed portion of the n-type PS layer not covered by the contacts can have a plurality of nanostructures deposited (e.g., nanostructure islands) on and/or within the n-type PS layer (e.g., a combined macroporous/nanoporous hybrid framework). The nanostructures can include, but is not limited to, a metal material, a metal oxide material, a metal oxynitride material, and combinations thereof. In an embodiment, the nanostructures can be discrete and/or clustered nanostructures and/or nanomaterials on and/or with the n-type PS layer. In another embodiment, the nanostructures can be deposited onto and/or within discrete areas of the n-type PS layer.

In an embodiment, the nanostructures can include nanoparticles such as a nanosphere, a nanowire, a nanodisk, and a nanobelt, where the nanoparticles can be uncoated or coated. For example, the nanostructure can be made of

metals and metal oxides such as silicon (Si), tin (Sn), chromium (Cr), iron (Fe), nickel (Ni), silver (Ag), titanium (Ti), cobalt (Co), zinc (Zn), platinum (Pt), palladium (Pd), osmium (Os), gold (Au), lead (Pb), iridium (Ir), rhodium (Rh), ruthenium (Ru), molybdenum (Mo), vanadium (V), aluminum (Al), aluminum oxide (Al_2O_3, AlO_x, x is 1 to 2), silicon oxide (SiO_x, x is 1 to 4), tin oxide (SnO_x, x is 2 to 4), chromia (Cr_2O_3), iron oxide (Fe_2O_3, Fe_3O_4, or FeO), nickel oxide (NiO), silver oxide (AgO), titanium oxide (TiO_2), cobalt oxide (Co_2O_3, Co_3O_4, or CoO), zinc oxide (ZnO), platinum oxide (PtO), palladium oxide (PdO), vanadium oxide (VO_2), molybdenum oxide (MoO_2), lead oxide (PbO), titanium oxide (TiO_2), titanium nitride (TiN_1), titanium oxynitride ($TiO_{2-x}N_x$), clustered oxides of each of these, other metal oxides, and a combination thereof. In this regard, by using a variety of metal and metal oxide materials, the conductometric PS sensor can be designed to provide selectivity for a particular gas.

In an embodiment, each nanostructure, a group of nanostructures, or a cluster of nanostructures, form an island on the n-type PS layer. In an embodiment, the islands are spaced apart so there is no cross talk between the islands that would impede, substantially impede, or substantially interfere with the detection of the gas(es) of interest.

Embodiments of the conductometric PS sensor having a plurality of nanostructures on the n-type PS layer can provide enhanced sensitivity (e.g., CO in the presence of SnO_2 nanostructures, NH_3 in the presence of gold clustered oxide nanostructures) and selectivity to certain gases (e.g., NH_3 in the presence of NO_N). In particular, concentrations of select gases can be measured in the presence with one or more additional gases, where selected gases are more strongly sensed (e.g., impedance change detected). In an embodiment, the selectivity to one gas over one or more others can be controlled by selection of the type or combination of types of nanoparticles.

As briefly mentioned above, the conductometric PS sensor responds and is operative to measure an impedance change (e.g., an impedance magnitude change) across a first contact and a second contact that corresponds to a concentration of a gas in contact with the PS surface. The sensitivity of the conductometric PS sensor is defined as the relative increase or decrease in impedance over a time frame following exposure to a concentration of a gas of interest. It should also be noted that the sensitivity is, in part, a function of the analyte gas of interest, the nature of the nanostructure deposites, and whether the extrinsic semiconductor is n- or p-type. In particular, relative to p-type conductometric PS sensors, the n-type conductometric PS sensors operate at lower relative pressures for a particular analyte gas.

The operating parameters of the conductometric PS sensor include, but are not limited to, a bias voltage, an AC voltage frequency, an AC voltage amplitude and combinations thereof. The conductometric PS sensors operate at a bias voltage between about 10 and 3000 millivolts DC. Also one can use an AC voltage frequency between 100 and 100,000 Hz, and an AC voltage amplitude between 1 and 1000 millivolts, or a combination thereof.

As mentioned briefly above, the impedance change can be measured with an impedance analyzer, a sensor and shunt circuit, or other impedance measurement devices. An embodiment of the sensor and shunt circuit uses a high impedance resistor in parallel with the sensor (conductometric PS sensor or components thereof). The resistor shunts the stray capacitance (removes high frequency noise), resulting in a resistive measurement.

The conductometric PS sensor can be used in a variety of ways including, but not limited to, a stand-alone detector, or a device including an array of stand-alone detectors (e.g., one or more types of n-type conductometric PS sensors and one or more typs of p-type conductometric PS sensors). The conductometric PS sensor can be used to detect gases (e.g., combustion generated gases such as carbon monoxide, carbon dioxide, sulfur dioxides, nitrogen oxides, and hydrogen sulfide). In particular, conductometric PS sensors, in accordance with the present disclosure, can provide a rapid and reversible response to analyte gases (e.g., including hydrogen chloride (HCl), ammonia (NH_3), phosphine (PH_3), carbon monoxide (CO), sulfur dioxide (SO_2), hydrogen sulfide (H_2S) nitric oxide (NO_x), and toluene) at room temperature. Additional details regarding analyte gases are described in the Examples.

In addition, the conductometric PS sensor can be used as an array, where multiple conductometric PS sensors (e.g., one or more types of n-type conductometric PS sensors and one or more types of p-type conductometric PS sensors) are uniquely sensitive to different gases of interest thereby enabling an array to measure the concentration of multiple gases simultaneously (e.g., an appropriately treated conductometric PS sensor can be made to respond more strongly to one gas over a second gas). In addition, an array of conductometric PS sensors can be used to enhance sensing selectivity as the array of conductometric PS sensors provide multiple data points per tested sample which can be analyzed in a matrix format to provide selectivity for one gas over another based on the individual conductometric PS sensors within the conductometric PS sensor array. Thus, an array of conductometric PS sensors includes conductometric PS sensors sensitive to one gas over another and, in this sense, to select gases. In this regard, the array of conductometric PS sensors can be used to detect multiple analytes simultaneously.

Embodiments of the present disclosure also include methods of making conductometric PS sensors. In general, the conductometric PS sensor can be fabricated by first providing an n-type silicon substrate (or other appropriate substrate) having a protective layer, such as a silicon carbide layer, disposed on a first portion of the silicon substrate. Then, a first area on the silicon substrate is converted into a n-type PS layer, where the first area does not have a silicon carbide layer disposed thereon. Next, a first contact (e.g., a first contact pre-coating (e.g., Ti or Cr) and the first contact (e.g., Au)) is formed onto a first portion of the n-type PS layer and onto a first portion of the silicon carbide layer. The first portion of the silicon carbide layer is contiguous with the first portion of the n-type PS layer as described above. A second contact (e.g., a second contact pre-coating (e.g., Ti or Cr) and the second contact (e.g., Au)) is formed onto a second portion of the n-type PS layer and onto a second portion of the silicon carbide layer. The second portion of the silicon carbide layer is contiguous with the second portion of the n-type PS layer as described above. A third portion of the n-type PS layer is between the contacted first portion and the second portion of the n-type PS layer. The first and second contacts can be formed at the same time. Specifically, the first and the second contact pre-coatings are formed and then the first and second contacts are formed on the first and second contact pre-coatings, respectively. The first and second contact pre-coatings are advantageous in that the first and second contacts enable a superior electrical connection to be formed. In addition, the first and second contacts can be formed using a shadow mask technique. One or more

types of nanostructures can be fractionally disposed on the n-type PS layer, where the nanostructure(s) form islands on the n-type PS layer.

Additional fabrication steps can be conducted. For example, an additional fabrication step includes cleaning the n-type PS layer with a mixture of one part hydrochloric acid (e.g., about 44%) in about five parts methanol for about four hours. In addition, a fabrication step for forming a nano-structured deposit on the porous silicon layer can be performed.

In an embodiment, the silicon substrate can be replaced with any extrinsic n-type semiconductor (e.g., GaP, InP, CdTe, and the like) onto which a porous microstructure can be generated. In an embodiment, the silicon substrate can include wafers, such as, but not limited to, n- or n$^+$-type doped wafers, n- or n$^+$-type phosphorous doped wafers. In an embodiment, the silicon substrate can include wafers, such as, but not limited to, n- or n$^+$-type doped silicon wafers, n- or n$^+$-type phosphorous doped silicon wafers.

In an embodiment, other materials can be used in place of the silicon carbide layer such as, but not limited to, a silicon nitride layer, a SiO_xN_y layer, an insulating dielectric film, and a ceramic layer.

In an embodiment, the n-type PS layer can be prepared by electrochemically etching a portion of the silicon substrate with acetonitrile, hydrofluoric acid, tetrabutylammonium-perchlorate (TBAP), and water, for example. Additional details regarding the preparation of the n-type PS layer are presented in more detail herein.

In an embodiment, the first contact pre-coating layer and the second contact pre-coating layer can be made from titanium or chromium, for example, and can be about 100 to 300 angstroms thick or about 200 angstroms thick. The first contact pre-coating and the second contact pre-coating can be disposed onto the two portions of the PS substrate via techniques such as, but not limited to, electron-beam evaporation, sputtering, electroless plating, and electroplating.

In an embodiment, the first and second contacts and can be made of metals, such as, but not limited to, gold (Au), and can be about 1000 to 4000 angstroms thick or about 3000 to 5000 angstroms thick to facilitate wire bonding. The first contact and the second contact can be disposed onto the two portions of the PS substrate via techniques such as, but not limited to, electron-beam evaporation, sputtering, electroless plating, and electroplating.

In an embodiment, the nanostructures can be can be disposed using techniques such, but not limited to, electron-beam evaporation, sputtering, silk-screen printing, electroless plating, and electroplating.

After the conductometric PS sensor is formed, the conductometric PS sensor can be validated. In this regard, embodiments of this disclosure include methods of selecting a conductometric PS sensor having certain performance characteristics, methods of analyzing the data measured using the conductometric PS sensor, and methods of measuring the concentration of a gas. In addition, the method of validating includes detecting false positives (e.g., determining that an impedance change is from the gas of interest and not a response caused by another source). Furthermore, the present disclosure provides methods of analyzing data for the conductometric PS sensor as well as for other devices and sensors.

EXAMPLES

Now having described the embodiments of the present disclosure, in general, the following examples describe some additional embodiments of the present disclosure. While embodiments of the present disclosure are described in connection with the examples and the corresponding text and figures, there is no intent to limit embodiments of the present disclosure to this description. On the contrary, the intent is to cover all alternatives, modifications, and equivalents included within the spirit and scope of the embodiments of the present disclosure.

Example 1

Brief Introduction

We describe a reversible response matrix and the dynamic interplay, as a moderately acidic NO_2 analyte interacts at room temperature with a TiO_2, SnO_x, Cu_xO (x=1, 2), and AxO (x>>1) metal oxide nanostructure deposited n-type nanopore coated microporous porous silicon (PS) interface. A significant variable response matrix is measured and the dynamic nature of analyte-interface processes characterizing the semiconductor-analyte interaction as NO_2 couples to the decorated semiconductor majority charge carriers. The competition for electrons between NO_2 and the TiO_2 decorated PS interface leads to distinct variations in sensor response as a function of increased TiO_2 concentration and displays a time variance as the extraction of electrons by NO_2 reaches a limiting charge carrier depletion and the decorated PS surface becomes electron withdrawing. This dynamic reversal is also demonstrated by distinct time-dependent PS interface responses to NO_2 and NO where the degree of electron extraction reaches a maximum and is again countered by the depleted n-type PS. Electron depleted SnOx and AuxO treated PS interfaces display a significant remnant effect as the decorated surface can become electron withdrawing for extended periods, forming a stronger acid and extracting electrons from NO_2. Exposure to NH3 also demonstrates the remnant effects of depletion.

Introduction:

We have outlined[1] an approach to "nanostructure directed electron transduction vs. chemisorption" on a sensor/micro-reactor interface. The fractional deposition of nanostructured metal oxide islands is used to modify sensitive surface layers created utilizing a hybrid nanopore covered micropo-rous matrix formed on "p- or n-type" silicon. The core of this approach is the Inverse Hard/Soft acid/base (Table 1/I) interaction model (IHSAB). This model provides a general approach to optimally design sensors with improved and variable sensitivity and conversion efficiency for a variety of gases, in an array-based format[5], by correlating the tenants of acid/base interaction and the properties of extrinsic semiconductors[1-4]. In the present study, we demonstrate not only the variable surface sensitivities that are introduced by the playoff between the untreated extrinsic semiconductor interface and the matrix of fractionally deposited nanostructured islands, but also the dynamic time-dependent response that exemplifies the manner in which these nanostructure decorated interfaces interact with the analyte NO_2, striking at the heart of the competitive electron dynamics that characterizes these systems.

The IHSAB principle correlates with a basis in directed electron transduction with minimized chemisorption, and is in complement to the HSAB principle for hard/soft acid/base interactions first put forth by Pearson et al.[6] and later correlated with density functional theory (DFT)[7,8] and Chemical Reaction Theory[9] by Pearson, Parr[7,8], Cohen et al.[9] and others[10]. In contrast to the HSAB principle which outlines a means to form strong ionic or covalent bonds via

hard/hard and soft/soft acid/base interactions, the driving principle to promote directed reversible interaction and efficient electron transduction to and from a semiconductor interface represents the inverse of that necessary to form strong chemical bonds[1]. The driving force of the IHSAB principle manifests through the interactions of the deposited metal oxide nanostructures as they influence the nature of analyte interaction with majority carriers in an n or p-type extrinsic semiconductor.

The IHSAB concept facilitates designed, highly variable, surface interactions using an available diversity of nanostructured "fractional" oxide depositions that act as gateways to focus the nature of the surface-interface interactions while minimizing the chemical interaction of an acidic or basic analyte with the semiconductor interface. These interactions are understood in terms of electron transfer to (base) or from (acid) the surface of an extrinsic semiconductor[2] which is controlled both by the nature of the extrinsic semiconductor and by the nanostructured metal oxides which are placed on its surface. Here, we exemplify and examine this interplay as we study the interaction of the created interfaces with the moderate acid NO_2. We demonstrate both the variable nanostructure sensitivity matrix and the intriguing competitive electron dynamics that occurs as a result of the interaction of NO_2 with the decorated PS interface. Here, the importance of the significant electron affinity of NO_2 becomes apparent in the interaction with n- and p-type porous silicon and is further emphasized by comparison with the time-dependent response to the amphoteric free radical NO with its extremely small electron affinity. The present study not only complements that of NO on p-type silicon[2] but also demonstrates the time-dependent behavior associated with the dynamic response associated with these two analytes.

We will emphasize the important roles played by (1) the electron affinity of the NO_2 analyte and (2) surface modification, with a fractional nanostructured island deposition, of an n-type extrinsic porous silicon surface. Measurements of the relative sensitivity of the decorated PS gas sensor interfaces at various NO_2 concentrations demonstrate not only a significant variance in response but also the dynamic nature of those processes that characterize the semiconductor-analyte interaction as NO_2 couples to the majority charge carriers of the decorated extrinsic semiconductor. The competition for electrons between NO_2 and a TiO_2 nanostructure decorated PS interface is found to lead to distinct variations in sensor response as a function of increased. TiO_2 deposition concentration as the time-dependent extraction of electrons by NO_2 reaches a limit in the depletion of the majority charge carriers as electron transduction is reversed and the decorated PS surface, now dominating NO_2, becomes electron withdrawing. This dynamic reversal is further demonstrated by comparing the distinct time-dependent responses of an extrinsic PS interface to NO_2 and the amphoteric NO radical where the degree of electron extraction reaches a maximum and is then countered by the depleted n-type PS interface. The electron depletion of SnO_x and Au_xO treated extrinsic semiconductor donor level population by NO_2 is found to display a significant remnant effect as the decorated n-type PS surface can become electron withdrawing for extended periods, forming a stronger acid and subsequently extracting electrons from NO_2. Experiments with NH_3 confirm the remnant effects of depletion. These dynamic effects form a backbone for the development of the sensitivity matrix.

It is to be noted that NO_2 detection is important since it contributes to vehicle exhaust emissions[5,11-19] and disease

detection[20,21], providing a non-invasive highly desirable clinical probe. The large quantities of NO produced in an asthmatic attack can combine with O_2 in breadth to produce NO_2. A simply constructed portable sensor capable of measuring significant NO (and NO_2) concentration changes in breath might be used on a regular basis to provide early detection for the onset of asthma attacks. NO_2 also represents a toxic air pollutant emitted by combustion engines and has been the focus of several research efforts in sensor technology[5,11-21] where levels as low as 12 ppb in dry air and 50 ppb in humid air have been reported for a p^+ substrate-based porous silicon sensor[5].

The Extrinsic Semiconductor Framework

FIG. 1.1 describes the variation in the position of the Fermi level with temperature for an n-type semiconductor[22]. This temperature dependence forms a basis for our considerations of electron transfer to and from the extrinsic semiconductor, the influence of electron transduction on the interaction with majority carriers in that semiconductor, and the corresponding effect which this transfer has on the semiconductor conductance. For an n-type semiconductor, donor electron levels lie just below the conduction band (FIG. 1.1). At moderate temperatures, the vast majority of the donor level electrons have been excited into the conduction band as eventually the semiconductor practically reverts to the behavior of an intrinsic material at temperatures above 300° C. Here, the Fermi level has shifted to the energy $E_{Fi} \approx E_g/2$ where E_g is the intrinsic semiconductor bandgap energy. From the temperature dependent behavior depicted in FIG. 1.1, it is apparent that population of donor level sites decreases with temperature. At 0K, the Fermi level lies at an energy E_d ($\approx$0.025 eV.)/2 below the conduction band. Here E_d corresponds to the donor level ionization energy for an n-type system. An acidic analyte withdraws electrons from an n-type extrinsic semiconductor. From the temperature dependent behavior depicted in FIG. 1.1, it is apparent that the removal of electrons from an "n-type" system should lead to an increase in resistance as majority charge carriers are removed, very much analogous to the effect of rising temperature. These effects, resulting from analyte interface interactions, have now been clearly observed. If, however, the extrinsic semiconductor interface is now modified by introducing additional metal oxide "island" sites to the micro/nanoporous PS interface in fractional deposition, these nanostructures act as gateways to influence the transit of electrons to and from the n-type semiconductor interface on which they are deposited.

EXPERIMENTAL

To create the framework to develop highly efficient nanostructure modified interfaces on either p- or n-type PS, the micro/nanoporous interface outlined in FIG. 1.1 must be generated[1]. Here a hybrid etch procedure is used to generate nanopore covered micropores. Schematic diagrams of the complete working sensor platform have already been presented[1,4,23]. The PS interface is generated by electrochemical anodization of 1-20 ohm-cm, n-type (phosphorous doped) (100) silicon wafers (Wafer World) or 7-13 ohm-cm, p-type (boron doped) (100) silicon wafers (Siltronix). The anodization of the n-type wafers[24,25] is done under topside illumination using a Blak-Ray mercury lamp. The wafer is etched in a 1:1 solution of HF and ethanol at a current between 8-15 mA/cm² (FIG. 1.2(a))[24,25]. The prepared n-type anodized sample is placed in methanol for a short period and then transferred to a dilute HF solution for a 30 minute period. This process creates a porous structure with

pore diameters of order 0.5-0.7 μm (FIGS. **2**(*b*) and (*c*)) and pore depths varying from 50 to 75 μm. These mircopores provide a medium for Fickian diffusion to the surface nanoporous layer.

Before the anodizations, an insulation layer of SiC (≈1000 angstroms) is coated onto the c-Si substrate by PEVCD methods and windows of 2×5 mm are opened in this layer by Reactive Ion Etching (RIE). The SiC layer serves two purposes. SiC makes it possible to form the hybrid micro/nanoporous PS structure in the specified windows during electrochemical anodization because of its resistance to HF. The SiC also aids the placement of gold contacts exclusively on the porous layer for resistance measurements and acts as an electrical insulator on the doped silicon. We continue to employ low resistance gold contacts whose formation has been discussed in detail previously. The PS hybrid arrays of nanopore covered micropores are tested at room temperature for their individual sensor response. In the present study, selected fractional nanostructure deposition is used to create an improved sensor response. The nature of this response is based on the application of the IHSAB acid/base principle. The selection of the nanostructures and the variable surface sensitivities that are produced as they form in-situ metal oxide deposits, introduces a distinct systematics of design, which can be predictably formatted. The approach is unique in that the nanostructures are deposited fractionally to the PS micropores and this fractional deposition does not require any time consuming self-assembly within the pores. This is not a coating technique or one that requires an exacting structural film arrangement but is, in fact, a much simpler process. The nanostructure deposition must be maintained at a sufficiently low level to avoid cross-talk between the nanostructures that, as it increases, leads to a noisy device and the eventual loss of functionality. Selected nanostructured metals, metal oxides, and nanoparticle catalysts can be deposited to the nanopore covered micropores to provide for distinct and variable sensitivities. In combination, these can be used as a basis to develop selectivity. In this study, nanostructured deposits generated from electroless gold, tin, and copper, as well as nanotitania provide for the detection of NO_2.

With the exception of the gold depositions, all of the nanostructured metals deposited to the PS surface are readily oxidized to SnO_x (x=2, 4) and Cu_xO (x=1, 2) as demonstrated by XPS measurements[23]. The initially introduced titania (anatase) may be crystalline, however, we cannot be certain of this crystallinity after deposition to the PS interface. The untreated PS hybrid structures are exposed to the electroless solutions for 10 to 30 seconds and are placed in DI H_2O and MeOH for consecutive 120 second periods. The oxidized electroless metal depositions when characterized before deposition correspond to amorphous structures displaying no diffraction patterns. Therefore, it is difficult to envision their crystallization during the short deposition and subsequent surface cleaning process. After deposition the decorated surfaces are cleaned for 120 s in DI and 120 s in methanol.

In all cases, the analyte gas being sensed is brought to the hybrid surface after entrainment at room temperature in UHP nitrogen (Matheson 99.999+%). The system is purged with UHP nitrogen for a minimum of 30 minutes before use. The typical resistances for the base PS structures range between 300 and 10,000 ohms at room temperature. The gas flow for the analyte and the entraining UHP nitrogen is controlled by MKS type 1179A mass flow controllers. The mass flow controllers used to control the anaylte gas and the entraining nitrogen flow responsed in less than 2 seconds.

The diffusion time of the analyte gas to the sensors, which provides the longest system time constant, varies from four to five seconds for the lowest anaylte concentrations to of order 1 to 2 seconds for concentrations greater than 2 ppm. These are the delay times for the observation of a signal due to the analyte in the supply line. The sensors respond to the analyte gas on a time scale much less than two seconds. The change in resistance is measured in one-second intervals using a DC current. This voltage bias used in these experiments is 3 volts to obtain an optimum signal to noise ratio. A NI DAQPad-6015 is used for gathering data and supplying the DC current. Labview software is used to control the experiment and record the results. MATLAB is used in the analysis of the data.

Results

NO_2 represents a moderately strong acid[26]. The interaction of this acid with an n-type PS interface, leads to a corresponding increase in resistance with analyte concentration, as NO_2 extracts electrons from the PS interface and removes majority carriers. Note, however, that the substantial electron affinity of NO_2 leads to a significantly different behavior with an n-type verses p-type[4] PS interface. For a p-type interface the extraction of electrons leads to an increase in the majority carriers (holes) and a decrease in resistance. We summarize the response changes for a particularly prepared and untreated n-type PS interface to NO_2 in FIG. **1.3**(*a*). Since there can be OH groups and hydrocarbons, originating from the air, deposited to the interface, we treat the system with UHP N_2 before use to insure that water is flushed from the surface. An N_2 flow onto the sensor is kept constant at 200 sccm at all times during the experiment The NO_2 is mixed (separately) with the N_2 flow which acts as an entrainment gas and diluent, as we test the system response for reversible sensitivity. In virtually all experiments, the deluted NO_2 was pulsed onto the interfaces with a 300 s half cycle followed by a 300 s half cycle UHP nitrogen cleaning. In addition, the sensors and system were purged with UHP nitrogen for 1800 s before operation.

In all of the experiments, an untreated sensor is prepared and measured for its response. The identical sensor is then treated and the relative sensor response is measured after the nanoparticle metal oxides are deposited to the PS interface. For the presently treated n-type systems, the positive resistance changes for NO_2 are found to vary linearly to at least 3 ppm and in some cases to 5 ppm. This behavior is in agreement with a simple 1D diffusion model simulation of the system which we have previously used to obtain a first order characterization of the naked PS gas sensor[27] This simple model solves the 1D diffusion equation numerically by comparing with the experimental sensitivity. We have evaluated the order of magnitude dimensions of the diffusion into the hybrid PS porous layer, and the relative time scales of both Fickian and Knudsen diffusion. For the saturated case we have calculate the gauge parameter D/L^2 and varied this parameter to get the best fit from the combination of experiment and simulation. The order of magnitude gauge parameters for Fickian diffusion into the mircopores and Knudsen diffusion into the nanopores are found to differ by approximately three orders of magnitude with an estimated Fickian to Knudsen diffusion coefficient of $10^{-5}/10^{-7}$ m^2/s. Further improvements of this numerical model can be accomplished by working in higher dimensions and with a more diverse pore structure. It is possible to improve the response equation through addition of other variables including the sticking coefficient, temperature, and humidity parameters. The results obtained demonstrate the dominant effect of diffusion at the lowest concentrations depicted in

FIGS. **1.3-1.9**. At concentrations in excess of 3 ppm, the response from the nanostructure deposited sensors begins to quench, as the depletion of the donor level population begins to saturate (bottom out) and the interface can subsequently become electron withdrawing. This clearly affects the diffusion dominated response.

The data in FIG. **1.3** corresponds to exposures of 1, 2, 3, 4, 5, and 10 ppm of test gas. This is denoted by the green saw-teeth in the figures which also indicate the range over which the analyte the gas is turned on and off. The untreated sensor interface in FIG. **1.3**(*a*) and the Cu$_x$O treated interface in FIG. **1.3**(*d*) for which the NO$_2$ signal varies linearly to 3 ppm are distinct from those for the untreated sensors in FIGS. **1.3**(*c*) and **1.3**(*e*) which are somewhat less responsive but display a linear response to 5 ppm. This less than linear increase in signal with concentration in FIGS. **1.3**(*c*) and **1.3**(*d*) indicates a more rapid approach to the limit of electron depletion which is reached at lower concentrations for the somewhat more sensitive devises. At concentrations in excess of 5 ppm all of the systems begin to display a quenching of the resistance response.

The results obtained for the PS interface treated with nanostructures of TiO$_2$ and SnO$_x$, both strong acids, with the moderate to weak acid Cu$_x$O, and with the very weak acid Au$_x$O, exemplify the dynamic interplay for these systems as the nanostructured oxides couple to the PS interface. The influence of this coupling is dictated by the IHSAB principle and the acid/base character of theses metal oxides. The results obtained with TiO$_2$ vividly demonstrate the important dynamic interplay induced by this strongly acidic nanostructure as it competes with NO$_2$ for electrons. The manifestation of the electron dynamics associated with these systems and donor level electron depletion are further characterized by remnant effects for the SnO$_x$ and Au$_x$O systems and, at elevated pressure, by the time dependent interaction of NO$_2$ and NO with an untreated PS surface.

As FIGS. **1.3**(*a-g*) demonstrate, the effect which SnO$_x$, Cu$_x$O, and Au$_x$O fractional nanostructured depositions have on the response of an n-type PS interface for each nanostructure deposited surface, the responses are distinct and do not have the same magnitude for the same concentration of the tested gas. This feature allows us to begin to develop a selectivity matrix for PS-NO$_2$ interaction and gas detection. For a 1 ppm exposure, the resistance change per base resistance for a nanostructure deposited vs. untreated sensor, Equation 1, is summarized in Table 1/II.

$$\Delta = \frac{\Delta R(\text{deposited})/R_0(\text{deposited})}{\Delta R(\text{untreated})/R_0(\text{untreated})} \qquad (1)$$

Dynamic Acid/Base Interactions and Competitive Electron Dynamics

In applying the ISHAB principle, we induce a "physisorptive" electron transduction by forcing the interaction of a moderate acid with a weakly basic metal oxide.[1,28] The opposite effect, the interaction of a strong acid with a strong base creates a chemisorptive interaction. FIG. **1.3**(*b*) demonstrates the effect, which the strong acid SnO$_x$ nanostructure deposit has on the NO$_2$ interaction with the PS interface. Here, both an acidic analyte and the nanostructure modified PS surface compete for electrons. If NO$_2$ and SnO$_x$ compete effectively for electrons, the competition might be expected to diminish the sensitivity of the interface, influencing directed electron transduction as measured by a significantly diminished resistance change. We do observe a muted

response. However, the weak and diffuse nature of the observed response after SnO treatment suggests that it is equally likely to be strongly influenced by chemisorption. While NO$_2$ is a moderate acid, NO$_2{}^-$, which can be formed as NO$_2$ extracts an electron from the n-type PS interface, corresponds to a moderate to strong base. Table 1/I suggests that an n-type PS surface corresponds to a borderline acidic surface. For this reason, we expect its chemical interaction (chemisorption) with NO$_2$ and NO$_2{}^-$ as dictated by the IHSAB/HSAB principle to be of only moderate effect. If, however, the PS surface is treated with nanostructured SnO$_x$, we expect a strong chemical interaction between this moderately strong acid and NO$_2{}^{-}$ [2,28]. We suggest that the muted and diffuse response with concentration in FIG. **1.3**(*b*) signals this chemisorption. It is to be emphasized that the base strength of NO$_2$" and the acid strength of SnO$_x$ are much more closely matched than those of either the much stronger acid, TiO$_2$, or the weaker acids Cu$_x$O and Au$_x$O. For this reason[1,28] we expect a chemisorptive interaction.

In contrast to SnO$_x$, the nanostructured deposition of Au$_x$O, a weak acid (Table 1/I) is observed to significantly enhance the rate of electron transfer to NO$_2$. However, in comparing FIG. **1.3**(*f*), where the Au$_x$O nanostructures are deposited in a ten second exposure, and FIG. **1.3**(*g*), where the PS interface is deposited for a 30 second exposure, with the data for the untreated PS interfaces in FIGS. **1.3**(*e*), we observe a significant relative enhancement at 10 s which is considerably diminished on exposure for 30 s. The decrease in sensitivity at higher Au$_x$O concentrations results as this exposure over-deposits the PS interface with electroless gold. Cross talk between the deposited nanostructures decreases the efficiency of electron transduction and leads to a notable decrease in response[1,2,23]. This emphasizes the requirement for careful fractional deposition to the PS interface. For the optimally deposited Au$_x$O system, the response verses the untreated PS surface is multiplied by a factor of approximately 5.

We find that the deposition of Cu$_x$O nanostructures in fractional deposition to the prepared n-type interface of FIG. **1.3**(*c*) (deposited surface **1.3**(*d*)) increases the system response by in excess of a factor of 2. The response of the Cu$_x$O treated interface rises linearly to 3 ppm, but much more rapidly than that of the untreated interface to. This response corresponds to an increase in the rate of electron removal which begins to quench at 4 ppm in contrast to the untreated PS interface. Further at 10 ppm we observe directly the effect of the dynamic behavior of the electron transduction. The resistance first increases sharply as NO$_2$ is extracting electrons. However, this extraction is soon countered as the donor level population is depleted to the extent that the decorated Cu$_x$O—PS interface begins to act as a stronger acid than NO$_2$. This effect is even more apparent in the TiO$_2$-based systems discussed below. Similar effects have been observed with the amphoteric NO radical[28].

FIGS. **1.4-1.7** demonstrate the effect that TiO$_2$ fractional nanostructured depositions have on the response of an n-type PS interface to NO$_2$. FIG. **1.4**(*b*) corresponds to the results obtained for low TiO$_2$ deposition times (≤10 s) or under conditions that do not produce sufficient concentrations of the strongly acidic TiO$_2$ to facilitate its ability to compete with NO$_2$, and attract electrons that are transferred to the PS interface. Here, the response to NO$_2$, which extracts electrons, leads to a resistance increase (conductance decrease). The TiO$_2$ treated system has a similar but weaker response than the untreated interface.

FIGS. **1.5**(*a-c*) demonstrate the effect that an intermediate TiO$_2$ fractional nanostructured deposition (20 s) has on the

response of an n-type PS interface to NO_2. FIG. **1.5**(a) corresponds to the response of the prepared untreated PS interface while FIG. **1.5**(b) demonstrates the response after TiO_2 is introduced. The results, demonstrated also in the overlapped response data of FIG. **1.5**(c), are striking. Here at the fractional concentrations deposited, the strong acid, $TiO_2^{1,28}$, competes quite effectively with the moderately strong acid, NO_2, for the available electrons in this system. The untreated PS interface (FIG. **1.5**(a)) displays a significant increase in resistance as NO_2 attracts electrons and depletes majority carriers. However, at the higher NO_2 concentrations, we observe a peaking in the resistance followed by a near exponential decay of the resistance to the point where the interface is no longer exposed to the NO_2. The rate of exponential decay observed in FIG. **1.5**(a) is seen to increase in magnitude with increasing NO_2 concentration in the range 4-10 ppm. The intensity is seen to maximize at ~3 ppm and the initial intensity maxima are similar for 3, 4, 5, and 10 ppm. We suggest that the effects of electron depletion and subsequent repopulation are manifest by the peak to a very similar maximum resistance and the subsequent exponential decay at the higher concentrations.

FIG. **1.5**(b) demonstrates striking results obtained after an intermediate TiO_2 nanostructure deposition. For those NO_2 analyte concentrations in excess of 2 ppm, as the response begins to increase with the introduction of NO_2, it is suddenly and rapidly quenched. This behavior is more pronounced at higher analyte concentrations. The spike-like response is also illustrated in FIG. **1.5**(c). As NO_2 is introduced to the decorated PS interface and attempts to extract electrons, the resistance rises rapidly to a point when the electron depletion reaches a limiting value. Here, the nanostructured TiO_2 islands coupled to the PS interface interact, preventing further electron withdrawal, and reversing flow of electrons so as to increase the donor and conduction level electron concentrations. This is manifest by a sharp decrease in the resistance. The affect clearly onsets at 2 ppm and increases in a manner proportional to concentration. The dynamic nature of this interplay is further evident as the resistance drops to a minimum value and then begins to again increase while the NO_2 is removed. As NO_2 is introduced in a new cycle the spike-like increase in resistance is again observed followed by a sharp drop in resistance. This behavior is explained as TiO_2 competes with and counteracts the extraction of electrons by NO_2, insures the flow of electrons to the decorated n-type PS interface, and increases the majority carrier concentration, leading to a significant decrease in resistance. The process of interaction is a dynamic one as TiO_2 and NO_2 vie for the available electrons. As a result the observed increase in resistance decreases by ~25% relative to the untreated PS interface.

The spike like features depicted in FIGS. **1.5**(b) and **1.5**(c) show a clear dependence on the NO_2 analyte concentration as the elapsed time to their appearance displays an inverse linear proportionality to the concentration. In addition, as the concentration of analyte increases the peak width of these features decreases and displays a sharp exponential decay. The dependent behavior of these features that are observed is distinct from that associated with analyte diffusion. FIGS. **1.5**(a) and **1.9** would suggest that the desorption kinetics associated with NO_2 is reasonably efficient. However, FIGS. **1.3**-**1.9** suggest that the efficiency of the adsorption process well exceeds that for desorption. While adsorption to the PS interface influences the observed processes we attribute to the nature of electron exchange, this observed behavior is difficult to relate to the adsorption/desorption process as it is more closely related to the interplay associated with electron

transduction. As opposed to response of these systems to adsorption and desorption kinetics (associated in part with gaseous diffusion) the observed behavior in FIGS. **1.5**(b) and **1.5**(c) as a function of analyte concentration is more easily associated that expected as analyte and interface compete for electrons.

FIG. **1.6**(b) demonstrates results at higher TiO_2 fractional deposition (30 s deposition time) Here, the TiO_2 coupled to the PS interface creates a surface which can overcome the electron withdrawing power of NO_2. Now, the response is that of a system which attracts electrons to the PS interface leading to a decrease in resistance (increase in conductance). By comparison, the data in FIG. **1.7** is intriguing in that it represents a variation of response as a function of NO_2 concentration. Here, we have converted the TiO_2 nanostructures deposited as in FIG. **6** to their corresponding oxynitride, $TiO_{2-x}N_x^{29}$. This creates a more basic interface and thus diminishes the ability of the deposited nanostructures to attract electrons. At NO_2 concentrations ≤5 ppm, the system again responds to the analyte by removing electrons from NO_2. This corresponds to a decrease in resistance although the decrease is notably less than that for the TiO_2 decorated system. However, an NO_2 concentration of 10 ppm is now sufficient to reverse this response, leading to a positive resistance change which results from a dominant electron extraction by NO_2.

For all of the systems studied, the electron affinity of NO_2 enhances its ability to withdraw electrons, eventually depleting the donor level electron population (FIG. **1.1**). The extent of this process and the dynamics of its time dependent reversal is pronounced as the interface, once depleted, becomes more electron withdrawing than NO_2. In compliment to the time-dependent behavior of the electron transduction in TiO_2, we find that the depletion process can lead to significant remnant effects. FIGS. **1.8**(a-d) demonstrates this remnant effect as we observe a response for both the SnO_x and Au_xO nanostructure modified and depleted surfaces which mimics that observed for interaction with an electron donating analyte. FIG. **1.8**(a) depicts the response of the SnO_x treated PS interface 24 hours after the initial experiments as described in FIGS. **1.3**(a) and **1.3**(b). The observed response is that which would be expected of an analyte that is contributing electrons to the SnO_x/n-type PS interface. The SnO_x decorated PS sample is now extracting electrons from NO_2. A similar behavior is observed for the Au_xO decorated PS (initially FIGS. **1.3**(f) and **1.3**(g)), which now extracts electrons from NO_2. FIG. **1.8**(b) demonstrates a resistance decrease for the 10 s exposed interface and FIG. **1.8**(c) indicates a slightly smaller decrease for the 30 s Au_xO exposed interface consistent with the nature of their initial depositions ~24 hours earlier. Even more compelling are the results obtained in FIG. **1.8**(d) when the system, treated for 10 s with Au_xO, is subsequently treated with NH_3, again 24 hours after the experiments depicted in FIG. **1.3**. FIG. **1.8**(d) indicates a significant resistance decrease and minimal quenching even at concentrations of 10 ppm. We suggest that NH_3, as a strong base, contributes electrons which provide the repopulation of a strongly depleted donor level population.

The IHSAB principle which we describe briefly above and elsewhere[1,3] dictates the means to obtain an initial dominant directed electron transduction and minimal chemisorption with respect to the acidic analyte NO_2. Because of the potential for the chemisorbed interaction-reaction of SnO_x with surface generated NO_2^-, the interaction leading to directed electron transduction enhanced via coupled gold clustered oxide Au_xO (x>>1) nanostructure

deposits provides a more efficient means for the initial "reversible" extraction of donor level electrons (FIG. **1.3**). However, FIG. **1.8** demonstrates that this previously treated and apparently depleted tin oxide surface now appears to the depleted Au_xO surfaces capturing electrons to populate the donor levels and subsequently decreasing the system resistance (increasing conductance).

The dynamic nature of electron depletion and exchange is also demonstrated at elevated concentrations of NO_2 and NO interact with an untreated PS interface. FIG. **1.9** depicts observed responses for an untreated PS interface to NO_2, and NO at concentrations in excess of 10 ppm. The data for NO_2 and NO in FIGS. **1.9**(*a*)-(*d*) reflect a clear dynamic interplay. The data for NO at 10 ppm display a rise to a maximum resistance as electrons are attracted by this analyte. A similar rise is observed for NO_2 although the change in resistance is considerably greater. At 20 ppm and again at higher concentrations, the NO response at first peaks and then decays. On the time resolution of FIGS. **1.9**(*a*) and **1.9**(*c*) these features appears as a sharp initial resistance increase, which at higher time resolution, are seen to decay as a slow, near exponential tail to a subsequent limiting value. The NO_2 responses at 20 and 30 ppm again display a rise to a maximum resistance during exposure, although the rise appears muted at 30 ppm. At 40 and 50 ppm, NO_2 also displays a signal which first peaks and then decays at a much faster rate than that observed at lower concentrations. An indication of this slow near exponential decay at higher time resolution and analyte gas concentrations of 80 ppm is presented in FIGS. **1.9**(*b*) and **1.9**(*d*). The onset of this behavior at lower concentrations for the NO system would suggest an origin for this phenomenon. The substantial electron affinity for NO_2[26] versus NO[30] dictates that NO_2 withdraws electrons considerably more efficiently than does the amphoteric NO radical, which has a small if not negligible electron affinity[30]. As NO_2 and NO withdraw donor level electrons, the n-type PS interface is depleted to the point where it begins to compete for available electrons. Because of its much more substantial electron affinity, NO_2 competes more favorably for these available electrons than does the amphoteric NO radical. Hence the dynamic signal decay onsets at higher concentrations. We suggest that the near exponential decays depicted in FIGS. **1.9**(*b*) and **1.9**(*d*) correspond to the process whereby the degree of electron extraction reaches a maximum and is then counteracted by the depleted n-type PS interface which now acts as a stronger acid than either NO_2 or NO.

Discussion

The results presented in FIGS. **1.3**-**1.9** for the transduction of NO_2 with both untreated and fractional nanostructure treated n-type porous silicon clearly indicate a very much more dynamic reversible interaction for acids and bases with majority electron carriers than with holes[1,3,27]. Further, the influence of the nanostructured metal oxides, fractionally deposited to the PS interface, appears to be notably more pronounced for n-type systems than it is for p-type systems. This is at least in part due to the effective masses.

The materials selected for the nanostructured islands serve the role of guiding antennas that can force a dominant directed electron transduction or a chemisorbtive interaction at the decorated extrinsic semiconductor interface. The data in FIGS. **1.4**-**1.7** and **1.9** now displays an important dynamic interplay which influences the electron transduction as it results from the dynamics of electron exchange. The nanoporous coating provides a phase match for the unique fractional deposition of select nanostructures. The selection of these nanostructures for sensor applications with both

p-type and n-type PS is well predicted by the hard and soft nature of the interacting constituents and the IHSAB model (Table 1/I) as this model dictates the coupling of analyte/interface acid-base interactions with the properties of the majority carriers in an extrinsic semiconductor. The results obtained for TiO_2 decoration in FIGS. **1.4**-**1.7** and the results obtained for the interaction of NO_2 and NO with an untreated PS interface at elevated pressure (FIG. **1.9**) now demonstrate the dynamic nature of the electron transduction process.

We suggest that the data presented in FIGS. **1.3**-**1.9** demonstrate important correlations with the schematic temperature dependence of an extrinsic semiconductor presented in FIG. **1.1**. First the temperature dependence for both p and n-type semiconductors is such that one can expect vacant donor levels for an n-type system and available holes for a p-type system at room temperature[22]. If an analyte acts to add electrons to the vacant donor electron levels of an n-type extrinsic semiconductor, we anticipate that the population of these levels will "top-out" as the resistance will reach a limiting lower value. An analogous decrease to a minimum resistance is observed for a p-type PS system. Here, NO_2 extracts electrons, augmenting the population of holes and enhancing conductance. FIG. **10** demonstrates the previously seen bottoming-out of the resistance as NO_2 interacts with an untreated p-type PS interface maximizing the removal of electrons.

At elevated analyte concentrations, NO_2 and NO are found to reach a limit in the degree of electron extraction from an untreated n-type PS interface[28] followed by the reversal of the electron exchange process. The data in FIGS. **1.3**-**1.9** now begin to provide a wider window to the dynamic process of electron withdrawal and exchange. At lower concentrations, it is apparent that the nature of the nanostructure deposition can have a strong and variable impact on the control of analyte electron extraction. This is demonstrated by the variations in the TiO_2 decorated PS interfaces in FIGS. **1.4**-**1.7**. The possibility exists to reverse the process of electron extraction whenever an acid is countered by an interface modified by a strongly acidic nanostructured deposition (FIGS. **1.3**-**1.9**). In all these cases the extrinsic semiconductor is depleted to the extent that it, in effect, becomes a stronger acid than NO_2. We suggest that the plateau resistance observed for the NO and NO_2 systems at elevated concentration (FIG. **1.9**) corresponds to the equilibration of the Fermi levels for the analyte-semiconductor interface to a position intermediate to that above the donor levels and the limit of energy corresponding to the Fermi level for the intrinsic semiconductor (FIG. **1.1**).

Conclusion

The interaction of NO_2, a moderately strong acid, with a nanostructure modified n-type PS interface demonstrates a diverse analyte-extrinsic semiconductor electon dynamics. Most intriguing are (1) the competition between NO_2 and strongly acidic TiO_2 nanostructures for the available electrons on the n-type PS interface and (2) the remnant effects which are observed subsequent to the depletion on and SnO_x and Au_xO treated PS interface. The observed initial behavior of these surfaces is dictated in large part by the IHSAB[1,27] principle. This model combines the basic tenants of acid/base chemistry (the ability of bases to donate electrons and acids to extract electrons) and with the physics of extrinsic semiconductors and their majority charge carriers to form devices sensitive to the ppb level. The nanoporous coating of microchannels[1,27] provides a unique phase match for the subsequent fractional deposition of select nanostructure islands that decorate the microchannel. The materials

selected in this study for the nanostructured islands to force a dominantly directed electron transduction (vs. chemisorbtion) at the decorated extrinsic semiconductor interface, insuring that the IHSAB principle dominates. The IHSAB principle and the intriguing electron dynamics which accompanies its application should be the subject of future study.

REFERENCES

Each of which is Incorporated Herein by Reference

1. J. L. Gole and S. Ozdemir, *Chem Phys Chem.*, 11, 2573-2581 (2010).
2. S. Ozdemir, T. Osburn, and J. L. Gole, *Journal of the Electrochemical Society*, 158(7), J201-J207 (2011).
3. (a) J. Gole, S. Ozdemir, and T. S. Osburn ECS Transactions, 33(8), 239-244 (2010).(b) S. Ozdemir and J. Gole, *ECS Transactions*, 33(8), 111-115 (2010).(c) J. L. Gole, S. Ozdemir, S. M. Prokes, and D. A. Dixon, *MRS Proceedings*, 1257-O09-04 (2010).
4. 4. J. Campbell, J. A. Como, N. Larsen, and J. L. Gole, *Journal of Electrochemical Society*, 155, D128-D132 (2008).
5. L. Pancheri, C. J. Oton, Z. Gaburro, G. Soncini, and L. Pavesi, *Sens. and Actuators B*, 89, 237-239 (2003).
6. See for example (a) R. G. Pearson, *Coordin. Chem. Rev.* 1990, 100, 403-25. (b) R. G Pearson, *J. Am. Chem. Soc.* 85, 3533-3539 (1963). (c) R. G Pearson, Chemical Hardness, John Wiley VCH, Weinheim, (1997). (d) R. G Pearson, *J. Chem. Sci.* 117(5), 369-377 (2005). (e) R. G Pearson, *Inorg. Chem.* 27, 734-740. (1988)
7. (a) R. G Parr, R. G Pearson, *J. Am. Chem. Soc.*, 105, 7512-7516 (1983). (b) R. G Parr, W. Yang. Density Functional Theory of Atoms and Molecules, Oxford University Press, New York, (1989)
8. (a) R. G. Parr, R. A. Donnelly, M. Levy, W. E. Palke, *J. Chem. Phys.*, 68, 3801.(1978)(b) W. Yang, R. G. Parr, *Proc. Natl. Acad. Sci. USA*, 82, 6723 (1985). (c) W. Yang; R. G. Parr, R. Pucci, *J. Chem. Phys.* 81, 2862. (1984) (d) R. G. Parr, W. J. Yang, *J. Am. Chem. Soc.* 106, 4049 (1984).
9. M. H. Cohen, A. Wasserman, *J. Phys. Chem.* 111, 2229-2242 (2007).d
10. C. G. Zhan, J. A. Nichols, D. A. Dixon, *J. Phys. Chem. A* 107(20), 4184-4195 (2003). (b) Geerlings, P.; De Proft, F.; Langenaeker, W. *Chem. Rev.* 109, 1793 (2003).
11. G. Williams and G. S. V. Coles, *Sens. and Actuators B*, 15-16, 349-353 (1993)
12. G. Sberveglieri, S. Groppelli, and P. Nelli, *Sens. and Actuators B*, 4, 457-461 (1991).
13. L. Boarino, C. Baratto, F. Geobaldo, G. Amato, E. Comini, A. M. Rossi, G. Faglia, G. Lerondel, G. Sberveglieri, *Mat. Sci. Eng. B Solid*, 69-70, 210-214 (2000).
14. S. Ozdemir, J. L. Gole, *Curr. Opin. Solid Stater Mater. Sci.* 11, 92-100 (2007).
15. C. Burratto, G, Faglia, E. Comini, G. Sberveglieri, A. Taroni, V. La Ferrara, L. Quercia, and G. Francia, *Sens. and Actuators B*, 77, 62-66 (2001).
16. M. J. Sailor, in: L. Canham (Ed.), Properties of Porous Silicon. IEE, London, UK, 1997, pg. 364.
17. S. R. Morrison, *Sensors and Actuators*, 2, 329-341 (1982).
18. S. R. Morrison, *Sensors and Actuators*, 12, 425-440 (1987).
19. G. Heiland, *Sensors and Actuators*, 2, 343-361 (1982).
20. (a) W. Miekisch, J. K. Schubert, G. F. E. Noeldge-Schomburg, *Clinica Chemica Acta*, 347, 25-39 (2004); (b)

P. P. R. Rosias, E. Doompeling, H. J. E. Hendriks, J. W. C. M. Heijnens, R. A. M. G. Donckerwolcke, Q. Jobsis, *Pediatric Allergy and Immunology*, 15, 4-19 (2004).
21. (a) M. R. Zeilder, E. C. Kleerup, D. P. Tashkin, *Current Opinions in Pulmonary Medicine*, 10, No. 1:31-36 (2004); (b) S. A. Kharitonov, P. J. Barnes, *Biomarkers*, 7, 1-32 (2002).
22. M. N. Rudden and J. Wilson, *Elements of Solid State Physics, John Wiley and Sons editors*
23. S. Ozdemir and J. L. Gole, *Sensors and Actuators B*, 151, 274-280 (2010).
24. C. Levy-Clement, A. Lagoubi, and M. Tomkiewicz, *J. Electrochem. Soc.* 141, 958-967 (1994).
25. H. Foell, M. Christophersen, J. Carstenson, and G. Hasse, Materials Science and Engineering R280, 1-49 (2002).
26. (a) K. M. Ervin, J. Ho, W. C. Lineberger, Ultraviolet Photoelectron Spectrum of NO2-, *J. Phys. Chem.*, 92, 5405 (1988); NO2(EA)=2.2730±0.0050 eV (b) L. Pancheri, C. J. Oton, Z. Gaburro, G. Soncini, and L. Pavesi, *Sens. and Actuators B*, 89, 237-239 (2003); (c) G. Williams and G. S. V. Coles, *Sens. and Actuators B*, 15-16, 349-353 (1993). (d) G. Sberveglieri, S. Groppelli, and P. Nelli, *Sens. and Actuators B*, 4, 457-461 (1991). (e) L. Boarino, C. Baratto, F. Geobaldo, G. Amato, E. Comini, A. M. Rossi, G. Faglia, G. Lerondel, G. Sberveglieri, *Mat. Sci. Eng. B Solid*, 69-70, 210-214 (2000).
27. S. Ozdemir and J. L. Gole, *ECS Transactions*, 33(8), 111-115 (2010).
28. J. L. Gole, E. C. Goode, and W. Laminack, *Chem Phys Chem*, 13, 549-561 (2012).
29. (a) J. L. Gole, J. D. Stout, C. Burda, Y. B. Lou and X. B. Chen, *Journal of Physical Chemistry B*, 108, 1230 (2004); (b) X. B. Chen, Y. B. Lou, A. C. S. Samia, C. Burda and J. L. Gole, *Advanced Functional Materials*, 15, 41 (2005).
30. (a) Travers, M. J.; Cowles, D. C.; Ellison, G. B., Reinvestigation of the Electron Affinities of O2 and NO, Chem. Phys. Lett., 164, 449 (1989); NO(EA) =0.0260±0.0050 eV; (b) W. Miekisch, J. K. Schubert, G. F. E. Noeldge-Schomburg, *Clinica Chemica Acta*, 347, 25-39 (2004); (c) P. P. R. Rosias, E. Doompeling, H. J. E. Hendriks, J. W. C. M. Heijnens, R. A. M. G. Donckerwolcke, Q. Jobsis, *Pediatric Allergy and Immunology*, 15, 4-19 (2004).

Example 2

Brief Introduction

A unique new approach to sensor design and construction has been conceptualized and initially validated. Implemented in basic science and technology, the Inverse Hard/Soft Acid/Base (IHSAB) model links chemical selectivity to the mechanism of sensor response for both doped semiconductor and nanowire sensors. This IHSAB model provides a simple-to-use prescription for design, which relates rationally and generally the physics and chemistry of specific nanostructure interfaces. The model combines the basic tenants of acid/base chemistry and semiconductor physics so as to form a road map for the implementation of readily constructed, cost effective, rapidly responding, deployable devices, sensitive to the ppb level. The mechanism of selectivity relies on the use of a nanopore coated microchannel array, which combines optimized analyte diffusion with maximum interface interaction. The nanoporous coating of the microchannel provides a unique phase match for

the subsequent fractional deposition of select nanostructure islands that decorate the microchannel. The materials selected for the nanostructured islands serve the role of guiding antennas to force a dominantly physisorbtive (vs. chemisorbtive) interaction at the decorated extrinsic semiconductor interface. The process can be reversed for microreactor applications. The selection of these nanostructures and the variable and controllable physisorbed (reversible) interaction they introduce for sensor applications, is well predicted by the IHSAB model. The IHSAB model the coupling of analyte/interface acid-base interactions with the properties of the majority carriers in an extrinsic semiconductor. The approach is unique in that the nanostructures are deposited fractionally to semiconductor micropores; this fractional deposition DOES NOT require any time consuming self-assembly within the pores and is far simpler to implement than traditional thin film or alternate coating techniques. The selection of the nanostructures that are deposited to the nanopore covered microchannels and the variable surface sensitivities that are produced, as they form in-situ metal/metal oxide deposits, can now be predicted not in a random fashion or based on limited previous observations, but in a clearly designed procedure based on established molecular properties.

Introduction—the IHSAB Model for Porous Silicon Sensors and Microreactors

Despite significant effort, much of the basic science and technology that can provide a general means to link sensor and micro-reactor design, in a framework applicable to detect and transform gas phase analytes and analytes in aqueous solution, has not yet been developed. In this chapter we will outline a novel, rational, and general approach to generate efficient interfaces which are being designed to detect, sequester, and destroy harmful analytes. At the heart of the conceptual approach is the combination of the basic tenants of acid/base chemistry and semiconductor physics This structured approach can be demonstrated to be relatively simple to follow and implement, leading to the future likelihood of cost effective, deployable devices sensitive to the ppb level. This can provide systems operating in an unsaturated mode over a wide temperature and pressure range, complemented by pulsed mode operation, which ensures low energy consumption and high analyte selectivity. The defining constraints offered by the combination of acid/base and semiconductor theory can enable the selection of device materials which target specific gas analytes. The degree to which this combination allows the tailoring of interfaces, through an understanding of their physics and chemistry, offers the means to construct a framework for analyte sensing and transformation. Further, the extension of this concept for sensor and microreactor development, on appropriate extrinsic semiconductor interfaces, might be coupled with solar energy conversion to enhance the potential for combining conductometric sensor suites and active photocatalysts, with application to the development of solar pumped sensing.

The enhanced activity of nanoscale structures can have a profound effect on the development and mediation of MEMS/NEMS sensing/microreactor technology, providing new inroads to create hybrid devices with greatly enhanced sensitivity, electivity, and chemical transformation efficiency. Within this framework, we consider a new approach to the formation of optimal sensor interfaces and arrays and transducing interfaces that can function across a broad temperature and pressure range (Seals et al. 2002; Lewis et al. 2005, 2007; Gole and Ozdemir 2010). The method of sensor design shows the potential to replace traditional metal

oxide sensor systems (usually SnO_2-based), especially in elevated temperature environments. Also inherent to this approach is the developing general concept of nanostructure directed physisorption (electron transduction) versus chemisorption at a doped semiconductor interface. Coupling the trends in the acid/base character of an analyte and an extrinsic semiconductor interface with the inherent nature of majority charge carriers in p and n-type semiconductors affords the potential to design a sensitive and controllable means of transferring electrons to build distinct sensor matrix arrays or modify in a controlled manner chemical transformations at an interface. In complement, the modification of this approach to sensor design to produce strong chemical interactions and dominant chemisorptions, has potential broader implications for microreactor technology including the sequestering and destruction of contaminants. The coupling of acid/base and semiconductor technology facilitates analyte-semiconductor interactions. This promotes enhanced sensor and microreactor capability and an enhanced combined microstructure-directed nanostructure conversion capability via the action of modifying nanostructures as they are introduced to a nanopore covered microporous semiconductor interface (Gole and Ozdemir 2010; Gole et al. 2011).

The Inverse Hard/Soft Acid/Base (IHSAB) principle/approach, as it correlates with a basis in physisorption (electron transduction), complements the HSAB principle for hard/soft acid/base interactions first put forth by Pearson (1963, 1990, 1997, 2005) and later correlated with density functional theory (DFT) (Parr et al. 1978; Yang et al. 1984; Yang and Parr 1985; Parr and Yang 1989; Geerlings et al. 2003) and Chemical Reaction Theory by Parr and Pearson (1983), Cohen and Wasserman (2007), and others (Zhan et al. 2003). The basis for correlation follows the principle that soft-soft acid/base interactions produce significant covalent bonding and hard-hard combinations produce significant ionic bonding. The HSAB principle states that hard acids prefer to coordinate to hard bases and soft acids prefer to coordinate to soft bases. In contrast, the driving principle to promote physisorption (electron transduction) represents the inverse of that necessary to form strong chemical bonds (Gole et al. 2011; Gole and Ozdemir 2010). This principle is manifest through the interactions of metal oxide nanostructures as they influence the nature of the majority carriers in a p- or n-type semiconductor. Nanoporous silicon layers positioned on porous silicon (PS) micropores facilitate the deposition of nanostructured metal/metal oxides which provide distinctly higher variable sensitivities and selectivity for a given extrinsic semiconductor interface. It is necessary that one treat the PS surface with fractional depositions, much less than a monolayer to insure that the nanostructures do not begin to cross talk and, in so doing diminish signal to noise. This deposition can be made to produce a dominant physisorptive (sensors) or chemisorptive (micro-reactors) character at the semiconductor interface as the deposited nanostructures act to focus the nature of the surface interaction. However, the nature of the extrinsic semiconductor, the manner in which its donor and/or acceptor levels can be manipulated, and its transformation to intrinsic character also represent important variables.

The dynamic natures of "n" and "p-type" silicon extrinsic semiconductors must be evaluated and compared, focusing on the controlled manipulation of these semiconductors as they are modified with nanostructures and interact with gaseous or aqueous analytes. The observed semiconductor responses correlate well with the temperature dependence of an extrinsic semiconductor as it is manipulated in the

transformation to intrinsic character. This is intimately tied to the population of donor or acceptor levels, and the inherent mobilities of electrons. When considering the inherent mobilities of electrons and holes, it is not surprising that the response of modified n-type semiconductors is found to exceed that of comparable p-type systems. The IHSAB concept can be extended to address the properties of several additional semiconductor interfaces including nanowires. The results obtained not only pertain to sensor and microreactor array design but also suggest the importance of the dynamic changes created as the majority charge carrier concentrations of the interacting extrinsic semiconductors are manipulated and their Fermi energies are modified through chemical and light interaction.

The Interface on Extrinsic Semiconductors

The widespread use of interfaces for chemical sensors and reactive transduction, including that introduced by catalysis, is a function of stability, speed, ease of manufacture, ease of calibration, and ease of use. Recently Korotchenkov and Chou (2010) have discussed these requirements and the advantages of porous silicon (PS). It is a crystalline material of large interfacial surface area, which is microelectronics (CMOS) compatible and can be simply fabricated with inexpensive equipment. However, with this simple mode of fabrication, it has been necessary to overcome problems of stability and reproducibility by applying several new fabrication and testing methods (Kottke et al. 2009; Ozdemir and Gole 2010a; Korotcenkov and Cho 2010). When this is done, it is possible to generate devices with continued improvements in sensitivity, which can operate for several months and be readily rejuvenated.

Porous silicon (PS) nano/microporous interfaces, illustrated in FIGS. **2.1** and **2.2**, are produced by a simple hybrid etch procedure described in detail elsewhere (Levy-Clement et al. 1994; Foell et al. 2002; Ozdemir and Gole 2008a) creating the desired interfacial support structure. The format for design and fabrication is applicable to virtually any extrinsic semiconductor into which a nanopore coated microporous framework can be generated.

The silicon structure or layers and the porous silicon (PS) structures, devices, and methods, can be replaced with any alternate extrinsic semiconductor (e.g., GaP, InP, CdTe) onto which a porous microstructure can be generated. Further, the configuration in FIG. **2.1** can be adapted to form a pass-through microporous membrane (Campbell et al. 2008; Gole et al. 2009). This greatly broadens the range of nanostructure-interface combinations that can be potentially exploited, as the alternate extrinsic semiconductors can be a p-type, a p^+-type, a n-type, or a n^+-type substrate.

A nanoporous (shown in green) coated micropore array (FIG. **2.1**) with micropores ideally 1-1.5 microns in diameter. The arrays from p, n, p^+, and n^+ extrinsic semiconductor substrates are fabricated using a variety of anodization techniques discussed in detail elsewhere (Levy-Clement et al. 1994; Foell et al. 2002; Ozdemir and Gole 2008a). Before anodization, a silicon wafer is cleaned in HF (49%) and a SiC layer 1000 angstroms in thickness is coated onto the polished surface of the silicon wafer by Plasma Enhanced Chemical Vapor Deposition (PECVD). SiC is used since this layer is highly durable in HF-based solutions (Nassiopoulos 1997). 2 mm×5 mm windows were opened in the SiC layer by Reactive Ion Etching (RIE). After the anodization process, a gold layer (3500-5000° A) is coated onto the sensor by an e-beam evaporation method. These processes create the overall sensor depicted in FIG. **2.3**. The conductometric PS gas sensors typically operate in the 1-5 V range, but it is

possible to use the sensors with a 100 mV or smaller bias voltage (Seals et al. 2002; Lewis et al. 2005).

The nanoporous coating process (FIG. **2.1**) provides a phase matching for the subsequent deposition of selected nanostructured islands (FIG. **2.1**, FIG. **2.2**). These surface-attached nanoparticles possess unique size dependent and electronic structural properties that form a basis for extrinsic silicon, measured by circuitry (ex: microprobes as in FIGS. **2.3** and **2.4**) attached to the electrodes shown in FIGS. **2.1** and **2.3** as gold contacts (Ozdemir and Gole 2010a). The nanopore covered microporous structure of the interface has been created specifically to facilitate highly efficient gaseous diffusion (Fickian) to the highly active nanostructure (FIG. **2.1**) modified nanoporous (FIG. **2.1**) coating (Ozdemir and Gole 2010b). While the room temperature operation of this interface serves many applications, the appropriate installation on heat sinks can allow operation at several hundred degrees C. This provides a key element whereby the developed interface can operate under conditions which are not amenable to typical metal oxide systems. Further, when coated with nanoparticle photo-catalysts, the interface can operate as a nanostructure-modified microreactor for efficient chemical transformations.

The approach to interface development in PS sensors also follows a basic concept that is elucidated in a distinct systematics of design. The selection of the nanostructures and the variable surface sensitivities that are produced as they form in-situ metal oxide deposits are predictable (Gole et al. 2011; Gole and Ozdemir 2010). The chemical concepts of acids and bases are coupled with the extrinsic properties of a semiconductor support structure to provide an ordered approach to the generation of an activity matrix for a given analyte gas. The nanopore coated micropores can be treated with a wide array of selective nanostructures (metals, metal oxides, or catalysts-FIG. **2.1**) deposited into the microporous channels. This process can be made to create a selective environment for either the physisorption (electron transduction) or the chemisorption of an analyte by correctly correlating the acidic or basic character of the nanostructure modified interface with the acid/base characteristics of the analyte of interest. Further, the degree of physisorption (electron transduction) vs. chemisorption can be varied to create a matrix (array) of responses for a sensor (physisorption (electron transduction) dominated) or a variable degree of chemical activity to produce chemical transformation (chemisorption dominated). Acidic analytes act to withdraw electrons from the nanostructure modified semiconductor interface whereas basic analytes act to donate electrons. As the nanostructure islands are chosen to force degrees of physisorption (electron transduction) they also act as antennas, to increase the sensor sensitivity. The nano-size of these deposits provides for high sensitivities that vary as a function of nanostructure, creating the framework for selectivity. In the physisorption (electron transduction) dominated mode, amenable to the formation of a reversible sensor response, the transfer to or removal of an electron from the semiconductor surface produces an interaction with the majority charge carriers of the semiconductor which greatly increases or decreases the resistance of a nanostructure modified PS interface (Gole et al. 2011; Gole and Ozdemir 2010). The response will depend both on whether the analyte is an acid or a base and whether the semiconductor is "p-type" or "n-type.

The IHSAB Concept as the Basis for Nanostructure-Directed Physisorption (Electron Transduction) at Sensor Interfaces

The concept of chemical hardness/softness first developed by Pearson (Gole et al. 2011) is based on the nature of metal ion complexation in aqueous solution and is a generalization of the Lewis acid/base concept. The HSAB concept, as it is correlated with chemical reactivity theory (CRT), was given a deep foundation in terms of density function theory by Parr and coworkers (Parr et al. 1978; Yang et al. 1984; Yang and Parr 1985; Parr and Yang 1989; Geerlings et al. 2003), following an initial correlation with molecular properties established by Pearson (1963, 1988, 1990, 1997, 2005). More recently, conflicts underlying the correlation of the DFT and CRT theories have been largely resolved by Cohen and Wasserman (2007) to obtain a further refinement of the concepts of electronegativity and hardness.

The properties of acids and bases can be described as hard and soft based upon the correlation of several atomic/molecular properties which include the ionization potential, I, the electron affinity, A, and the chemical potential, μ, in connection with the HOMO-LUMO gap concept from molecular orbital (MO) theory as the Kohn-Sham orbitals replace the MOs (Parr and Yang 1989; Geerlings et al. 2003; Yang et al. 1984; Parr et al. 1978; Yang and Parr 1985).

Examples in terms of the groups of hard, borderline, and soft acids and bases are given in Table 2/1 (Pearson 1988). For a soft acid, the acceptor atom is of low positive charge, large size, and has easily polarizable outer electrons. The acceptor atom of a hard acid is of small size and not easily polarized. In a soft base, in precise contrast to a hard base, the donor atom is of low electronegativity, easily oxidized and highly polarizable with low-lying empty molecular orbitals. The HSAB principle was initially based on empirical observations. However, as it groups acids and bases, the HSAB basis has been developed in terms of DFT. The basis follows the principle that soft-soft combinations depend mainly on covalent bonding and hard-hard combinations depend mainly on ionic bonding. Further the HSAB principle states that hard acids prefer to coordinate to hard basis whereas soft acids prefer to coordinate to soft bases (Gole et al. 2011).

Within the HSAB-DFT framework, the electronic chemical potential (Pearson 1963, 1990, 1997, 2005; Parr and Yang 1989; Geerlings et al. 2003; Yang et al. 1984; Parr et al. 1978; Yang and Parr 1985; Zhan et al. 2003) given by Equation (3.1),

$$\mu = \left(\frac{\partial E(N)}{\partial N}\right)_{v_e} = \left(\frac{\delta E}{\delta \rho}\right)_{v_e} \qquad (3.1)$$

is a global quantity. Here E(N) is the ground state energy of a system of N electrons in the electrostatic potential energy, v_e, due to its nuclei (fixed) and E is a functional (Eq. (3.1)) of the electron density, ρ. The three point finite difference approximation for $\partial E(N)/\partial N$ gives $\mu \approx (I+A)/2$ with I the ionization potential and A the electronegativity so that μ is the negative of the Mulliken electronegativity χ_M (Equation (2)):

$$X_M \approx -\mu \approx \frac{(I+A)}{2} \qquad (3.2)$$

The absolute hardness of a species, η (Pearson 1963, 1988, 1990, 1997, 2005; Parr et al. 1978; Yang et al. 1984;

Yang and Parr 1985; Parr and Yang 1989; Geerlings et al. 2003; Zhan et al. 2003), is defined by Eq. (3.3):

$$\eta = \left(\frac{\partial^2 E(n)}{\partial N^2}\right)_{v_e} = \left(\frac{\partial \mu}{\partial N}\right)_{v_e} \approx (I - A) \qquad (3.3)$$

and the absolute softness (Yang and Parr 1985) is the inverse of the hardness (Eq. (3.4)):

$$S = \eta^{-1} = \left(\frac{\partial N}{\partial \mu}\right)_{v_e} \qquad (3.4)$$

The approximation in Eq. (3.3) arises from the use of the finite difference formula.

Unlike the chemical potential, the hardness is not constrained to be constant everywhere throughout a system, having local values for which η is simply a global average. Parr and coworkers (Parr and Yang 1989; Geerlings et al. 2003; Yang et al. 1984; Parr et al. 1978; Yang and Parr 1985) have defined a local hardness that corresponds to the change in chemical potential with electron density in different parts of a molecule, complex or simply a system. Cohen and Wasserman (2007), in their formulation of CRT, define a generalization to include a hardness matrix that incorporates both the self-hardness of individual species and the mutual hardness for pairs of species combining in a system. They also provide a description of local softness as they demonstrate how the reactivity of a species depends on its chemical context. Within this context, as interacting constituents separate, the hardness matrix becomes diagonal in the self-hardness. It is possible to establish a more general description of electronegativity (Eq. 2) equalization. Cohen and Wasserman's (2007) generalization realizes that reactivity indices are chemical-content dependent, not unique properties of an isolated system as an electron can move on and off of a species, interacting with its chemical environment. The electron need be associated with that species only part of the time as, for example, when a Lewis acid/Lewis base interaction takes place. Of equal importance are the correlations which define the connection between CRT and DFT theories as they can be used to provide a description of those molecular orbitals (MO's) involved in the process of electron transfer from an acid to a base.

Within the context outlined, if two systems B and C are brought together, electrons will flow from the system of lower χ (Eq. (3.2)) to that of higher χ to equilibrate the chemical potentials. If we consider that in solid-solid interactions, the equilibration of the Fermi levels is the analog of the chemical potential, it is not difficult to envision the extrapolation of these concepts to the interaction of a molecule with an interface.

Within the context of interacting molecular systems B and C, as a first approximation to an acid-base interaction, the fractional number of electrons transferred can be defined by Gole et al. (2011)

$$\Delta N = \frac{X_C - X_B}{2(\eta_C + \eta_B)} \qquad (3.5)$$

where the difference in electronegativity drives the electron transfer and the sum of the hardness parameters acts as a resistance. This expression, while approximate, is useful

because it expresses the nature of the initial interaction between B and C using properties of the isolated systems providing the backdrop for the first order categorizations given in Table 2/1. Whereas the absolute chemical potential and hardness are molecular parameters, the flow of electrons is from a specific occupied molecular orbital of B to a specific empty orbital in C so that the overlap between the exchanging orbitals will be critical in determining energy change and the nature of chemical interaction.

The correlation of hardness and softness with molecular orbital theory follows readily from the Frontier orbital concept of chemical reactivity theory (Fukui et al. 1952). Within the context of Koopman's theorem, the frontier orbital energies can be correlated with the expressions for chemical potential (Eqs. (3.1) and (3.2)), hardness (Eq. (3.3)), and softness (Eq. (3.4)) as

$$-\epsilon_{HOMO}=I, -\epsilon_{LUMO}=A \qquad (3.6)$$

where now the concept of hardness reduces to the statement: hard molecules have a large HOMO-LUMO gap and soft molecules have a small HOMO-LUMO gap (Pearson 1988). This concept must be carefully applied. In formal DFT, the location to which the electron transits corresponding to the electron affinity is not the LUMO but actually the first excited state. In practice, the application of the concept in this manner usually applies, but it is not formally rigorous (Dixon 2010). A further issue in MO theory is that for an infinite basis set, if the EA is negative, the HOMO-LUMO gap is equal to the IP. This means that the outlined concept must be applied carefully to systems that do not have a positive EA and bind an electron (Dixon 2010). The criteria that hard acids prefer to coordinate to hard bases and soft acids to soft bases is, in one sense, a HOMO-LUMO matching criteria. Politzer (1987) has shown that the softness of atoms correlates with their polarizability whereas Huheey (1978) has shown that softness is the ability to accept charge. Within this framework, we promote a HOMO-LUMO mismatch to induce physisorption (electron transduction).

The foundation of the HSAB concept can be used in complement to create a framework for chemisorptive interactions and the formation of a micro-reactor interface. In contrast, to create sensitive, rapidly responding, and reversible PS gas sensors, processes that lead to strong ionic or covalent bonding must be avoided. The following sections of this monograph emphasize that a general approach to conductometric chemical sensor development should follow the inverse of the HSAB concept of acid-base chemical interaction. The changes in response to nanoparticle modified PS interfaces outlined in the following discussion can be correlated with this inverse (IHSAB) behavior.

The Extrinsic Semiconductor Framework

The position of the Fermi level varies with temperature for n-type and p-type semiconductors as shown in FIG. 2.5 (Rudden and Wilson 1993). This temperature dependence forms a basis for our considerations of electron transfer to and from an extrinsic semiconductor the nature of the interaction with majority carriers in that semiconductor, and the corresponding influence that this transfer has on the semiconductor conductance and transduction (Gole et al. 2011). For an n-type semiconductor, donor electron levels lie just below the conduction band (FIG. 2.5a). At 0° K, the Fermi level lies at an energy E_d ($\approx$0.025 eV.)/2 below the conduction band. Here E_d corresponds to the donor level ionization energy for an n-type system. At moderate temperatures, the vast majority of donor level electrons have been excited into the conduction band as eventually the

semiconductor almost reverts to that of an intrinsic material at temperatures above 600 K. At this point, the Fermi level has shifted to the energy $E_{Fi}\approx E_g/2$ where E_g is the intrinsic semiconductor bandgap energy. A similar situation holds for a p-type semiconductor (FIG. 2.5(b)) as electrons are excited to acceptor levels (holes are excited into the valence band) at an energy $E_a\approx$0.036 eV (Rudden and Wilson 1993) above the valence band. At 0° K, the Fermi level lies at an energy $E_d/2$ above the valence band, however, FIG. 2.5b depicts the corresponding shift of E_{Fp} as it transcends with temperature to the value $E_{Fi}\approx E_g/2$ for the corresponding intrinsic semiconductor.

A basic analyte can donate electrons to a "p-type" porous silicon (PS) semiconductor surface and these electrons can fill empty acceptor levels or combine with holes. This reduces the number and the formation of majority charge carriers, leading to an increased resistance. The process is effectively reversed for an "n-type" semiconductor as the majority charge carriers, electrons, increase within the donor levels that are not populated at room temperature, and therefore the conductance increases and the resistance decreases. The opposite effect should be observed for an acidic analyte as it withdraws electrons. From the temperature dependent behavior depicted in FIG. 2.5, it is apparent that vacant donor level sites and valence band hole sites increase with temperature. It is also apparent that the addition of electrons to an n-type system should contribute to and eventually "top-out" the donor level population, whereas the removal of electrons and increase in resistance is very much analogous to the effect of temperature rise. In contrast, the removal of electrons from a p-type system can potentially maximize conductance (decrease resistance to a minimum value), whereas an influx of electrons is very much analogous to the effect of temperature rise. These effects, resulting from analyte interface interactions, the preparation of the interface, and the population of donor and/or acceptor levels, have now been clearly observed for several of the sensor systems we consider. Further, the Fermi level shifts that accompany these dynamic interactions are significant. They must also be considered if one is to correctly evaluate solar pumping experiments.

If the extrinsic semiconductor interface is now modified by introducing additional metal oxide "island" sites (FIG. 2.1) in fractional deposition, these nanostructures form a superstructure on the semiconductor interface. These nanostructures act as antennas to influence the transit of electrons to and from the semiconductor interface on which they are deposited and the available donor and acceptor levels.

In a p-type porous silicon (PS), semiconductor surface electrons are being excited from a valence band either into acceptor levels or the conduction band as holes. These represent the majority charge carriers that are created in the valence band. If an analyte donates electrons to a p-type semiconductor, these electrons can combine with holes, thus reducing the number of majority charge carriers, leading to an increased resistance. To first order, the process should be reversed for an n-type semiconductor as the majority charge carriers, electrons, increase the population of the donor levels. If an analyte donates electrons the conductance increases, and the resistance, is expected to decrease. However, the process is more complex, in part, because the majority charge carriers, now electrons, have higher mobilities. The dynamics of these charge carriers can be influenced by the fractional nanostructure coverage of the semiconductor interface. While the increase or decrease in resistance (decrease or increase in conductance) associated with the response to a given analyte is determined predominantly by

the p or n-type character of the selectively nanostructure modified semiconductor interface, the dynamics of conduction (Laminack et al. 2012) can be modified as a result of the acid/base strength of the fractionally deposited nanostructures.

Following the framework of the IHSAB concept (Gole and Ozdemir 2010; Gole et al. 2011), selected nanostructured islands (FIG. **2.1**), are placed on the semiconductor to act as antennas to promote physisorption (electron transduction). The HSAB principle manifest at surfaces (Parr and Yang 1989; Geerlings et al. 2003; Gole and Ozdemir 2010; Yang et al. 1984; Parr et al. 1978; Yang and Parr 1985 Pearson 1963, 1990, 1997, 2005; Gole et al. 2011), promotes chemisorption. These two principles can be applied in complement to the behavior of an extrinsic semiconductor to provide a range of responses. Thus, a matrix of signatures for a given analyte in a physisorption (electron transduction) dominated sensor mode or, with appropriate modification, a range of reactions in a microreactor configuration might be developed.

Physisorption (Electron Transduction) and the Response of a Nanostructure Modified Sensor Platform

The introduction of nanostructures to the nanopore coated microporous framework can selectively modify the resistance response of the PS interface. The selection of the nanostructures that are deposited to the nanopore covered microchannels and the variable surface sensitivities that are produced, as they form in-situ metal/metal oxide deposits, can be predicted in a clearly designed implementation of the outlined concepts above. These predictions are based on established molecular properties, as the chemical concepts of acids and bases are coupled with the extrinsic properties of a semiconductor support structure. As the nanopore coated micropores of a p- or n-type PS surface (hybrid PS) are treated with a wide array of selective nanostructures deposited into the microporous channels, they create a selective environment for either the physisorption (electron transduction) or the chemisorption of an analyte by correctly correlating the acidic or basic character of the nanostructure modified interface with the acid/base characteristics of the analyte of interest. Physisorption (electron transduction) can be made to dominate chemisorption by applying the IHSAB principle and can be varied to create a matrix (array) of sensing responses. Alternatively, the HSAB concept applied to a semiconductor surface might be used to create a variable degree of chemical activity (chemisorption dominated).

Basic analytes contribute electrons whereas acidic electrolytes act to withdraw electrons from the nanostructure modified semiconductor interface. When chosen to force degrees of physisorption (electron transduction), the nanostructured metal oxide islands also act as antennas to increase the sensor sensitivity. In this physisorption (electron transduction) dominated mode, amenable to the formation of a reversible sensor response, the transfer to or removal of an electron from the semiconductor surface results in a modification of the semiconductor majority charge carriers, which greatly increases or decreases the resistance response of the modified PS interface. As we have noted, this will depend both on whether the analyte is an acid or a base and whether the semiconductor is p-type or n-type.

Lewis acids accept electrons and Lewis bases donate electrons. They can be classified in a range from hard to soft where these categorizations are a function of several properties including the electron affinity and ionization potential (Gole, et al. 2011). Hard acids react with hard bases to form strong ionic bonds and soft acids react with soft bases to form strong covalent bonds (HSAB concept (Pearson 1963,

1990, 1997, 2005; Parr and Yang 1989; Geerlings et al. 2003; Yang et al. 1984; Parr et al. 1978; Yang and Parr 1985; Zhan et al. 2003; Cohen and Wasserman 2007; Parr and Pearson 1983)) accompanied by a strong matchup of molecular orbitals (MO's). In a gas-surface interaction this produces strong chemisorption. The IHSAB concept is based on the reversible interaction of hard-acid surfaces with analytes that represent soft bases or hard-base surfaces with analytes that represent soft acids. It requires the combination of a modified semiconductor interface and analyte materials which can be used to direct a strongly dominant electron transduction (vs. chemisorption) interaction (avoiding the formation of a strong bond which inhibits reversibility). For example, as demonstrated in FIG. **2.6**, the fractional in-situ nanostructure deposition of SnO_2, a strong acid, to a p-type PS interface leads to a maximum impedance increase for the weak base NO. In contrast, a weak acid, Au_xO (x>>1), nanostructure deposition leads to a maximum impedance increase for the strong bases NH_3 and PH_3 (FIG. **2.7**). The corresponding impedance change for an acidic analyte on the modified p-type PS interface decreases, exemplified for the moderate acid NO_2 in FIG. **2.8**. These impedance changes are easily measured, show significant variation and are reproducible. Importantly, the increase or decrease in impedance is dictated predominantly by the nature of the semiconductor interface, especially for p-type systems. The data for the gas phase bases in Table 2/2 correspond to comparisons of the positive resistance change produced as SnO_x, NiO, Cu_xO, and Au_xO (x>>1) fractional nanostructure deposits are used to modify an untreated PS interface. FIG. 2/9 demonstrates that the nature of these deposits have been verified by XPS spectroscopy. Here, the magnitude of the response changes observed relative to an untreated PS interface forms the basis for the materials positioning diagram in FIG. **2/10**.

To first order, the interactions are reversed for an "n-type" semiconductor where the majority charge carriers, electrons, can be made to increase upon "physisorbed" interaction with a basic analyte (conductivity increases as resistance decreases) and decrease upon interaction with an acidic analyte. However, the increased mobility of donor level electrons, in contrast to holes, is also manifest as is the effect of the fractionally deposited nanostructured oxides. Table 2/3 compares and contrasts the details of analyte interaction on primarily n-type PS for the strong base NH_3, the amphoteric NO radical, and the moderate acid NO_2. The n-type PS interface is treated with fractional nanostructured depositions of nanostructured oxides including TiO_2, SnO_x, NiO, Cu_xO, and Au_xO (Gole et al. 2011). The data in Table 2/3 should be compared with the results obtained for the fractional deposition of nanostructures on a p-type PS interface (Table 2/2). This comparison indicates that there are clear and significant differences between the n- and p-type systems. However, at the same time, there is an underlying complementary structure created by the nanostructure deposits.

The concentration of SnO_x and Au_xO nanostructures deposited to the PS interface to produce the enhanced sensitivities relative to PS indicated in FIG. **2.6**, is notably less than the nanostructure deposition illustrated in FIG. **2.2**. It is necessary that the deposited nanostructures be sparsely interspersed onto the micro/nanoporous framework to avoid crosstalk. Table 2/2 as it summarizes the results for several nanostructure modified p-type PS surfaces for the gases NH_3, PH_3, and NO at one ppm level, indicates significant differences for the ratios of resistance change given for the various nanostructure deposited interfaces relative to an

untreated PS structure. In addition, the data (FIG. **2.6**) obtained for CO, a weak base, demonstrates a significant response increase upon exposure of this gas to an SnO_2 (hard acid, Table 2/1) nanostructure coated surface whereas the data obtained for H_2S (Gole et al. 2004) (an intermediate base, Table 2/1) indicates a significant increase in response (1.5-2) for an Au_xO nanostructured oxide (weak acid) deposited interface. The SnO_x deposited sensors, in particular, allow the room temperature detection of CO at the sub-ppm level notably below the sensitivity of other PS sensors (Foucaran et al. 1997; Moseley 1997; Schechter et al. 1995). This SnO_2 deposited sensor can be compared with PS-based sensors whose resistances exceed hundreds of $k\Omega$ operating on a 2 V bias (Foucaran et al. 1997), SnO_2 sensors operating at 300° C.-500° C. (Moseley 1997) and similar gas sensors operating at 2-5 V (Schechter et al. 1995). The data obtained for SO_2 (Table 2/2) demonstrate that this radical acts like a moderate base in the absence of a hydrating environment.

The basic hybrid PS sensor micro/nanoporous surface has been considerably improved through the refinement of etch techniques. With this improvement, electroless gold treatments of the improved PS interface have led to a substantial increase in sensitivity (signal/noise) for ammonia (Ozdemir and Gole 2008b) so that responses in the several hundred ohm/ppm range are possible. This forms the basis for low ppb concentration detection at sensitivity ratios relative to untreated PS as indicated in Table 2/2. The relative sensitivity ratios in Table 2/2 and 2/3 are maintained quite closely over time and as detection sensitivity is improved. The results obtained for phosphine, exemplified in FIG. **2.7** and summarized in Table 2/2, are difficult to obtain as PH_3 is known to display an even greater degree of interaction with a nanostructured surface and have a higher sticking coefficient than NH_3 (Lewis et al. 2005; Ozdemir and Gole 2010a). The tendency toward the equilibration of adsorption and desorption, also manifest in ammonia, can produce a gradual increase in the sensor baseline. Although we operate the sensors in an unsaturated mode (Lewis et al. 2005; Ozdemir and Gole 2010a), the sensor response and recovery time scales are distinctly different. The observed drift can also result from weak chemisorptions of PH_3 superimposed on a dominant physisorption (electron transduction) (Ozdemir and Gole 2010a). Purging the sensor surface with ultrahigh purity (UHP) nitrogen for longer durations, following exposure to the 300 s PH_3 gas pulse (FIG. **2.7**), enhances the return to the initial baseline (Gole and Ozdemir 2010; Lewis et al. 2005; Ozdemir and Gole 2010a). This return to baseline can be further improved by more tightly constraining the gas flow path to the sensor surface from its current design for operation at atmospheric pressure. In addition, the application of FFT pulsing techniques, considered in a following section, can be used to average out the effects of this baseline drift (Lewis et al. 2007).

FIGS. **2.6** and **2.7** and Table 2/2 suggest that the proper combination of nanocoating techniques could be used to produce combinations of array-based multiple sensor devices of varying sensitivity to a variety of basic gases. The matrix of array responses could be correlated to selectively analyze gas mixtures. For example, a sensor array consisting of an untreated SnO_x nanostructure coated and gold clustered oxide nanostructure coated sensor can be used to sensitively test for the presence and relative concentrations of ammonia and nitric oxide (current limits NO<500 ppb, NH_3<50 ppb). A nanostructured $PS/SnO_2/Au_xO$ sensor combination could provide the basis for developing a sensitive room temperature detector that could be installed as a simple sensor system for asthmatics (Lewis et al. 2005; Gole and

Ozdemir 2010) where one requires the ability to simultaneously monitor the increase in NO, NH_3, and NO_2.

Table 2/3 has summarized data for several nanostructure modified n-type PS interfaces. NO_2 represents a moderate acid (Ervin et al. 1988) whereas NH_3 corresponds to a strong base (Grant et al. 2009). We expect these analytes to induce the opposite response from an n-type and p-type semiconductor interface. NO, however, is an amphoteric free radical (Travers et al. 1989) and, for this reason, its interactions are far less straightforward. In FIG. **2.11**, we summarize the response changes for an untreated n-type PS interface to NO_2, NO, and NH_3. Here, the surfaces are carefully purged of hydroxyl and hydrocarbon contamination before they are characterized. The positive resistance changes for NO_2 and NO vary linearly and correspond to an exposure to 1, 2, 3, 4, 5 ppm (10 for NO_2) of test gas. The recorded signal for NO_2 on n-type PS is that of an acid which has a significant electron affinity (Ervin et al. 1988) and withdraws electrons from the PS interface. In contrast, as NO_2 withdraws electrons from p-type PS (FIG. **2.8**), we observe a decrease in resistance. The recorded signal for NO on n-type PS corresponds to 100 Ohms/ppm which considerably exceeds the 2 Ohm/ppm signal recorded for p-type PS (Ozdemir et al. 2011). For both n- and p-type PS, the observed change in response corresponds to an increased resistance. Thus, with n-type PS, the amphoteric NO radical acts like an acid withdrawing electrons whereas with p-type PS, the NO radical (Travers et al. 1989) acts like a weak base, contributing electrons but at a much lower rate. The response for the moderately strong base, NH_3 (FIG. **2.11***a*) (Grant et al. 2009), corresponds to a significant drop in resistance. This response, which corresponds to an increase in conductance as NH_3 contributes electrons to the majority carriers (donor level electrons) is linear to 4 ppm, begins to saturate at pressures in excess of 5 ppm and is partially quenched at 10 ppm.

With the outlined data, it is possible to consider whether the underlying IHSAB principle described above dictates the response observed for several sensor, basic and acidic gas, interactions. The principle can then be extended to the detection of additional gases with the development of a selective nanostructure deposition approach that facilitates physisorption/electron transduction. By monitoring the trends in hard and soft acid and base behavior, first order selections can be made for the appropriate modification of the PS hybrid interface with nanostructured metal/metal oxide coatings to create a range of selectivities as is apparent from Tables 2/2 and 2/3 for a number of gases (Ozdemir and Gole 2008b, 2010a; Wang et al. 2011). The development of selective nanostructured coatings that reversibly complex with a gas can be based in an IHSAB concept which relies, counter to that of Pearson et al. (Pearson 1963, 1990, 1997, 2005; Parr and Pearson 1983) on the combination of hard Lewis acids with soft Lewis bases or soft Lewis acids with hard Lewis bases (counter to that of Pearson et al. (Parr and Pearson 1983; Pearson 1963, 1990, 1997, 2005). To establish this combination, we follow the trends established for the classification of the hard and soft nature of acids and bases (Pearson 1963, 1990, 1997, 2005; Parr and Yang 1989; Geerlings et al. 2003; Yang et al. 1984; Parr et al. 1978; Yang and Parr 1985; Zhan et al. 2003; Cohen and Wasserman 2007; Parr and Pearson 1983).

A first order comparison of the response data in Table 2/2 with the exemplary list of hard, borderline and soft acids and bases in Table 2/1 clearly demonstrates that hard bases such as ammonia (and ~ phosphine) respond most strongly (resistance change) when exposed to a nanostructured Au_xO

surface corresponding to the soft acid ($Au^{0,+1}$). The data outlined in Table 2/2 corresponds to a rise in resistance (decrease in conductance) as NH_3 contributes electrons to a p-type PS interface, canceling the majority carriers which are holes. This is most easily done for Au_xO. In contrast, as NH_3 contributes electrons to an n-type PS interface, we observe a decrease in resistance (increase in conductance) as NH_3 contributes to the majority carriers which are electrons. However, if we compare the data for NH_3 in Tables 2/2 and 2/3, we see that they follow a very similar trend. This trend correlates with the mismatch of analyte and nanostructure modified PS interface MO's and the mismatch in hard and soft acid/base character. In contrast to the strong bases NH_3 and PH_3, the soft bases CO and NO display a maximum response (change in resistance) upon interaction with the borderline to hard acid SnO_x ($Sn^{+2,+4}$). Note also the minimum response of the untreated PS surface to CO and the subsequent decrease for the Au_xO nanostructure treated surface displayed in FIG. 2.6. These properties have not changed over an extended period as we observe no clearly measureable response with an untreated and gold nanostructure treated PS surface. For CO, the decrease in an already small, almost negligible, resistance response versus hybrid PS is consistent with the expected effect of chemisorption for the interaction of a weak acid with a weak base to create a covalent chemical bond that does not facilitate electron transfer.

The responses outlined in Table 2/2, in concert with FIGS. 4 and 5 and Table 2/1, can be correlated further as one generates the materials positioning depicted in FIG. 2.10. This positioning diagram is generated based on the relative responses to the analytes studied as they are exposed to several nanostructured deposits. The results obtained remain constant over an extended period. We position the five bases NH_3, PH_3, H_2S, NO, and CO relative to the porous silicon ($Si^{+1\ to\ +4}$)(Wang et al. 2011) and the PS modified acidic interfaces generated with a nanostructured TiO_2(Ti^{+4}), SnO_x ($Sn^{+2,+4}$), Al_2O_3 (Al^{-+3}), NiO (Ni^{+2}), Cu_xO ($Cu^{+1,+2}$), and Au_xO ($Au^{0,+1}$) deposit. The rationale for the positioning of H_2S in FIG. 2.3 is the correlation of the relative responses for one ppm H_{2S} with an Au_xO deposited surface compared to an untreated PS surface (Ozdemir and Gole 2010b) and to the data for NH_3, PH_3, and NO in Table 2/2. Based on ionization potential as well as proton affinity data, H_2S lies close to the soft acid side of PH_3. The basis for the positioning of CO is its virtually non-existent response to Au_xO and its substantial response to SnO_2 summarized in FIG. 2.6. Data for Al_2O_3 deposits has been generated only for phosphine for which the response is found to be virtually identical to the hybrid PS interface. Thus, the acid strength of the alumina modified PS surface as well as the untreated PS surface and the base strength of PH_3 are closely aligned.

There are several additional factors contributing to the construction of FIG. 2.10. A larger resistance change associated with SnO_2 suggests that ammonia lies closer to porous silicon than to the extremely strong Sn^{+4} acid site. The inherently hard basic character of ammonia is also consistent with the strong resistance change observed for its interaction with the Au_xO nanostructure deposited surface (Table 2/2). The behavior of ammonia is also strongly mimicked by phosphine, which displays an expected strong increased resistance change relative to the p-type PS surface associated with the Cu_xO and Au_xO nanostructure modified interfaces. The results obtained with ammonia for an n-type PS interface (Table 2/3) are quite similar. We observe a decrease in the magnitude of the resistance response increase relative to the untreated PS surface as a result of a (Ni^{+2}) oxide

nanostructure deposition. This suggests that the (Ni^{+2}) treated surface lies to the soft acid side of the untreated hybrid PS interface. The remaining interactions with NO and NH_3 suggest a (Ni^{+2}) acid strength in closer proximity to untreated PS. This defines the broader relative response for the Ni^{+2} and hybrid PS regions indicated in FIG. 2.10. As we have noted for phosphine, the responses to the hybrid PS structure and an Al_2O_3 nanostructure treated p-type PS surface appear virtually identical. Therefore, we anticipate that phosphine lies equally close to Al_2O_3 and PS with NH_3, a stronger base, on the hard base side of PH_3. This also suggests that the acid character of Sn^{+4} considerably exceeds that of Al^{+3}. For PH_3, more recent results obtained working with surfaces treated with TiO_2 nanostructures prepared using sol-gel methods (Gole et al. 2004) show a significant increase in resistance, 4 to 5 times that of untreated PS, for p-type surfaces. Similarly, NH_3 shows a 3.5 to 4 fold increase in resistance compared to the untreated hybrid PS interface response to NH_3. These responses, thought to be dominated by the action of Ti^{+4}, suggest the response of a harder acid than Sn^{+4} with the moderately strong bases, NH_3 and PH_3. As we will demonstrate, the extremely hard acid strength of TiO_2 can play a very significant role (Gole et al. 2011).

The NO radical has a considerably different molecular orbital makeup and electron shell structure than ammonia or phosphine and represents a weak base. The open shell nature of NO would suggest a very different interaction with hybrid PS and nanostructure treated PS surfaces. In addition, NO is in fact amphoteric as it can bind an electron, if only weakly, which NH_3 and PH_3 cannot. The behaviour of NO with p and n-type nanostructure treated PS is quite distinct. For the p-type PS interface (Table 2/2), the soft base-hard acid interaction of NO with a SnO_2 nanostructured coating leads to a substantial resistance change relative top-type PS. This is the signature of the reversible interaction of a strongly acidic surface with a weak base. Further, the response to gold, copper, and nickel treated surfaces, while considerably muted relative to the tin treated surface, suggests that NO should be positioned directly below the copper ($Cu^{+1,+2}$) systems and intermediate to gold ($Au^{0,+1}$) and nickel (Ni^{+2}). The interaction of NO with Ni^{+2} suggests a greater separation from nickel than from gold. While PS and Ni^{+2} may lie in a similar intermediate region, the larger resistance change observed for NO with a Ni^{+2} surface suggests that the (Ni^{+2}) modified PS surface lies to the hard acid side of PS, acting as a harder acid deposited to the PS surface. This again suggests a broader range for the relative response of the Ni^{+2} and PS regions as indicated in FIG. 2.10. The results obtained for n-type PS appear to offer a very different picture. However, to understand the data in Table 3, the amphoteric character of NO and the hard acid character of both SnO_2 and TiO_2 must be considered. FIG. 2.11 demonstrates the response of an untreated PS interface to NO, the changes corresponding to a decrease in the semiconductor conductance as NO extracts electrons. However, because NO is amphoteric, the strong acidic character of TiO_2 and to a lesser degree SnO_2 overcomes the ability of NO to extract electrons. Instead electrons are extracted from NO and transferred to the n-type PS interface to increase the conductance. This is vividly demonstrated in FIG. 2.12.

FIG. 2.12 compares the response for a prepared n-type PS interface with that for the same PS interface treated with TiO_2, SnO_x, NiO, Cu_xO, and Au_xO nanostructures. In all cases relative measurements for the treated and untreated PS samples exposed to NO at 1, 2, 3, 4, 5, and 10 ppm are considered. The stark changes observed for the TiO_2 and

SnO_2 nanostructure treated PS interfaces (FIGS. **2.12**b and **2.12**c) are apparent as the conductance of these systems is reversed relative to the untreated device described below and in FIG. **2.11**. The observed responses for the untreated samples are virtually linear to 5 ppm although a slight delay in the gas system flow to the sensor and its response is evident below 2 ppm. The observed response again does not double from 5 to 10 ppm, indicating the onset of saturation manifest as a decrease in the rate of conductance increase at the highest NO concentrations.

The variations in response observed for the nanostructure treated PS interfaces, while reflecting the donor level population, demonstrate the important role played by the deposited nanostructures and the nature of acid/base interaction they direct. The observed trends also correlate well with the relative responses observed as NO interacts with p-type PS (Table 2/2). The acid strength of the nanostructures deposited to the n-type PS interface decreases from the strongest acid TiO_2 to the weakest acid Au_xO in the order $TiO_2 > SnO_x > NiO > Cu_xO > Au_xO$. FIGS. **2.12**e-**2.12**h demonstrate that the deposition of both Au_xO and Cu_xO nanostructures increases the response of the PS interface (Table 2/3) and that the increase is greater for the weaker acid Au_xO. As observed for the nanostructure modified p-type interface, the data suggest that the acid/base strengths of NO and Cu_xO are comparable. Here, Au_xO and Cu_xO act to enhance the electron withdrawing power of the NO radical, which suggests that they represent weaker acids on the n-type PS interface. The effect of the enhanced rate of transfer is apparent (FIGS. **2.12**(e) and (f)) and evidenced by a decrease in the rate of conductance increase with concentration and a decrease in response with time at the highest concentrations.

NiO displays an intriguing intermediate acid behavior. FIG. **2.12**d demonstrates that at the lowest NO concentrations the response of the n-type PS interface is enhanced as the ratio of the responses (2 ppm/1 ppm) increases significantly relative to that for the untreated n-type PS. However, at an NO concentration of 3 ppm, the dynamic response at first increases to a maximum, subsequently decreases, oscillates and again increases. This dynamic behavior is even more pronounced at 4, 5, and 10 ppm. As the NO concentration increases, the transfer of electrons to NO increases to a maximum. However, this transfer reaches a limit when the decorated n-type PS interface is sufficiently depleted that it acts as a stronger acid than the amphoteric NO radical. At this point electrons are extracted from NO (acting as a base) accompanied by a decrease in the measured dynamic resistance (increase in conductance) as the semiconductor donor levels are repopulated. Thus, at the lowest concentrations the NiO nanostructure deposited interface mimics the dynamic behavior of the weak acids Cu_xO and Au_xO and at higher concentrations it is transmuted to a surface similar to that treated with the stronger nanostructured acids TiO_2 and SnO_x. As a function of concentration, NO acts as both an acid and a base. However, the intermediate behavior observed for NiO also appears to correlate with the results obtained for p-type systems as exemplified in FIG. **2.10**. Here again, NO as an analyte interacting with the p-type PS interface was placed as a weak base (Seals et al. 2002) in a region close to the region between Cu^{+2} and Ni^{+2}. This is, in effect, the fulcrum region for the Acid/Base Diagram 10, which is also observed for the n-type PS interface.

The Underlying IHSAB Principle

The underlying IHSAB principle, which we describe briefly above dictates the physisorption (electron transduction) directed response observed for a number of basic, acidic, and amphoteric analytes as they interact with nano-structure deposited p and n-type PS extrinsic semiconductor interfaces. A first order comparison of the response data in Tables 2/2 and 2/3 with the exemplary list of hard, borderline and soft acids and bases in Table 2/1 demonstrates that hard bases such as NH_3 respond most strongly when exposed to an Au_xO nanostructure treated PS surface. Within the framework of the IHSAB principle, this is not surprising since Au_xO is a soft acid ($Au^{0,+1}$). The results which we obtain for the amphoteric NO radical demonstrate the importance of the relative acidity (Table 2/1) of nanostructured metal oxide deposits, which is more strongly manifest on an n-type as opposed to a p-type PS interface. Their ability to direct electron flow dictates whether NO acts as either a weak acid or weak base. The responses outlined in Table 2/3, FIG. **2.11** and FIG. **2.12** for an n-type PS interface can be correlated to demonstrate consistency with the materials positioning diagram of FIG. **2.10**. Because of the significant catalogue of information on metal oxides, this principle can be extended to the detection of additional gases with the development of a selective nanostructure deposition approach which facilitates reversible physisorption (electron transduction). By monitoring the trends in hard and soft acid and base behavior, first order selections can be made for the modification of the PS hybrid interface (or any extrinsic semiconductor interface into which a microporous structure can be formed) with nanostructured metal oxide deposits to create a range of selectivities for a number of gases.

The data in Tables 2/2 and 2/3 to correlate the materials positioning indicated in FIG. **2.10**, within especially similar molecular analogs, with a focus to sensor array development. FIG. **2.10** is constructed within the framework of the acid and base character outlined in Table 2/1 considering, to first order, the hard acid strength which we associate with a Ti^{+4} (TiO_2) or Sn^{+4} (SnO_2) configuration, the soft acid strength to be associated with an $Au^{0,+1}$ (Au_xO) configuration, and the intermediate (borderline) acid strength we associate with the porous silicon hybrid surface. Here, the silicon oxidation state (Si_xO_y) is considered to vary from +1 to +4 (Wang et al. 2011). Superimposed relative to this structure, we insert the results outlined in Table 2/2 for the intermediate acid Ni^{+2}, the soft and intermediate acids $Cu^{+1,+2}$ and the comparatively strong acid state with which we associate Al^{+3} (Al_2O_3) to begin to formulate a user's table for the IHSAB principle.

The introduction of the nanostructured metal oxides to the nanoporous PS surface modifies the sensing process by transforming the surface of the chemically sensitive doped PS nanoporous layer. The sensor resistance increases for "basic" gases which are oxidized (NO, CO, NH_3, PH_3, H_2S) on p-type PS. This process is amplified through the interaction of a modified acidic metal oxide surface. If an electron is donated to a p-type PS surface, this process will act to reduce the number of majority carriers (holes) and thus will promote an increase in resistance. In contrast, the interaction of a gas that is reduced on p-type silicon, exemplified by the acidic gas NO_2, removes electrons from the p-type PS surface, increases the majority charge carriers and decreases resistance (FIG. **2.8**) (Gole et al. 2011; Laminack et al. 2012; Ozdemir et al. 2011). In effect, the nanostructures act as antennas to transduce charge. The process is reversed for n-type interfaces.

The process of physisorption (electron transduction) must involve the interaction of high-lying occupied (low lying unoccupied) molecular orbitals of each individual gas. These gases are the electron donors (acceptors) with the electron acceptor (donor), represented by the acidic (basic) metal oxides used to modify the p or n-type PS interface.

This process will differ from gas to gas with changes in the nanostructured deposit. However, the nature of the interaction, as it provides for increased physisorption (electron transduction) and minimizes chemical bond formation (chemisorption), therefore influencing the flow of electrons from a gaseous molecule to the sensor, provides the basis for the observed resistance changes. The presence of a fractional nanostructured oxide coating on the PS surface promotes further interaction with the interface. The process whereby a gas transfers or withdraws electrons as it interacts with that surface will be strongly influenced by the balance of chemical bonding, which greatly inhibits electron flow, and physical absorption, which can facilitate the process.

Given the limits of the system considered, we note the considerable increase in sensitivity inherent to the n-type vs. that observed for the p-type systems. The n-type systems, while displaying quenching at concentrations in excess of 5 ppm, are apparently capable of operation at much lower concentrations than the p-type systems, possibly extending to the low ppb or ppt levels. Concomitantly, the p-type systems appear to provide a linear response to notably higher pressures than do the n-type systems (Gole et al. 2011; Lewis et al. 2007; Lewis et al. 2005). As the pore structure for these systems can be further optimized, the sensitivity ranges can be expanded.

The precise details of the mechanism for the resistance change which appears to be characteristic of virtually all oxidized (increased resistance) and reduced (decrease in resistance), gases on the individually modified hybrid p-type PS interfaces and their counterparts in an n-type system will require further experimentation and modeling. If we, however, consider an appropriate sensor mechanism for interaction with oxide surface subgroups, the fractional nanostructure coating of either a p-type or an n-type sensor is consistent with the changes in resistance that we outline above. Basic analytes will provide an electron to the PS interface whereas acidic analytes will remove an electron, leading to a decrease or increase in the number of majority carriers. This, of course, will affect the observed conductance.

The temperature dependence shown in FIG. 2.5 for both p- and n-type semiconductors indicates that one can expect vacant donor levels for an n-type system and available holes for a p-type system at room temperature (Korotcenkov and Cho 2010). If an analyte acts to add electrons to the vacant donor electron levels of an n-type extrinsic semiconductor, it can be anticipated that the population of these levels will "top-out" and the resistance will reach a limiting lower value. This limit in resistance is likely demonstrated when NO, acting as a base is exposed to the TiO_2 decorated (FIG. 2.12b) n-type PS interface. An analogous decrease to a minimum resistance is observed for the p-type PS system. Where NO_2 extracts electrons and enhances conductance. FIG. 2.8 demonstrates the bottoming-out of the resistance associated with the removal of electrons as would be expected from FIG. 2.5. The outlined results obtained with NO_2 allow us to position this acid in FIG. 2.10.

The outlined correlations associated with FIG. 2.3 point to an additional aspect of the dynamic nature of these systems. The Fermi level is dynamic and the change in the Fermi level energy must be evaluated as we consider processes initiated with extrinsic semiconductor interfaces. This will have significant consequences as one attempts to employ these prepared interfaces in transduction processes which include any type of dynamic electron transfer and, for that matter, solar pumping involving these systems. While many approaches focus on the bandgap when considering inter-

actions associated with an extrinsic semiconductor, this focus lacks appropriate dynamic considerations. The effect of process on energy increments in a dynamic system and especially on the Fermi level should be strongly considered.

Application to Nanowire Configurations

The considerations we have outlined within the IHSAB framework can also be applied to semiconductor nanowire configurations. Li et al. (2010) have recently reported enhanced gas sensing for H_2S by assembling Pd nanoparticles on SnO_2 nanowires (FIG. 2.13). These observations are readily explained within the IHSAB model. The interaction of H_2S, a moderate base, gives up electrons to the n-type SnO_2 nanowire. This process, which increases the majority carrier concentration and the conductance, is made more efficient due to the presence of the weak acid Pd nanoparticle islands. Here, the weak acid (Pd-Table 2/1) interacts with the moderately strong base, H_2S, promoting physisorption (electron transduction) and a more efficient electron transfer.

Kim et al. (2010) have studied gas sensing for O_2 on In_2O_3 nanowires enhanced with Pt nanoparticle depositions. These authors transformed continuous Pt shell layers into cubic Pt nanoparticles deposited to In_2O_3 (FIG. 2.14). "In an O_2 sensing test, the Pt-functionalized In_2O_3 nanowires revealed exceptionally higher sensitivity and faster response than did the bare In_2O_3 nanowires. Here again the IHSAB model explains the experimental observations. The interaction of O_2, a moderate base with p-type In_2O_3 leads to a decrease in conductance. A resultant increase in sensor resistance is again promoted by the weak acid Pt which promotes a "physisorbed" interaction with O_2.

Recently, Kolmakov et al. (2005) studied the response of a Pd-functionalized SnO_2 nanostructure to sequential hydrogen and oxygen pulses at 473 and 543 K (FIG. 2.15). Here, a strong increase in resistance is noted at both temperatures upon hydrogen introduction. No response is observed for oxygen at 473K but a drop in resistance is monitored at 543K. These results can be readily explained within the IHSAB model. The strong acid hydrogen interacts with n-type SnO_2, removing majority carriers and leading to an increase in resistance. At the higher temperatures, the formation of O_2^-, a moderate to strong base, on the SnO_2 surface provides additional electrons to increase conductance, again enhanced by the presence of the weak acid Pd nanostructured islands.

Application to Additional Semiconductors

Finally we should note that the silicon or layers and the porous silicon (PS) structures, devices, and methods, described in the following discussion can be replaced with any alternate extrinsic semiconductor (e.g., GaP, InP, CdTe) onto which a porous microstructure can be generated (Levy-Clement et al. 1994). Further, the configuration in FIG. 2.1 can be adapted to a pass-through microporous membrane. This greatly broadens the range of nanostructure-interface combinations which can be potentially exploited as the alternate extrinsic semiconductors can be a p-type substrate, a p^+-type substrate, or an n-type substrate.

Time Varying Operation and False Positives-Sensing in an Unsaturated Mode

To further improve the sensitivity and stability of the porous silicon sensors, we have developed the method of pulsed system frequency analysis (PSFA). Here, methods of acoustic theory are applied to signal analysis. The benefits of this approach include improved measurement sensitivity, isolation of periodic noise sources, and the ability to evaluate the trade-off between the precision and duration of measurement to aid the design of an experimental system. A

defined gas pulsing technique is combined with FFT signal analysis to allow a sensor gas response to be measured, without saturation, and filtered on a drifting baseline, so as to eliminate false positives and the effects of external noise (as might be associated with pressure, temperature, and humidity variation). FIG. **2.16** depicts a test in which the concentration of ammonia (in N_2) being delivered to the sensor was pulsed between 0 and 5 ppm at a frequency of $\frac{1}{60}$s (0.017 Hz). The baseline for the device increases during the test as the adsorption and desorption of ammonia begin to equilibrate, however, the magnitude of the signal at the beginning and end of the pulsing sequence and throughout the sequence remains virtually the same as we operate in an unsaturated mode. The baseline can also be affected by low frequency changes in temperature and pressure, however, because of the pulsed mode of operation which has been introduced to run all of the sensor systems this drift can be both "locked out" and monitored (Lewis et al. 2007). By introducing an FFT analysis to the reversibly, linearly, responding, PS gas sensor, the gas response can be acquired and filtered on a drifting baseline or in the presence of external noise sources (FIGS. **2.17** and **2.18**).

FIG. **2.17** shows an example of the raw data and the high fidelity outputs after FFT analysis and filtering with the PSFA technique. The benefits of this approach include improved measurement sensitivity, and isolation of periodic noise sources. This technique, closely aligned with the advantages of the PS versus other sensors, does not require stability in the baseline resistance or low thermal sensitivity. With this method, thermal noise, random fluctuations, and long settling times are mitigated. Additional benefits include the ability to detect gas signals when environmental signals are dominant, and the testing time can be greatly reduced. The FFT data analysis method for the PS gas sensor also offers the ability to operate below saturation and provides several safeguards against false positives. If the false positive is associated with the delivered gas, attributes of the "time-delay" module become unstable and the dataset is withdrawn (Lewis et al. 2007).

Sensor Rejuvenation

If a sensor is poisoned due to contamination or extensive exposure to a deleterious component of a gas mixture, which might be a strong acid, it is advantageous to have available a rejuvenation process. In most cases the rejuvenation of a sensor is difficult, at best; however, the simple open structure inherent to the porous silicon sensor facilitates this process. FIG. **2.19** demonstrates the results of a straightforward and repeatable rejuvenation process that can be applied to poisoned sensors (Ozdemir and Gole 2008b). This facilitates their cycling and decreases the long-term expense of a sensor device.

Summary of Sensor Attributes

A correctly developed porous interface sensor has several attributes. (1) its rapid response (~2 s), sensitivity (sub-ppm), and reversibility, (2) its operation at room temperature as well as at stable, readily accessible elevated temperatures with an insensitivity to temperature drift, (3) its potential operation in a heat-sunk configuration allowing reliable performance to a surface temperature of 80° C. even in highly elevated temperature (combustion or flue gas) environments (in sharp contrast to metal oxide sensors), (4) its ease of modification with a diversity of clearly mapped gas-selective nanostructured materials, providing a range of sensitivities for a given gas and the format for sensor arrays, (5) its low cost of fabrication usually with a single nano-structure modification, (6) its ease of operation combining micro- and nanotechnology, (7) its low power consumption (power requirements less than a watch battery), (8) its ease of rejuvenation following contamination, (9) its ability to rapidly assess false positive signals using FFT techniques, operating the sensor in a pulsed gas mode, and (10) its potential for use in the development of solar pumped sensors.

Extension to Phytocatalysis-Enhanced System

Photocatalysts, formed as the nanostructured metal oxides or their modification, can be used to further enhance the activity of the nanopore coated microporous PS interface (FIG. **2.1**) through their interaction with solar radiation. In such a way, the sensor array configurations that we have been developing can be extended to behave as microreactors in which visible light absorbing quantum dot (QD) photo-catalysts are placed within the pores of PS microarray and excited using PS electroluminescence or photolumines-cence. Properly employed, these microreactors might then be used to form "solar pumped" sensors. The quantum dots are exemplified by the highly efficient light absorbing tita-nia-based nanocolloids which we have produced in a nanoscale synthesis at room temperature, (Gole et al. 2004; Kumar et al. 2005; Chen et al. 2005; Gole et al. 2006a; Prokes and Carlos 2005; Lewis et al. 2007; Ogden et al. 2008; Gole, et al. 2010) and that can be nitridated in seconds to produce nitrogen doped, stable, and environmentally benign $TiO_{2-x}N_x$ photocatalysts whose optical response can be tuned across the entire visible region. Tunability through-out the visible is found to depend upon the degree of nanoparticle agglomeration and upon the ready ability to seed the nanoparticles with metals (metal ions) including Pd and additional active dopants including the transition metals (Chen et al. 2005). These photocatalyts are found to readily photodegrade methylene blue and gaseous ethylene. They can also be used to eliminate environmental contaminants.

FIG. **2.20** demonstrates the photocatalytic efficiency of nitrided anatase $TiO_{2-x}N_x$ quantum dots generated using the sol-gel technique and Degussa P25 (Chen et al. 2005), a well-known nanocatalyst. The photodegradation of methyl-ene blue is not only 4 times more efficient than P25 at 390 nm, P25 at 390 nm, but also the nitrided quantum dots show a photocatalytic efficiency in the visible (540 nm) which virtually eclipses that of P25.

It is significant that these oxynitride ($TiO_{2-x}N_x$) quantum dots can be transformed from liquids to gels, and, in addi-tion, can be placed on the PS surface in a sensor-microre-actor based conformation in order to produce a photocata-lytically enhanced "solar pumped sensor" response.

Mixed Gas Format

The sensors which we have outlined, operated for iden-tification of a given analyte can be made to function in an array-based format on the bases of a row matrix response to a given analyte. They can be operated in a mixed gas format, creating a sensor array matrix. Sensor array selectivity is another very important sensor operating characteristic which must be demonstrated. However, we exemplify the inherent selectivity that a nano/microporous surface can display in a mixed gas configuration in FIG. **2.19**. Here, with an untreated PS interface (even before treatment with Au_xO nanostructures), the analysis for 1 and 3 ppm NH_3 can be carried out in the presence of 20 ppm NO_x (Lewis et al. 2005). We note that the introduction of an Au_xO nanostruc-tured deposit can considerably improve the relative sensi-tivity to ammonia and that the introduction of a SnO_x nanostructured deposit leads to a substantial increase in NO sensitivity. These three sensors, in tandem, produce three distinct responses to an NH_3+NO mixture.

Comparison of Some Embodiments to Alternate Technologies

One can compare (Ozdemir et al. 2011) the positive aspects of an embodiment of the sensor platform with competing and complementary technologies that are currently available or in the process of becoming available. The two main sensor technologies are (1) Electrochemical based, and (2) Metal Oxide based sensors. Each of these technologies have unique advantages, however, both are also plagued with drawbacks. For example, electrochemical sensors are known for low power operation, rapid response, and insensitivity to humidity; but they have poor sensitivity and are inherently complex and expensive to produce and replace.

The metal oxide sensors (FIG. **2.22**), when compared to electrochemical sensors are slightly less costly to produce, but are still significantly more complex than the technology that we propose. However, the main drawbacks of the metal oxide sensor include low sensitivity, poor selectivity, high power requirements, and most importantly, the need to operate at elevated temperatures. The latter requirement is a major drawback for several reasons. First, a power consuming heating element must be provided with the sensor housing to precisely control the temperature of the sensor element. This is, in large part, intimately tied to the correct identification of the gas of interest. A formaldehyde sensor will operate at one temperature whereas an ethanol sensor will operate at another. Otherwise the devices are virtually identical. Distinguishing one gas from another thus requires that the heating element and sensor be well separated (channel) from the remaining electronics. This in turn means that this configuration can be greatly affected by an impinging combustion or flue gas, rendering moot the correct identification of gaseous species in the flow. In contrast the PS sensor configuration depicted in FIG. **2.1** is far simpler and does not require the complexity of a system separated sensor/heater configuration. In a heat sunk environment, it is potentially capable of operation in a high temperature gas flow. This simplicity and capability of operation thus represents a revolutionary change. Further, the attributes of an extrinsic semiconductor technology developed by combining array generation through the coupling of acid/base chemistry with the properties of extrinsic semiconductors suggests a general road map for array development, and the importance of further understanding the nuances of this process. We provide an important element to combine with well-developed fabrication and CMOS technologies that greatly simplifies device fabrication and costs relative to optical technologies.

Chemisorption and the Analog of the HSAB Principle

As the IHSAB model applies to the general development of a sensor interface so to does an extrapolation of the HSAB model apply to the development of a Microreactor model. However, in order to develop the model it is necessary to modify the interface of FIG. **2.1** so that it is more compatible with microreactor design. This dictates that one attempt to develop flow-through configurations. It is significant that the oxynitride ($TiO_{2-x}N_x$) quantum dots which we have previously discussed can be transformed from liquids to gels, and, in addition, can be placed on the PS surface in a sensor-microreactor based conformation to produce a photocatalytically enhanced "solar pumped sensor" response. Of possibly greater importance to microreactor applications is a recently developed microfilter configuration (Campbell et al. 2008; Gole et al. 2009). This technology represents the first single step etch-liftoff procedure (one step separation) which allows the removal of macroporous PS layers. FIG. **2.23** demonstrates that filters with pore diameters ranging from 1

to 2 microns and thickness from 3 to 70 micrometers have been produced. These silicon-based filters carry a polarizing negative charge and represent an alternative to porous alumina films (pore diameter not yet in the one to three micron range) with a capability for operating at significantly elevated temperatures as compared to polymer films. Pt and Cu have been introduced to these filters to create an effective reducing surface.

Physisorption (Electron Transduction) Versus Chemisorption

In developing sensor and microreactor configurations using the IHSAB and HSAB concepts one need be continuously mindful of the dynamics of interaction as the process of electron transfer takes place. FIG. **2.24** demonstrates the effect which the strong acid SnO_x has on the NO_2 interaction with the PS interface (Laminack et al. 2012). Here, both an acidic analyte and the nanostructure modified PS interface compete for electrons. If NO_2 and SnO_x compete effectively for electrons, the competition might be expected to diminish the sensitivity of the interface and influence physisorption (electron transduction) as measured by a significant resistance change. One does observe a muted response after. However, the weak and diffuse nature of the observed response after SnO_x treatment suggests that it is equally likely to be the result of the strong influence of chemisorption. While NO_2 is a moderate acid, NO_2^-, which can be formed as NO_2 extracts an electron from the n-type PS interface, corresponds to a moderate to strong base. Table 2/1 suggests that an n-type PS surface corresponds to a borderline acidic surface. For this reason, one might expect a chemical interaction (chemisorption) with NO_2 and NO_2^- as dictated by the IHSAB/HSAB principle to be of only moderate effect. If, however, the PS surface is treated with nanostructured SnO_x, it is possible to obtain a strong chemical interaction between this strong acid and NO_2^-. The muted and diffuse response with concentration in FIG. **2.24***b* may signal this chemisorption. It is to be emphasized that the base strength of NO_2^- and the acid strength of SnO_x are much more closely matched than those of either the much stronger acid, TiO_2, or the weaker acids Cu_xO and Au_xO. Thus (Gole and Ozdemir 2010) one anticipates a chemisorptive interaction.

REFERENCES

Each is Incorporated Herein by Reference

Andzelm J. (ed.) (1991) *Density Functional Methods in Chemistry*. Springer-Verlag, New York

Campbell J., Como J. A., Larsen N. and Gole J. L. (2008) Development of porous-silicon-based active microfilters. *J. Electrochem. Soc.* 155, D128-D132; DOI 10.1149/1.2811868

Chen X., Lou Y., Samia A. C. S., Burda C. and Gole J. L. (2005). Formation of oxynitride as the photocatalytic enhancing site in nitrogen-doped titania nanocatalysts: comparison to a commercial nanopowder. *Adv. Funct. Mater.* 15, 41-49; DOI: 10.1002/adfm.200400184

Cohen M. H. and Wasserman A. (2007). On the foundations of chemical reactivity theory. *J. Phys. Chem. A* 111, 2229-2242; DOI: 10.1021/jp066449h

Dixon D. A. and Gole J. L. (1997). Suggested correlation between the visible photoluminescence and the fourier transform infrared spectrum of a porous silicon surface. *J. Phys. Chem. B* 101, 8098-8102; DOI: 10.1021/jp971177r.

Dixon D. A. and Gole J. L. (2005). Time dependent density functional theory predictions of the vertical excitation

49

energies of silanones as models for the excitation process in porous silicon. *J. Phys. Chem. B* 109, 14830-14835; DOI: 10.1021/jp050538x

Dixon D. A. (2010) Private discussions

Ervin K. M., Ho J. and Lineberger W. C. (1988). Ultraviolet photoelectron spectrum of nitrite anion. *J. Phys. Chem.* 92, 5405-5412; DOI: 10.1021/j100330a017.

Foell H., Christophersen M., Carstenson J. and Hasse G. (2002). Formation and application of porous silicon. *Mater. Sci. Eng. R.* 280, 1-49;

Foucaran A., Pascal-Delannoy F., Giani A., Sackda A., Commette P. and Boyer P. (1997) Porous silicon layers used for gas sensor applications. *Thin Solid Films.* 297, 317-320; http://dx.doi.org/10.1016/S0040-6090(96)09437-0

Fukui K., Yonezawa T. and Shingu H. (1952) A molecular orbital theory of reactivity in aromatic hydrocarbons. *J. Chem. Phys.* 20, 722-725 DOI:10.1063/1.1700523

Geerlings P., De Proft F. and Langenaeker W. (2003) Conceptual density functional theory. *Chem. Rev.* 103, 1793-1874; DOI: 10.1021/cr990029p.

Gole J. L., Dudel F. P., Grantier D. and Dixon D. A. (1997) "Origin of porous silicon photoluminescence: evidence for a surface bound oxyhydride-like emitter," *Phys. Rev. B.* 56, 2137-2153; DOI:10.1103/PhysRevB.56.2137

Gole J. L. and Dixon D. A. (1998a) Potential role of silanone and silylenes in the photoluminescence-excitation, visible-photoluminescence-emission, and infrared spectra of porous silicon, *Phys. Rev. B.* 57, 12002-12016; DOI: 10.1103/PhysRevB.57.12002

Gole J. L. and Dixon D. A. (1998b) "Electrochemical methoxylation of an HF-etched porous silicon surface," *J. Phys. Chem. B.* 102, 1768-1774; DOI: 10.1021/jp980140j

Gole J. L. and Dixon D. A. (1998c) "Evidence for oxide formation from single and multiphoton excitation of a porous silicon surface or silicon nanoparticles", *J. Appl. Phys.* 83, 5985-5990; doi:10.1063/1.367464

Gole J. L. and Dixon D. A., (2000) "Isomerization of fluorophors on a treated silicon surface," *J. Phys. Chem. B.* 104, 1777-1782; DOI: 10.1021/jp9933469

Gole J. L., Fedorov A. G., Hesketh P. and Burda C. (2004) From nanostructures to porous silicon: sensors and photocatalytic reactors. *Phys. Stat. Sol. C.* 1(S2), S188-197; DOI: 10.1002/pssc.200405139

Gole J. L., Stout J., Burda C., Lou Y. and Chen X. (2004). Highly efficient formation of visible light tunable $TiO_{2-x}N_x$ photocatalysts and their transformation at the nanoscale. *J. Phys. Chem. B.* 108, 1230-1240; DOI: 10.1021/jp030843n

Gole J. L., Prokes S. M., Stout J. D., Glembocki O. J. and Yang R. (2006a) Unique properties of selectively formed ZrO_x nanostructures—light enhancement from a metal oxide. *Adv. Mater.* 18, 664-667; DOI: 10.1002/adfm.200400184

Gole J. L., Veje, E., Egeberg, R. G., Ferreira da Silva A., Pepe I. and Dixon D. A. (2006b) Optical analysis of the light emission from porous silicon: a hybrid polyatom surface-coupled fluorophor, *J. Phys. Chem. B.* 110, 2064-2073; DOI: 10.1021/jp0555302

Gole J. L., Lewis S., and Lee S. (2007) Nanostructures and porous silicon: activity at interfaces in sensors and photocatalytic reactors. *Phys. Stat. Solids (a).* 204(5), 1417-1422; DOI: 10.1002/pssa.200674369

Gole J. L., Ozdemir S., Prokes S, and Shin H-C. (2009) Active microfiltered sensor interfaces, photocatalytic

50

reactors, and microbatteries using combined micro/nano-porous interfaces. *Phys. Stat. Solid.* 6, 1773-1776; DOI: 10.1002/pssc.200881009

Gole J. L., Prokes S. M., Qiu X., Burda C. and Glembocki O. J. (2010) Study of concentration-dependent cobalt ion doping of TiO_2 and $TiO_{2-x}N_x$ at the nanoscale. *Nanoscale.* 2, 1134-40; DOI: 10.1039/c0nr00125b

Gole J. L. and Ozdemir S. (2010). Nanostructure directed physisorption vs. chemisorption at semiconductor interfaces: the inverse of the hard-soft acid-base (HSAB) concept. *Chem Phys Chem.* 11, 2573-2581; DOI: 10.1002/cphc.201000245

Gole J. L., Goude E. C. and Laminack W. (2012) Nanostructure driven analyte-interface electron transduction: a general approach to sensor and microreactor design. *Chem Phys Chem.* 13(2), 549-561; DOI: 10.1002/cphc.201100712

Grant D. J., Matus M. H., Anderson K. D., Camaioni D. M., Neufeldt S., Lane C. F. and Dixon D. A. (2009) Thermochemistry for the dehydrogenation of methyl-substituted ammonia borane compounds. *J. Phys. Chem. A.* 113, 6121-6132. DOI: 10.1021/jp902196d

Grant G. H. and Richards W. G. (1995) *Computational Chemistry.* Oxford University Press, Oxford.

Hehre W. J., Radom L., Schleyer P. R. and Pople J. A. (1986) *Ab Initio Molecular Orbital Theory.* John Wiley and Sons, New York.

Hirst D. M. (1990) *A Computational Approach to Chemistry.* Blackwell Scientific, Oxford.

Huheey J. E. (1978) *Inorganic Chemistry.* 2nd ed. Harper and Row, New York.

Kim S. S., Park S. Y., Choi S-W., Kim H. S., Na H. A., Yang J. C. and Kim H. W. (2010) Significant enhancement of the sensing characteristics of In_2O_3 nanowires by functionalization with Pt nanoparticles. *Nanotechnology.* 21(41) 1-7; DOI:10.1088/0957-4484/21/41/415502

Kolmakov A., Klenov D. O., Lilach L., Stemmer S, and Moskovitz M. (2005) Enhanced gas sensing by individual SnO_2 nanowires and nanobelts functionalized with Pd catalyst particles. *Nanoletters.* 5, 667-673; DOI: 10.1021/nl050082v

Korotcenkov G. and Cho B. K. 2010) Porous Semiconductors: Advanced Material for Gas Sensor Applications. *Crit. Rev. Solid St. Mater. Sci.* 35(1), 1-37; DOI 10.1080/10408430903245369

Kottke P. A. Fedorov A. G. and Gole J. L. (2009) Multiscale mass transport in porous silicon gas sensors. In: Schlesinger M. (ed.) *Modern Aspects of Electrochemistry*, Vol. 43. Springer, New York, N.Y., 139-168; http://dx.doi.org/10.1007/978-0-387-49582-8

Kumar S., Fedorov A. G. and Gole J. L. (2005) Photodegradation of ethylene using visible light responsive surfaces prepared from titania nanoparticle slurries. *Appl. Catal. B.* 57, 93-107; http://dx.doi.org/10.1016/j.apcatb.2004.10.012

Laminack W., Pouse N. and Gole J. L. (2012) The dynamic interaction of NO_2 with a nanostructure modified porous silicon matrix: the competition for donor level electrons. *J. Electrochem. Soc.* submitted

Lévy-Clément C. (2002) Encyclopedia of Electrochemistry Chapter 3.2, Semiconductor electrodes and photoelectrochemistry, S. Licht, Editor, ISBN 3-527-30250-6 (Vol. 6 in"Encyclopedia on Electrochemistry," A. Bard, Series Editor), WILEY-VCH, Weinheim, Germany

Levy-Clement C., Lagoubi A., and Tomkiewicz M. (1994) Morphology of porous n+ type silicon obtained by pho-

toelectrochemical etching. *J. Electrochem. Soc.* 141, 958-967; http://dx.doi.org/10.1149/1.205f65

Lewis S. E., DeBoer J. R., Gole J. L., and Hesketh P. J. (2005) Sensitive, selective, and analytical improvements to a porous silicon gas sensor. *Sens. Actuators B.* 110, 54-65; http://dx.doi.org/10.1016/j.snb.2005.01.014

Lewis S. E., DeBoer J. R., and Gole J. L. (2007) Pulsed system frequency analysis for device characterization and experimental design. *Sens. Actuators B.* 122(1), 20-29; http://dx.doi.org/10.1016/j.snb.2006.04.113

Li H., XU J., Zhu Y., Chen X., and Xiang X. (2010) Enhanced gas sensing by assembling Pd nanoparticles onto the surface of SnO_2 nanowires. *Talanta.* 82, 458-463; http://dx.doi.org/10.1016/j.talanta.2010.04.053

Moseley P. T. (1997) Solid state gas sensors. *Meas. Sci. Technol.* 8, 223-237; doi:10.1088/0957-0233/8/3/003

Nassiopoulos A. G. (1997) Local formation and patterning of porous silicon. In: Canham L. (ed.), *Properties of Porous Silicon.* IEE-Books, London, 77-80.

NIST (2003) X-ray Photoelectron Spectroscopy Database, Version 3.5 National Institute of Standards and Technology, Gaithersburg, (http://srdata.nist.gov/xps/).

Ogden A., Fedorov A., Hong J., and Gole J. L. (2008) Maintaining particle size in the transformation of anatase to rutile titania nanostructures. *J. Phys. & Chem. of Solids,* 69, 2898-2906; DOI: 10.1016/j.jpcs.2008.07.016

Ozdemir S. and Gole J. L. (2008a) The potential of porous silicon gas sensors. *Currents opinions in Solid State and materials Science.* 11, 92-100; DOI: 10.1016/j.cossms.2008.06.003

Ozdemir S, and Gole J. L. (2008b) Porous silicon gas sensors for room temperature detection of ammonia and phosphine. Chemical Sensors 8: Chemical (Gas, Ion, Bio) Sensors and Analytical Systems, *ECS Transactions,* 16(11), 379-387; ISBN 1566776570, 9781566776578

Ozdemir S. and Gole J. L. (2010a) A phosphine detection matrix using nanostructure modified porous silicon gas sensors. *Sens. Actuators B.* 151, 274-280; http://dx.doi.org/10.1016/j.snb.2010.08.016

Ozdemir S, and Gole, J. L. (2010b) Gas transport and response in porous silicon sensors. Materials Research Society Spring Meeting, Apr. 5-9, 2010, San Francisco, Abstract K5.33.

Ozdemir S., Osburn T. and Gole J. L. (2011) Transient conversion of NO to NO_2 on a nanostructure modified porous silicon gas sensor detection matrix *J. Electrochem. Soc.* 158(7), J201-J207; http://dx.doi.org/10.1149/1.3583368

Parr R. G., Donnelly A. A., Levy M. and Palke W. E. (1978) Electronegativity: the density functional viewpoint *J. Chem. Phys.* 68, 3801-3807; DOI: 10.1063/1.436185

Parr R. G. and Pearson R. G. (1983) Absolute hardness: companion parameter to absolute electronegativity. *J. Am. Chem. Soc.* 105, 7512-7516. DOI: 10.1021/ja00364a005

Parr R. G. and Yang W. (1989) *Density functional theory of atoms and molecules.* Oxford University Press, New York.

Pearson R. G. (1963) Hard and soft acids and bases. *J. Am. Chem. Soc.* 85, 3533-3539; DOI: 10.1021/ja00905a001

Pearson R. G. (1988) Absolute electronegativity and hardness: application to inorganic chemistry. *Inorg. Chem.* 27, 734-740; DOI: 10.1021/ic00277a030

Pearson R. G. (1990) Hard and soft acids and bases—the evolution of a chemical concept. *Coord. Chem. Rev.* 100, 403-425; DOI 10.1016/0010-8545(90)85016-L

Pearson R. G. (1997) *Chemical hardness.* Wiley-VCH, Weinheim.

Pearson R. G. (2005) Chemical hardness and density functional theory. *J. Chem. Sci.* 117, 369-377; DOI: 10.1007/BF02708340

Politzer P. (1987) A relationship between the charge capacity and the hardness of neutral atoms and groups. *J. Chem. Phys.* 86, 1072; doi:10.1063/1.452296

Prokes S. M. and Carlos W. E. (2005) Defect related optical behavior in surface modified TiO_2 nanostructures. *Adv. Funct. Mater.* 15, 161-167; DOI: 10.1002/adfm.200305109

Rudden M. N. and J. Wilson (eds.) (1993) *Elements of solid state physics.* John Wiley and Sons, New York, N.Y.

Schechter I., Ben-Chorin M. and Kux A. (1995) Gas sensing properties of porous silicon. *Anal. Chem.* 67, 3727-3732; DOI: 10.1021/ac00116a018

Seals L., Tse L. A., Hesketh P. J. and Gole J. L. (2002) Rapid, reversible, sensitive porous silicon gas sensor *J. Appl. Phys.,* 91, 2519-2523; doi:10.1063/1.1436556

Travers M. J, Cowles D. C. and Ellison G. B. (1989) Reinvestigation of the electron affinities of O_2 and NO *Chem. Phys. Lett.* 164, 449-455. http://dx.doi.org/10.1016/0009-2614(89)85237-6

Wang T., Gole J. L., White M. G., Watkins C., Street S. C., Fang Z. and Dixon D. A. (2011) The surprising average oxidation state of fumed silica and the nature of water binding to the silicon oxides and hydroxides, *Chem. Phys. Lett.* 501, 159-165 http://dx.doi.org/10.1016/j.cplett.2010.11.013

Yang W., Parr R. G. and Pucci R. (1984) Electron density, Kohn-Sham frontier orbitals, and Fukui functions *J. Chem. Phys.* 81, 2862-2863; DOI: 10.1063/1.447964

Yang W. and Parr R. G. (1985) Hardness, softness, and the Fukui function in the electronic theory of metals and catalysis *Proc. Natl. Acad. Sci.* USA 82, 6723-6726

Zhan, C. G., Nichols J. A. and Dixon D. A. (2003) Ionization potential, electron affinity, electronegativity, hardness, and electron excitation energy: molecular properties from density functional theory orbital energies. *J. Phys. Chem.* A 107, 4184-4195; DOI: 10.1021/jp0225774

Ziegler T. (1991) Approximate density functional theory as a practical tool in molecular energetics and dynamics. *Chem. Rev.* 91, 651-667; DOI: 10.1021/cr00005a001.

It should be noted that ratios, concentrations, amounts, and other numerical data may be expressed herein in a range format. It is to be understood that such a range format is used for convenience and brevity, and thus, should be interpreted in a flexible manner to include not only the numerical values explicitly recited as the limits of the range, but also to include all the individual numerical values or sub-ranges encompassed within that range as if each numerical value and sub-range is explicitly recited. To illustrate, a concentration range of "about 0.1% to about 5%" should be interpreted to include not only the explicitly recited concentration of about 0.1 wt % to about 5 wt %, but also include individual concentrations (e.g., 1%, 2%, 3%, and 4%) and the sub-ranges (e.g., 0.5%, 1.1%, 2.2%, 3.3%, and 4.4%) within the indicated range. In an embodiment, the term "about" can include traditional rounding based on numerical value and the measurement techniques. In addition, the phrase "about 'x' to 'y'" includes "about 'x' to about 'y'".

It should be emphasized that the above-described embodiments of the present disclosure are merely possible examples of implementations, and are set forth only for a clear understanding of the principles of the disclosure. Many variations and modifications may be made to the above-described embodiments of the disclosure without departing substantially from the spirit and principles of the disclosure.

All such modifications and variations are intended to be included herein within the scope of this disclosure.

The invention claimed is:

1. A device, comprising:
a conductometric porous silicon gas sensor including a n-type silicon substrate having a porous silicon layer, wherein the n-type silicon substrate is an n^+-type silicon substrate, wherein a plurality of nanostructures are disposed on a portion of the porous silicon layer, wherein the conductometric porous silicon gas sensor is operative to transduce the presence of a gas into an impedance change, wherein the impedance change correlates to the gas concentration.

2. The device of claim 1, wherein the nanostructure provides a fractional coverage on the porous silicon layer.

3. The device of claim 2, wherein the nanostructure is a metal oxide.

4. The device of claim 2, wherein the nanostructure is selected from the group consisting of: tin (Sn), chromium (Cr), iron (Fe), nickel (Ni), silver (Ag), titanium (Ti), cobalt (Co), zinc (Zn), platinum (Pt), palladium (Pd), osmium (Os), gold (Au), lead (Pb), iridium (Ir), molybdenum (Mo), vanadium (V), aluminum (Al), an oxide of each of these, and a combination thereof.

5. The device of claim 2, wherein the nanostructure is selected from the group consisting of: aluminum oxide (Al_2O_3, AlO_2), silicon oxide (SiO_x, x is 1 to 4), tin oxide (SnO_x, x is 2 to 4), chromia (Cr_2O_3), iron oxide (Fe_2O_3, Fe_3O_4, or FeO), nickel oxide (NiO), silver oxide (AgO), titanium oxide (TiO_2), cobalt oxide (Co_2O_3, Co_3O_4, or CoO), zinc oxide (ZnO), platinum oxide (PtO), palladium oxide (PdO), vanadium oxide (VO_2), molybdenum oxide (MoO_2), lead oxide (PbO), titanium oxide (TiO_{2-x}, x is 1 to 2), titanium nitride (TiN_1), titanium oxinitride ($TiO_{2-x}N_x$), gold oxide (Au_xO, x>>1), copper oxide (Cu_xO, x is 1 to 2), and a combination thereof.

6. The device of claim 2, wherein the nanostructure is selected from the group consisting of: tin oxide (SnO_x, x is 2 to 4), nickel oxide (NiO), titanium oxide (TiO_2), titanium oxide (TiO_x, x is 1 to 2), titanium nitride (TiN_1), titanium oxinitride ($TiO_{2-x}N_x$), gold oxide (Au_xO, x>>1), copper oxide (Cu_xO, x is 1 to 2), and a combination thereof.

7. The device of claim 6, wherein the nanostructure is a nanoparticle.

8. The device of claim 1, wherein the porous silicon region has a hybrid microporous/nanoporous framework, wherein the walls of the microporous framework are superimposed with a nanoporous layer.

9. The device of claim 8, wherein the macroporous framework includes pores approximately 1 to 2 μm wide and 0.5 to 20 μm deep.

10. The device of claim 1, wherein the conductometric porous silicon gas sensor is operative to measure the impedance change corresponding to a gas concentration at less than 100 parts per billion.

11. The device of claim 1, wherein the conductometric porous silicon gas sensor is operative to measure the impedance change at room temperature.

12. The device of claim 1, further comprising a p-type conductometric porous silicon gas sensor.

13. The device of claim 1, further comprising an array of n-type conductometric porous silicon gas sensors and p-type conductometric porous silicon gas sensors.

14. A method of detecting a concentration of a gas, comprising:
providing a conductometric porous silicon gas sensor including a n-type silicon substrate having a porous

silicon layer, wherein a plurality of nanostructures are disposed on a portion of the porous silicon layer, wherein the conductometric porous silicon gas sensor is operative to transduce the presence of a gas into an impedance change, wherein the impedance change correlates to the gas concentration;
introducing the gas to the sensor; and
measuring an impedance change in the sensor at room temperature.

15. The method of claim 14, wherein measuring includes obtaining an impedance value from an impedance analyzer.

16. The method of claim 14, wherein measuring includes obtaining a resistive value from a sensor and shunt circuit.

17. The method of claim 14, further comprising: correlating the impedance change to the concentration of the gas.

18. The method of claim 17, wherein correlating includes computing a magnitude of the impedance change, computing the time over which the magnitude of the impedance change occurs, and computing a slope from the ratio of the magnitude of the impedance change and the time to determine the concentration of the gas.

19. A device, comprising:
a conductometric gas sensor including a n-type substrate having a porous layer, wherein a plurality of nanostructures are disposed on a portion of the porous layer, wherein the nanostructure provides a fractional coverage on the porous layer, wherein the conductometric gas sensor is operative to transduce the presence of a gas into an impedance change, wherein the impedance change correlates to the gas concentration, wherein the n-type substrate is selected from the group consisting of: n- or n^+-type doped wafer and n- or n^+-type phosphorous doped wafer.

20. The device of claim 19, wherein the n-type substrate is an extrinsic n-type semiconductor.

21. The device of claim 19, wherein the n-type substrate is selected from the group consisiting of: silicon, GaP, InP, and CdTe.

22. The device of claim 19, wherein the nanostructure is a metal oxide.

23. The device of claim 22, wherein the nanostructure is selected from the group consisting of: tin (Sn), chromium (Cr), iron (Fe), nickel (Ni), silver (Ag), titanium (Ti), cobalt (Co), zinc (Zn), platinum (Pt), palladium (Pd), osmium (Os), gold (Au), lead (Pb), iridium (Ir), molybdenum (Mo), vanadium (V), aluminum (Al), an oxide of each of these, and a combination thereof.

24. The device of claim 19, further comprising a p-type conductometric porous silicon gas sensor.

25. The device of claim 19, further comprising an array of n-type conductometric porous silicon gas sensors and p-type conductometric porous silicon gas sensors.

26. A device, comprising:
a conductometric porous silicon gas sensor including a n-type silicon substrate having a porous silicon layer, wherein a plurality of nanostructures are disposed on a portion of the porous silicon layer, wherein the conductometric porous silicon gas sensor is operative to transduce the presence of a gas into an impedance change, wherein the impedance change correlates to the gas concentration, wherein the porous silicon region has a hybrid microporous/nanoporous framework, wherein the walls of the microporous framework are superimposed with a nanoporous layer.

27. The device of claim **26**, wherein the macroporous framework includes pores approximately 1 to 2 μm wide and 0.5 to 20 μm deep.

28. The device of claim **26**, wherein the nanostructure provides a fractional coverage on the porous silicon layer.

29. The device of claim **26**, wherein the nanostructure is selected from the group consisting of: tin (Sn), chromium (Cr), iron (Fe), nickel (Ni), silver (Ag), titanium (Ti), cobalt (Co), zinc (Zn), platinum (Pt), palladium (Pd), osmium (Os), gold (Au), lead (Pb), iridium (Ir), molybdenum (Mo), vanadium (V), aluminum (Al), an oxide of each of these, and a combination thereof.

30. The device of claim **26**, wherein the conductometric porous silicon gas sensor is operative to measure the impedance change corresponding to a gas concentration at less than 100 parts per billion.

31. The device of claim **26**, wherein the conductometric porous silicon gas sensor is operative to measure the impedance change at room temperature.

32. A device, comprising:
a conductometric porous silicon gas sensor including a n-type silicon substrate having a porous silicon layer, wherein a plurality of nanostructures are disposed on a portion of the porous silicon layer,
wherein the conductometric porous silicon gas sensor is operative to transduce the presence of a gas into an impedance change, wherein the impedance change correlates to the gas concentration,
wherein the conductometric porous silicon gas sensor is operative to measure the impedance change corresponding to a gas concentration at less than 100 parts per billion.

33. The device of claim **32**, wherein the porous silicon region has a hybrid microporous/nanoporous framework, wherein the walls of the microporous framework are superimposed with a nanoporous layer.

34. The device of claim **32**, wherein the nanostructure provides a fractional coverage on the porous silicon layer.

35. The device of claim **32**, wherein the nanostructure is selected from the group consisting of: tin (Sn), chromium (Cr), iron (Fe), nickel (Ni), silver (Ag), titanium (Ti), cobalt (Co), zinc (Zn), platinum (Pt), palladium (Pd), osmium (Os), gold (Au), lead (Pb), iridium (Ir), molybdenum (Mo), vanadium (V), aluminum (Al), an oxide of each of these, and a combination thereof.

36. The device of claim **32**, wherein the conductometric porous silicon gas sensor is operative to measure the impedance change corresponding to a gas concentration at less than 100 parts per billion.

37. The device of claim **32**, wherein the conductometric porous silicon gas sensor is operative to measure the impedance change at room temperature.

38. A device, comprising:
a conductometric porous silicon gas sensor including a n-type silicon substrate having a porous silicon layer, wherein a plurality of nanostructures are disposed on a portion of the porous silicon layer,
wherein the conductometric porous silicon gas sensor is operative to transduce the presence of a gas into an impedance change, wherein the impedance change correlates to the gas concentration,
wherein the conductometric porous silicon gas sensor is operative to measure the impedance change at room temperature.

39. The device of claim **38**, wherein the porous silicon region has a hybrid microporous/nanoporous framework,

wherein the walls of the microporous framework are superimposed with a nanoporous layer.

40. The device of claim **38**, wherein the nanostructure provides a fractional coverage on the porous silicon layer.

41. The device of claim **38**, wherein the nanostructure is selected from the group consisting of: tin (Sn), chromium (Cr), iron (Fe), nickel (Ni), silver (Ag), titanium (Ti), cobalt (Co), zinc (Zn), platinum (Pt), palladium (Pd), osmium (Os), gold (Au), lead (Pb), iridium (Ir), molybdenum (Mo), vanadium (V), aluminum (Al), an oxide of each of these, and a combination thereof.

42. The device of claim **38**, wherein the conductometric porous silicon gas sensor is operative to measure the impedance change corresponding to a gas concentration at less than 100 parts per billion.

43. A device, comprising:
a conductometric gas sensor including a n-type substrate having a porous layer, wherein a plurality of nanostructures are disposed on a portion of the porous layer, wherein the nanostructure provides a fractional coverage on the porous layer,
wherein the conductometric gas sensor is operative to transduce the presence of a gas into an impedance change, wherein the impedance change correlates to the gas concentration,
wherein the conductometric porous silicon gas sensor is operative to transduce the presence of a gas into an impedance change, wherein the impedance change correlates to the gas concentration.

44. The device of claim **43**, wherein the n-type substrate is an extrinsic n-type semiconductor.

45. The device of claim **43**, wherein the n-type substrate is selected from the group consisiting of: silicon, GaP, InP, and CdTe.

46. The device of claim **43**, wherein the n-type substrate is selected from the group consisting of: n- or n^+-type doped wafer and n- or n^+-type phosphorous doped wafer.

47. The device of claim **43**, wherein the nanostructure is selected from the group consisting of: tin (Sn), chromium (Cr), iron (Fe), nickel (Ni), silver (Ag), titanium (Ti), cobalt (Co), zinc (Zn), platinum (Pt), palladium (Pd), osmium (Os), gold (Au), lead (Pb), iridium (Ir), molybdenum (Mo), vanadium (V), aluminum (Al), an oxide of each of these, and a combination thereof.

48. A device, comprising:
a conductometric gas sensor including a n-type substrate having a porous layer, wherein a plurality of nanostructures are disposed on a portion of the porous layer, wherein the nanostructure provides a fractional coverage on the porous layer,
wherein the conductometric gas sensor is operative to transduce the presence of a gas into an impedance change, wherein the impedance change correlates to the gas concentration,
wherein the porous silicon region has a hybrid microporous/nanoporous framework, wherein the walls of the microporous framework are superimposed with a nanoporous layer.

49. The device of claim **48**, wherein the n-type substrate is an extrinsic n-type semiconductor.

50. The device of claim **48**, wherein the n-type substrate is selected from the group consisiting of: silicon, GaP, InP, and CdTe.

51. The device of claim **48**, wherein the n-type substrate is selected from the group consisting of: n- or n^+-type doped wafer and n- or n^+-type phosphorous doped wafer.

52. The device of claim **48**, wherein the nanostructure is selected from the group consisting of: tin (Sn), chromium (Cr), iron (Fe), nickel (Ni), silver (Ag), titanium (Ti), cobalt (Co), zinc (Zn), platinum (Pt), palladium (Pd), osmium (Os), gold (Au), lead (Pb), iridium (Ir), molybdenum (Mo), vanadium (V), aluminum (Al), an oxide of each of these, and a combination thereof.

53. A device, comprising:

a conductometric gas sensor including a n-type substrate having a porous layer, wherein a plurality of nanostructures are disposed on a portion of the porous layer, wherein the nanostructure provides a fractional coverage on the porous layer,

wherein the conductometric gas sensor is operative to transduce the presence of a gas into an impedance change, wherein the impedance change correlates to the gas concentration,

wherein the conductometric porous silicon gas sensor is operative to measure the impedance change corresponding to a gas concentration at less than 100 parts per billion.

54. The device of claim **53**, wherein the n-type substrate is an extrinsic n-type semiconductor.

55. The device of claim **53**, wherein the n-type substrate is selected from the group consisiting of: silicon, GaP, InP, and CdTe.

56. The device of claim **53**, wherein the n-type substrate is selected from the group consisting of: n- or n$^+$-type doped wafer and n- or n$^+$-type phosphorous doped wafer.

57. The device of claim **53**, wherein the nanostructure is selected from the group consisting of: tin (Sn), chromium (Cr), iron (Fe), nickel (Ni), silver (Ag), titanium (Ti), cobalt (Co), zinc (Zn), platinum (Pt), palladium (Pd), osmium (Os),

gold (Au), lead (Pb), iridium (Ir), molybdenum (Mo), vanadium (V), aluminum (Al), an oxide of each of these, and a combination thereof.

58. A device, comprising:

a conductometric gas sensor including a n-type substrate having a porous layer, wherein a plurality of nanostructures are disposed on a portion of the porous layer, wherein the nanostructure provides a fractional coverage on the porous layer,

wherein the conductometric gas sensor is operative to transduce the presence of a gas into an impedance change, wherein the impedance change correlates to the gas concentration,

wherein the conductometric porous silicon gas sensor is operative to measure the impedance change at room temperature.

59. The device of claim **58**, wherein the n-type substrate is an extrinsic n-type semiconductor.

60. The device of claim **58**, wherein the n-type substrate is selected from the group consisiting of: silicon, GaP, InP, and CdTe.

61. The device of claim **58**, wherein the n-type substrate is selected from the group consisting of: n- or n$^+$-type doped wafer and n- or n$^+$-type phosphorous doped wafer.

62. The device of claim **58**, wherein the nanostructure is a metal oxide.

63. The device of claim **58**, wherein the nanostructure is selected from the group consisting of: tin (Sn), chromium (Cr), iron (Fe), nickel (Ni), silver (Ag), titanium (Ti), cobalt (Co), zinc (Zn), platinum (Pt), palladium (Pd), osmium (Os), gold (Au), lead (Pb), iridium (Ir), molybdenum (Mo), vanadium (V), aluminum (Al), an oxide of each of these, and a combination thereof.

* * * * *